

UC Merced

UC Merced Electronic Theses and Dissertations

Title

A Rechargeable Aluminum Battery Electrolyte Based on Aluminum Trifluoromethanesulfonate in Tetrahydrofuran: The Role of Chloride and Hydride Additives

Permalink

<https://escholarship.org/uc/item/91n696cn>

Author

Slim, Zaher

Publication Date

2022

Peer reviewed|Thesis/dissertation

UNIVERSITY OF CALIFORNIA, MERCED

**A Rechargeable Aluminum Battery Electrolyte Based on
Aluminum Trifluoromethanesulfonate in Tetrahydrofuran:
The Role of Chloride and Hydride Additives**

A dissertation submitted in partial satisfaction of the requirements for the
degree of DOCTOR OF PHILOSOPHY

in

Chemistry and Chemical Biology

by

Zaher Slim

Dissertation Committee:

Professor Erik J. Menke, Advisor

Professor Ryan Baxter

Professor Min Hwan Lee

Professor Hrant P. Hratchian, Chair

2022

Chapter 2 © 2020 American Chemical Society

Chapter 3 © 2022 American Chemical Society

All other Chapters © 2022 Zaher Slim

All rights reserved

The dissertation of Zaher Slim is approved, and it is acceptable in quality and form for publication on microfilm and electronically:

Erik J. Menke, Advisor

Ryan Baxter

Min Hwan Lee

Hrant P. Hratchian, Chair

University of California, Merced

2022

Dedicated to my mother Nawal, my father Afif, my brothers Hassan, Ali and Mohammad, my partner Samar Zaidi, and my advisor Erik J. Menke...

She had studied the Universe all her life, but had overlooked its clearest message: For small creatures such as we, the vastness is bearable only through love —Carl Sagan

Table of Contents

Acknowledgements	vii
Curriculum Vitae	viii
List of Figures	ix
List of Schemes	xi
List of Tables	xii
Abstract	xiii
Chapter 1: Aluminum Batteries: A Literature Review	1
1.1 Motivation.....	1
1.2 Brief overview on the development of aluminum batteries.....	3
1.3 Haloaluminate ionic liquids	5
1.4 Organic electrolytes	7
1.4.1 Aluminum halide electrolytes	8
1.4.2 Active-halide-free electrolytes.....	10
1.5 Cathodes.....	11
1.6 References.....	13
Chapter 2: Comparing Computational Predictions and Experimental Results for Aluminum Triflate in Tetrahydrofuran	21
2.1 Introduction.....	21
2.2 Materials and Methods.....	22
2.2.1 Density functional theory calculations.....	22
2.2.2 Experimental details.....	23
2.3 Results and Discussion	24
2.3.1 Coordination structures.....	24
2.3.2 Determination of ionic association between aluminum and triflate in THF using infrared spectroscopy	25
2.3.3 Stability predictions and electrochemical profiling	28
2.4 Conclusions.....	32
2.5 References.....	32
Chapter 3: Aluminum Electrodeposition from Chloride-Rich and Chloride-Free Organic Electrolytes	35
3.1 Introduction.....	35
3.2 Materials and Methods.....	38
3.2.1 Density functional theory calculations.....	38
3.2.2 Experimental details.....	38
3.3 Results and Discussion	39
3.4 Conclusion	47
3.5 Outlook	47
3.6 Supporting Information.....	48
3.7 References.....	58

Chapter 4: Hydride-Enhanced Plating and Stripping of Aluminum from Triflate-Based Organic Electrolytes	64
4.1 Introduction.....	64
4.2 Materials and Methods.....	66
4.2.1 Density functional theory calculations.....	66
4.2.2 Electrolyte preparation.....	66
4.2.3 Materials characterization.....	67
4.3 Results and Discussion	68
4.4 Outlook and Future Work	78
4.5 Supporting Information.....	79
4.6 References.....	88
Appendix A.....	92
Copyright permission for chapter 2	92
Copyright permission for chapter 3	93

Acknowledgements

My journey as a graduate student at the University of California, Merced has been exhilarating and full of exciting scientific endeavors primarily because of the countless incredible individuals in my life who have inspired me to become a better person and a better scientist. First, I would like to thank my advisor and mentor, Prof. **Erik J. Menke**. Erik is a brilliant scientist and an extraordinary mentor, above all, an incredibly kind and considerate individual. His guidance and support throughout those past few years have been invaluable. His infectious positivity, faith in others, and cheerful personality made my Ph.D. journey a very delightful one. I am extremely lucky and privileged to have had the opportunity to work along his side, I could not have asked for a better a Ph.D. advisor. It goes without saying that none of the work in this dissertation would have been possible without him. I would like to thank all my family members, including my dedicated and compassionate mother **Nawal**, my wise, brilliant, and perseverant father **Afif**, my caring and amazing brothers **Hassan, Ali and Mohammad** and my kind, loving, and beautiful partner **Samar Zaidi** for all their love and support. My awesome friends around the world, and here at UC Merced, especially **Hassan Harb, Ali Aboutaka, and Samantha Bidwell** for being great friends and amazing colleagues and for all their help. I probably would not have made it through the first few weeks of graduate school if it weren't for their support and guidance. Hassan's friendship has played an integral part in my scientific journey. I discovered my love for science during secondary school when Hassan and I prepared a poster on Supernova. Since then, Hassan has continued to be an exceptionally kind and compassionate friend. Hassan spent numerous hours teaching me how to troubleshoot and run DFT calculations. Sharing my science with him throughout the years has brought me great deal of joy. Ali's friendship has also played a critical part in my Ph.D. studies. It was him who convinced me to apply to UC Merced in the first place, and I am very glad I listened. I'm very lucky to have shared my Ph.D. journey with such a talented, and tenacious individual. I am also incredibly lucky to have remarkable scholars as my dissertation committee members. My sincere gratitude to Prof. **Hrant P. Hratchian**, Prof. **Ryan Baxter**, and Prof. **Min Hwan Lee** for their help, guidance, and support throughout my Ph.D. studies. I am very grateful to **David Rice** for training me to use the NMR and FTIR instrumentation. I am also thankful to **Kennedy Nguyen** for training me to use the SEM, XRD, and XPS instrumentation. I am thankful to **Melissa Russel, Donna Jaramilo-Felin, Alyssa Hua**, and all chemistry teaching lab staff and instructors at UC Merced for all their help, support, and guidance. I would like to thank Prof. **David Kelley** and Prof. **Son Nguyen** for giving me permission to use their FTIR spectrometers. My sincere gratitude to the international student's office personnel, graduate division personnel and School of Natural Sciences personnel, especially **Joy Sanchez-Bell, Paul Roberts, Jesse Batther, Emily Huang, Becky Mirza** and **Lacey Long Vejar** for all their help and support. I would like to thank **Karnamohit Ranka, Bilal Overton, Riley Ball, Ryan Brisbin, Suzanne Sandin, Ajay Khanna, Will Spaller, Warren Nanney, Zachary Petrek, Jocelyn Ochoa, David Morgan, Randy Espinoza, Duy Nguyen, David Morgan, Pin Lyu** and many others for being awesome friends and amazing colleagues. Lastly, I would like to thank all the students I have had the privilege of teaching at UC Merced.

Curriculum Vitae

Education

- Ph.D. in Chemistry and Chemical Biology 2017 - 2022
Dissertation title: A Rechargeable Aluminum Battery Electrolyte Based on Aluminum Trifluoromethanesulfonate in Tetrahydrofuran: The Role of Chloride and Hydride Additives
- M.S. in Food Quality and Chemistry of Natural Products “Maxima Cum Laude” 2015 - 2017
Dissertation title: Polyphenol Extraction from *Origanum Dictamnus* using low-Transition Temperature Mixtures Composed of Glycerol and Organic Salts
- M.S. in Food Science and Technology 2013 - 2015
- B.S. in Agricultural Sciences 2010 - 2013

Publications

- Slim, Z.**; Menke, E. J. Hydride-Enhance Plating and Stripping of Aluminum from Triflate-Based Organic Electrolytes. **2022 (Under Review)**
- Slim, Z.**; Menke, E. J. Aluminum Electrodeposition from Chloride-Rich and Chloride-Free Organic Electrolytes. *J. Phys. Chem. C* **2022**, 126 (5), 2365–2373.
- Slim, Z.**; Menke, E. J. Comparing Computational Predictions and Experimental Results for Aluminum Triflate in Tetrahydrofuran. *J. Phys. Chem. B* **2020**, 124 (24), 5002–5008.
- Slim, Z.**; Jancheva, M.; Grigorakis, S.; Makris, D. P. Polyphenol Extraction from *Origanum Dictamnus* Using Low-Transition Temperature Mixtures Composed of Glycerol and Organic Salts: Effect of Organic Anion Carbon Chain Length. *Chem. Eng. Commun.* **2018**, 205 (10), 1494–1506.

List of Figures

Figure 1.1 Intrinsic properties of various metal anodes.....	1
Figure 1.2 Timeline showing overview of aluminum-based organic electrolytes	7
Figure 2.1 DFT optimized structures of Al speciation in $\text{Al}(\text{OTF})_3/\text{THF}$ electrolyte	24
Figure 2.2 FTIR spectra of Al-triflate/THF solutions.....	26
Figure 2.3 Displays the CV for $\text{Al}(\text{OTF})_3$ in THF electrolytes at different concentrations	30
Figure 2.4 Ionic conductivity of the solution as a function of aluminum triflate concentration.....	31
Figure 3.1 DFT optimized structures of Al-Triflate and Al-Chloride complexes	37
Figure 3.2 FTIR spectra of various concentrations of Al and/or Li salts in THF.....	40
Figure 3.3 CVs and chronoamperograms of $\text{Al}(\text{OTF})_3/\text{THF}$, AlCl_3/THF , and $\text{Al}(\text{OTF})_3+\text{LiCl}/\text{THF}$ electrolytes	44
Figure 3.4 SEM images of Al electrodeposits on Cu obtained from $\text{Al}(\text{OTF})_3/\text{THF}$, AlCl_3/THF , and $\text{Al}(\text{OTF})_3+\text{LiCl}/\text{THF}$ electrolytes	46
Figure 3.5 Illustration of OTF^- transfer from Al- to Li-cation based on DFT and FTIR..	52
Figure 3.6 CV shift as function of increasing concentration of AlCl_3/THF	52
Figure 3.7 Showing the similarity in CV profiles for various mole ratios of $\text{Al}(\text{OTF})_3:\text{LiCl}/\text{THF}$ electrolytes.....	53
Figure 3.8 Low magnification SEM images Al electrodeposits on Cu obtained from $\text{Al}(\text{OTF})_3/\text{THF}$, AlCl_3/THF and 1:3 $\text{Al}(\text{OTF})_3:\text{LiCl}/\text{THF}$ electrolytes	53
Figure 3.9 High magnification SEM images Al electrodeposits on Cu obtained from $\text{Al}(\text{OTF})_3/\text{THF}$, AlCl_3/THF and 1:3 $\text{Al}(\text{OTF})_3:\text{LiCl}/\text{THF}$ electrolytes	54
Figure 3.10 SEM images showing streaking patterns of Al electrodeposits on Cu from $\text{Al}(\text{OTF})_3/\text{THF}$	55
Figure 3.11 CV, chronomaperogram and SEM images for chloride-free aluminum electroplating from 0.2M $\text{Al}(\text{OTF})_3/\text{THF}$ electrolyte	56

Figure 3.12 XPS spectra of Al deposits from Al(OTF) ₃ /THF electrolyte	57
Figure 4.1 DFT optimized structures and FTIR spectra for Al-hydride electrolytes.....	68
Figure 4.2 CVs and chronoamperograms of triflate- and chloride-based electrolytes	71
Figure 4.3 Optical microscopy images and XRD spectra for Al electrodeposits on Cu ..	73
Figure 4.4 SEM images of Al electrodeposits on Cu substrate from triflate- and chloride-based electrolytes	75
Figure 4.5 XPS spectra for Al deposits from triflate- and chloride-based electrolytes	77
Figure 4.6 Showing the DFT calculated Al—H bond lengths in Al ₂ H ₇ ⁻ and Al ₂ Cl ₃ H ₄ ⁻ ...	80
Figure 4.7 CV for 1.5 M LiAlH ₄ /THF on gold working electrode	81
Figure 4.8 CV showing hydride activity, oxidative stability, and contribution from side reaction.....	82
Figure 4.9 Showing photographic images of Al electrodeposit on Cu substrate and region for XPS experiments	83
Figure 4.10 XPS spectra comparison of region 1 (before etching) and region 2 for Al electrodeposits triflate- and chloride-based electrolytes	83
Figure 4.11 SEM image of remaining Al electrodeposits on Cu substrate after etching experiments at region 1	84
Figure 4.12 Showing optical image and SEM image of Al electrodeposits streaking patterns on Cu and Al film obtained after 18 hours of plating	85
Figure 4.13 High magnification SEM images of Al electrodeposits from triflate- and chloride- based electrolytes.....	86
Figure 4.14 CV for 1:3 Al(OTF) ₃ :LiAlH ₄ /diglyme	87
Figure 4.15 CVs for 1:3 Al(OTF) ₃ :LiBH ₄ /THF and 1:3 AlCl ₃ :LiBH ₄ /THF	87

List of Schemes

Scheme 2.1 Born-Haber cycle used to calculate the changes in the standard solvation Gibbs Free Energy	28
--	----

List of Tables

Table 1.1 Intrinsic properties of various metal anodes	2
Table 2.1 Measured and computed vibrational frequencies of CF ₃ symmetric deformation, SO ₃ symmetric and antisymmetric stretching modes.....	25
Table 2.2 Gibbs Free Energies and absolute reduction potentials of solvent, anion and complexes	29
Table 3.1 Measured and computed vibrational frequencies of aluminum complexes.....	48
Table 3.2 Predicted reaction energies from DFT calculations (OTF ⁻).....	50
Table 3.3 Predicted reaction energies from DFT calculations (chloride).....	51
Table 3.4 Comparison of measured Al (2p) binding energies to literature values	57
Table 4.1 Measured and computed vibrational frequencies of aluminum complexes.....	79

Abstract

Rechargeable batteries based on multivalent ions (Mg^{2+} , Ca^{2+} , Al^{3+}) can have far-reaching applications such as portable electronics, electric vehicles, and grid storage. As the most abundant metal in the Earth's crust, Al is an ideal candidate. Metallic Al anodes can, in theory, provide exceptionally high charge capacities. However, the lack of non-corrosive electrolytes has been a bottleneck in the advancement of a practical rechargeable battery. This dissertation discusses the author's efforts to develop and understand organic electrolytes based on aluminum trifluoromethanesulfonate (referred to herein as Al-triflate or $\text{Al}(\text{OTF})_3$), an active-halide-free and commercially available Al salt. To investigate these systems, a wide range of computational and experimental techniques have been utilized, including density functional theory (DFT) calculations, Fourier transform infrared spectroscopy (FTIR), cyclic voltammetry (CV), electrochemical impedance spectroscopy (EIS), scanning electron microscopy (SEM), and X-ray photoelectron spectroscopy (XPS). From these, insights into Al-ion speciation and electrochemistry are brought to light, and Al electrodeposition is successfully achieved from several electrolyte systems. Ultimately, the work presented in this dissertation successfully tackles reversible Al electrodeposition from chloride-free organic electrolytes, a major hurdle that has prevented the incorporation of these systems in rechargeable Al batteries.

Chapter one includes a detailed review of historic and most recent developments in non-aqueous electrolyte chemistries for rechargeable aluminum batteries, including chloroaluminate ionic liquids and organic solutions.

Chapter two reports the results of research on an $\text{Al}(\text{OTF})_3$ in tetrahydrofuran (THF) electrolyte. Computational modelling by means of DFT and a variety of experimental techniques have revealed the predicted and measured spectroscopic and electrochemical features of aluminum ions in this electrolyte. Aluminum was found to be electrochemically active, in addition to the presence of two concentration dependent ionic environments for triflate anions (OTF^-). This work also introduces a method that provides a rationale for understanding redox potentials of Al-ions by comparing DFT calculations with cyclic voltammetry experiments.

Chapter three discusses the effect of lithium chloride (LiCl) as an additive to the $\text{Al}(\text{OTF})_3$ in THF electrolyte to investigate the role of chloride ions on speciation and the electrochemical behavior of aluminum. Successful electrodeposition of aluminum was carried out from chloride (Cl^-)-free (non-corrosive) and Cl^- -rich (highly-corrosive) Al electrolytes at room temperature, and a method to probe the progress of the reactions involving $\text{Al}(\text{OTF})_3$ and LiCl by utilizing the DFT-derived and FTIR-measured vibrational frequencies of the OTF^- was introduced.

Chapter four discusses the effect of hydrides (H^-) on Al speciation and electrochemistry by employing a LiAlH_4 additive to the $\text{Al}(\text{OTf})_3/\text{THF}$ electrolyte. Reversible room-temperature Al electrodeposition is demonstrated and compared to the chloride-based electrolyte. Using the method developed in chapter 3, and from DFT and FTIR analyses, Al-hydride speciation in these systems is explored, and a mechanism for reversible Al electrodeposition in OTf^- -based electrolyte is proposed. Insight into the chemical composition of the Al deposits from the OTf^- - and Cl^- -based electrolyte is revealed using depth-profile XPS analyses.

Chapter 1: Aluminum Batteries: A Literature Review

1.1 Motivation

The reliance on fossil fuels as the primary energy source has aggravated the impacts of global climate change.¹ To address the climate challenges and mitigate their impacts on society, global efforts have focused on exploiting renewable energy resources such as solar and wind power.² However, the intermittent nature of these green-energy resources necessitates the development of novel energy storage devices.³ Convenient storage of electrical energy can be fulfilled by using electrochemical storage devices.⁴ An example of such systems are rechargeable batteries. Providing on-demand access to energy with the possibility of reuse over an extended period of time, these devices, notably, Lithium-ion (Li-ion) batteries, play an essential role in our day-to-day lives.^{5,6} From portable electronic devices to electric vehicles, society's reliance on these batteries is continuously growing, and with that growth, a surge in demand for alternative and more advanced energy storage devices is inevitable.

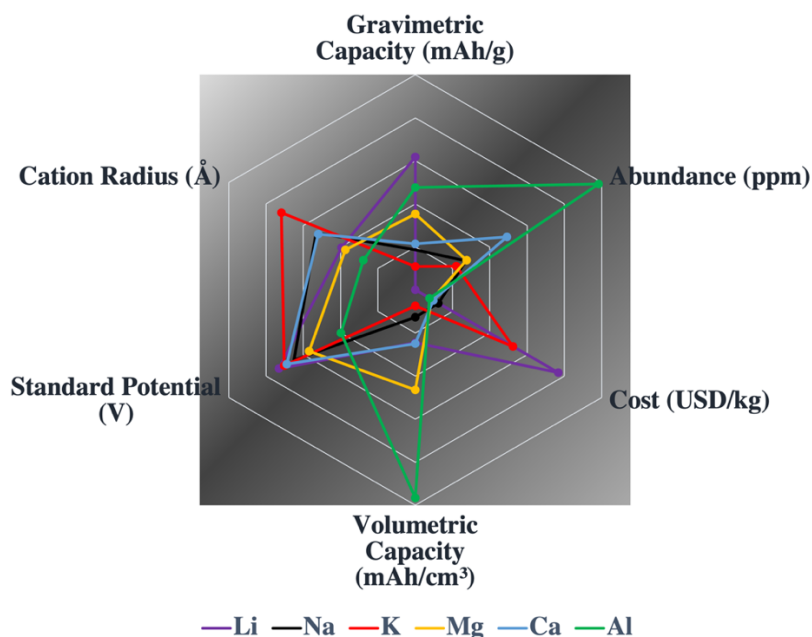


Figure 1.1 Intrinsic properties of various metal anodes. Abundance in Earth's crust, cation radius, standard potential, cost, gravimetric and volumetric capacity.

Table 1.1 Intrinsic properties of various metal anodes. Abundance in Earth's crust, cation radius, standard potential, cost, gravimetric and volumetric capacity of lithium (Li), sodium (Na), potassium (K), magnesium (Mg), calcium (Ca), and aluminum (Al) ⁷

Element	Gravimetric capacity (mAh/g)	Abundance (ppm)	Cost (USD/kg)	Volumetric capacity (mAh/cm ³)	Standard Potential (V vs NHE)	Cation radius (Å)
Li	3861	65	19.2	2042	-3.042	0.76
Na	1166	22700	3.1	1050	-2.71	1.02
K	685	18400	13.1	609	-2.925	1.38
Mg	2205	23000	2.2	3868	-2.37	0.72
Ca	1340	41000	2.4	2071	-2.87	1
Al	2980	82000	1.9	8046	-1.66	0.535

Aluminum (Al) is the most abundant metal and third most abundant element on Earth. Compared to its monovalent and divalent counterparts, Al exhibits the highest theoretical charge capacity per unit volume (8046 mAh/cm³), which is about 4 times that of Li (2042 mAh/cm³). (see Table 1.1 and Figure 1.1). This makes Al batteries an attractive candidate for personal electronic devices where portability is considered a key attribute. Also, Al's theoretical gravimetric capacity (2980 mAh/g) is lower than that of Li (3861 mAh/g), yet superior to that of the other metals. Additionally, among these metals, Al has the smallest ionic radius (0.535 Å) which suggests that intercalation-type cathodes, such as those used for Li-ion batteries, may be feasible.⁷

Because of these exceptional characteristics, and from an industrial standpoint, large-scale development of rechargeable batteries based on aluminum offer the possibility of high energy density with low cost when coupled with suitable electrolytes and cathodes materials.

To make use of Al as an anode material, reversible aluminum electrodeposition at high Coulombic efficiencies is an essential criterion. Unfortunately, this can only be achieved from a limited number of electrolyte systems, particularly those employing Al-halide molten salts (room-temperature and high temperature). Hence, these systems have been the spotlight of research on rechargeable Al batteries over the past decade, and several review articles on the topic have been published.⁷⁻¹⁵ In practice, however, these electrolytes are reactive towards cathode materials,^{16,17} corrosive towards stainless Steel current collectors,¹⁸ and Al anodes¹⁹ and may involve chlorine (Cl₂) generation side reactions.^{20,21} Consequently, alternative electrolyte systems are urgently needed.

On account of their successful incorporation into Li-ion batteries, organic electrolytes present an appealing choice for practical application of rechargeable Al batteries. However, a major challenge that has hindered the development of an organic electrolyte for rechargeable Al batteries is the lack of a suitable organic system.^{12,17} Ultimately, the electrolyte of choice should be active-halide-free, that is, the system should not include free halogen anions (Cl^- , Br^- , F^-) and halo-aluminate complexes (such as AlCl_4^- , Al_2Cl_7^-) while also promoting reversible aluminum electrodeposition. Additionally, the electrolyte should exhibit a wide electrochemical window to accommodate various types of cathode materials, and high ionic conductivity.

Although numerous investigations employing aluminum trichloride in organic solvents have been undertaken, very few active-halide-free Al electrolytes have been reported.^{23-27,101} To that end, this dissertation discusses the author's efforts to develop and understand electrolytes based on Aluminum trifluoromethanesulfonate, also referred to herein as Al-triflate or $(\text{Al}(\text{OTF})_3)$, in tetrahydrofuran (THF),²⁸ and the role of chlorides (Cl^-),²⁹ and hydrides (H^-) in aluminum electrochemistry.

1.2 Brief overview on the development of aluminum batteries

According to early literature reports, the first application of Al as an electrode material was in 1850, where it was used as a cathode rather than an anode material in an Al - Zinc battery.⁸ Later, in 1857, initial attempts to use Al as an anode were conducted. In this study, Al was coupled with a carbon cathode in a nitric acid electrolyte.³⁰ Almost a century later, a heavy duty Al - Chlorine (Cl_2) battery was reported. Despite offering reasonable discharge voltages, further progress in the development of this battery was probably hampered by the safety concerns involving the use of Cl_2 gas.³¹ In 1951, a Leclanché -type dry cell utilizing an Al anode and a MnO_2 cathode was developed. The cell employed a NaOH plus ZnO electrolyte and a porous separator.³² In the following years, the electrolyte was replaced by manganese chloride tetrahydrate and other separators.^{33,34} Attempts to commercialize these batteries were unsuccessful, primarily due to Al's innate ability to form an oxide layer which significantly lowers the battery's operating voltage.

Almost a decade later, in 1962, the Al-air battery, which utilizes the oxygen derived from air as a cathode, was developed. The battery was enabled by a concentrated KOH or NaOH electrolytes.³⁵ By employing strong base electrolytes, dissolution of Al was achieved and the challenges associated with the protective oxide layer were overcome. However, this occurs at the cost of high corrosivity, which significantly diminishes the capacity of Al anodes due to side reactions involving H_2 evolution, leading to lower practical operating cell voltages.^{14,36}

In 1972, the kinetics of Al electrodeposition/dissolution from binary ($\text{AlCl}_3 - \text{NaCl}$) and ternary ($\text{AlCl}_3 - \text{LiCl} - \text{KCl}$) high temperature molten salts were highlighted by Del Duca, and the conceptual framework for a rechargeable Al battery was brought to light.³⁷ Shortly after Del Duca's report, Holleck and Griner published two research articles on a $\text{AlCl}_3 - \text{KCl} - \text{NaCl}$ molten salts electrolyte. The first study focused on evaluating Al as an anode material in the molten salts.³⁸ While in the second study, the kinetics of Cl_2 reduction on a rotating-vitreous carbon disk electrode were elucidated.³⁹ Although these systems showed promise as energy storage devices, large-scale application of these batteries was probably hindered by the high operating temperatures of the molten salt electrolytes, electrode passivation during anodic and cathodic polarization, dendrite formation during Al electrodeposition which could short-circuit the battery during operation, and the challenges associated with the use of Cl_2 gas.³⁸

Several years later, in 1988, the Al- Cl_2 battery was revisited, this time however, a room-temperature molten salt was used as the electrolyte. By mixing AlCl_3 with 1,2-dimethyl-3-propyl-imidazolium chloride, Gifford and Palmisano developed a rechargeable battery which utilized reversible Al plating/stripping as the anodic reaction, and Cl_2 intercalation into carbon as the cathodic reaction. The battery exhibited a discharge voltage of 1.7V , and 35-40 mAh/g discharge capacities sustained for over 150 cycles.⁴⁰

Interest in rechargeable Al batteries re-emerged in 2010 when Paranthaman et al. investigated Mn_2O_4 as a cathode material with the room-temperature chloroaluminate molten salt consisting of AlCl_3 and 1-ethyl-3-methyl-imidazolium chloride ($[\text{EMIm}]\text{Cl}$) at 1.5:1 mole ratio.⁴¹ Unfortunately, intercalation/de-intercalation behavior with the Mn_2O_4 cathode was not measured.

One year later, using the same ionic liquid electrolyte, Jayaprakash et al. described a rechargeable aluminum battery that utilized V_2O_5 as a cathode.⁴² The study revealed compelling evidence for rechargeability in terms of capacity and cycling behavior which lead the researchers to conclude that Al-ion insertion/de-insertion into V_2O_5 was responsible for this electrochemical behavior. This hypothesis was later invalidated by Reed and Menke in 2013, who suggested that the V_2O_5 was electrochemically inactive in this system and that the measured capacities were likely due to a side reaction occurring with the stainless Steele current collector.¹⁸ These reports were probably what motivated Wen et al. to study the reactivity of the ionic liquid with the V_2O_5 .⁴³ A mechanism elucidating the chemical reactivity between said constituents was proposed. It was found that V_2O_5 reacts with the chloroaluminate species and produces electrochemically active degradation products including ($\text{VOCl}_3, \text{VO}_2\text{Cl}, \text{AlCl}_3\text{VO}_3^-$) which emphasizes the need for further investigation of the chemical reactivity of the chloroaluminate ionic liquids towards other cathodes material.

Following the work on the Al – V₂O₅ battery by Jayaprakash et al,⁴² and then Reed and Menke,¹⁸ and the work by Abood et al. on ionic liquid analogues in 2011,⁴⁴ an increasing number of studies on aluminum batteries utilizing room temperature chloroaluminate ionic liquids,^{45–59} high temperature molten salts,^{60–65} and ionic liquid analogues were reported.^{66–73} While many researchers carried on investigating and synthesizing novel cathode materials (as can be found in these reviews^{16,74}), Reed and Menke focused their efforts on developing active-halide-free organic electrolytes. In 2015, they reported the first known rechargeable Al battery based on an organic electrolyte.²⁵ The battery employed an Al(OTF)₃ in diethylene glycol dimethyl ether (diglyme) electrolyte and copper hexacyanoferrate cathode. Despite obtaining reversible intercalation behavior with the Prussian blue analogue cathode, the battery delivered relatively low discharge capacities and suffered from poor capacity retention. Still, this work opens new horizons for the use of Prussian-blue analogues as cathodes materials for rechargeable Al batteries.

1.3 Haloaluminate ionic liquids

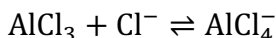
It is widely recognized that the discovery of ionic liquids occurred almost a century ago when Walden investigated the physical properties of ethylammonium nitrate, which was produced by reacting ethylamine with nitric acid.⁷⁵ Chloroaluminate melts are first generation ionic liquids⁷⁶ and are commonly investigated as electrolytes for rechargeable aluminum batteries.⁷⁹ These electrolytes can be produced by mixing RX with AlX₃, where R is an organic cation typically imidazolium or pyridinium, and X is an anion, typically a halogen (Cl, Br, or I).^{9,77}

Early investigations of these systems were those of Hurley and Wier in 1951, where an ionic liquid consisting of 2:1 mole ratio of AlBr₃ and 1-ethylpyridinium bromide was investigated for Al electrodeposition.⁷⁸ Because this system consisted of both bromides and chlorides, exploring chemical composition was complicated at the time. Almost 3 decades later, Gale et al. studied a similar system by Raman spectroscopy.⁷⁹ The electrolyte consisted of AlCl₃ and 1-butylpyridinium chloride and was investigated at mole ratios ranging from 0.75:1 to 2:1. A key finding reported in this study was that the formation of Al₂Cl₇⁻ was more facile in ionic liquids compared to high temperature molten salts, the significance of this Al complex will be discussed later.

As mentioned previously, electrodeposition of Al from high temperature molten salts was also investigated in the 1970s by Del Dulca.³⁷ Compared to ionic liquids, high temperature chloroaluminate molten salts are usually produced by reacting binary or ternary mixtures of AlX₃, with M⁺X⁻, where M an alkali metal (such as Li, K or Na) and X is a halogen (such as Br, or Cl).^{9,77} It is worth mentioning that the design rationale behind both high temperature chloroaluminate molten salts and room temperature chloroaluminate ionic liquids is the same, that is, combining a Al-halide salt such as AlCl₃ with another halogen source (organic cation or alkali metal salt) at specific mole ratios, produces a mixture that exhibits a significantly lower melting point in comparison to the melting points of the individual constituents. In the case of high temperature molten salts, this is usually achieved by heating the mixture, while room temperature ionic liquids are in the molten state at ambient conditions.

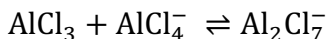
Furthermore, it is important to note that Al speciation in these mixtures is in the form of Al-complexes rather than free Al cations.¹⁴ However, the presence of Al-complexes in these mixtures does not guarantee successful Al electrodeposition/stripping. Speciation in both room-temperature ionic liquids and high temperature molten salts can be described by the following conditions:

In basic and neutral chloroaluminate melts, that is when the mole ratio of AlCl₃ to its corresponding chloride source is less than or equal to 1, the system is governed by following reaction²⁰:

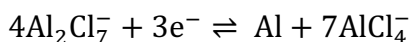


Al electrodeposition from these systems is possible in high temperature molten salts. On the other hand, in room temperature ionic liquids, the electrochemical reduction of Al complexes is preceded by electrochemical reduction of the organic cation, hence electrolyte decomposition occurs before Al plating can be achieved.⁸⁰

When excess amount of AlCl₃ is added to the system, self-ionization of haloaluminate species takes place, and the system is governed by the following reaction²⁰:



As a result of the coexistence of both AlCl₄⁻ and Al₂Cl₇⁻, reversible Al electrodeposition can be carried out, and the following reaction has been proposed^{20,77}:



Because room temperature chloroaluminate ionic liquids take advantage of this equilibrium at ambient conditions, these systems are widely explored as electrolytes for rechargeable Al battery application.

In addition to their compositional tunability, ionic liquids exhibit exceptionally high ionic conductivities (13-19 mS/cm at room temperature in the commonly used (AlCl₃: [EMIm]Cl)⁵⁹ comparable to those of lithium ion batteries and relatively wide electrochemical windows¹⁹ (~ 2.4V vs Al/Al³⁺ in the (AlCl₃: [EMIm]Cl)).¹⁷ Meanwhile, these electrolytes are extremely hygroscopic and highly corrosive towards stainless steel current collectors.¹⁸ Although, the corrosivity concern can be overcome by using molybdenum instead,^{17,81} this system still suffers from significant hurdles which have not yet been addressed, including the parasitic reaction involving Cl₂ gas generation,^{20,21} and the lack of a suitable cathode materials.¹⁷

1.4 Organic electrolytes

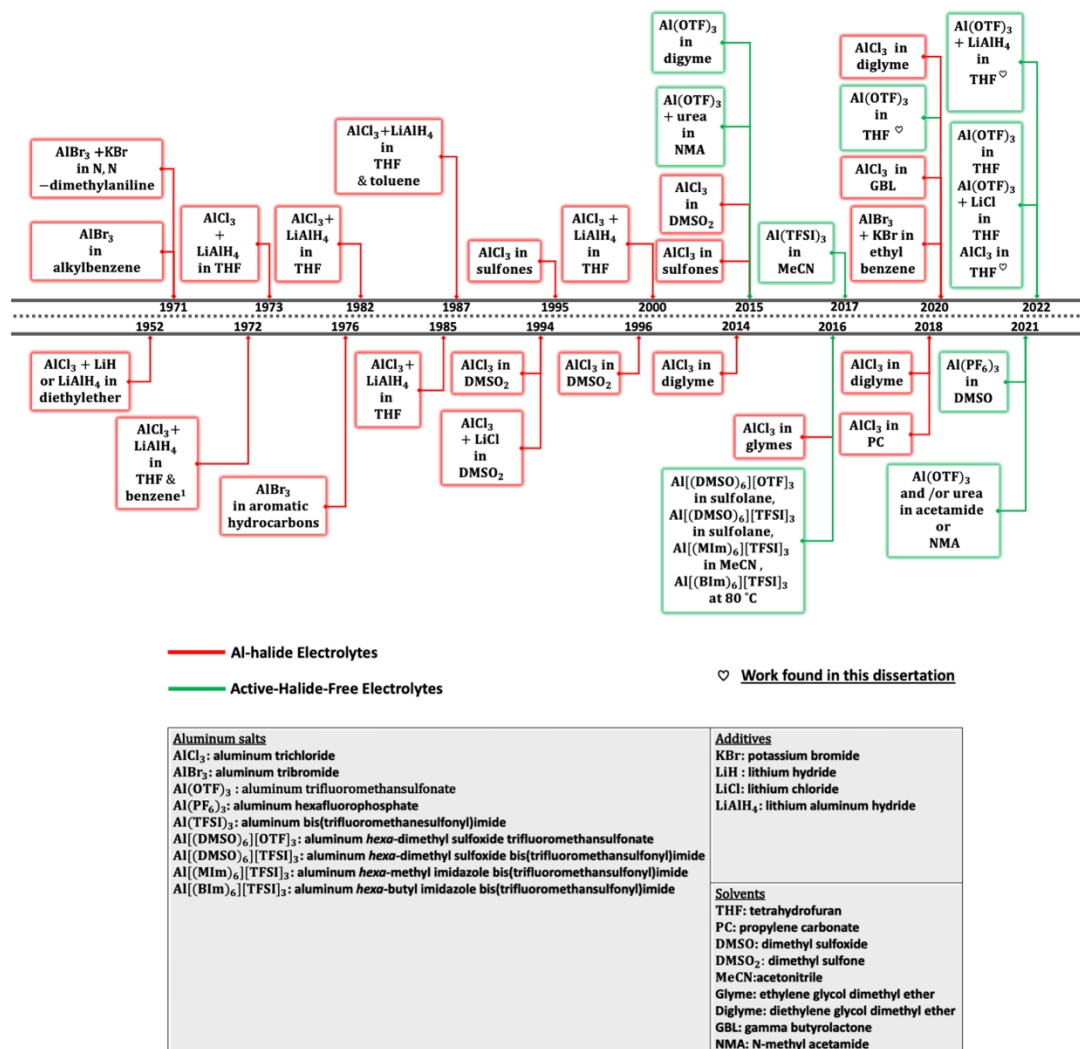


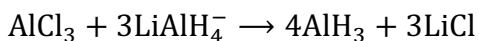
Figure 1.2 Timeline showing overview of aluminum-based organic electrolytes.^{23–29,82–107}

1.4.1 Aluminum halide electrolytes

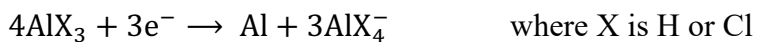
In 1952, Couch and Brenner developed an organic electrolyte from which Al electrodeposition was achieved.⁸² Their study was inspired by Plotnikov's work, which dates to 1899. The electrolyte consisted of a mixture of 2 - 3 M aluminum chloride and 0.5 - 1 M lithium hydride (LiH) or lithium aluminum hydride (LiAlH₄) in diethylether. This system was developed at the National Bureau of Standards and was the first to be implemented on an industrial scale.^{77,82,108} Following this work, considerable efforts were devoted to the investigation of similar electrolytes, a timeline showing the evolution of most of these efforts is shown in figure 1.2, and a detailed review article describing early literature attempts (before 2000) on Al electrodeposition from organic electrolytes can be found in reference.⁷⁷

In this dissertation, special consideration is given to the studies involving AlCl₃ and LiAlH₄. While the original report by Couch and Brenner discussed the use of a wide range of additives and solvents,^{82,109} in the following years, more detailed investigations were undertaken by other researchers. For example, in 1972, Ishibashi and Yoshio reported Al electrodeposition from a 3:1 mole ratio of AlCl₃ and LiAlH₄ in tetrahydrofuran-benzene.⁸⁵ It was reported that this solvent mixture significantly improved the operational longevity of the plating bath compared to diethyl ether. Another research article by Ishibashi and Yoshio was published in the following year.⁸⁶ In this study, THF was used as the sole solvent for AlCl₃ plus LiAlH₄ mixture. It was found that the current densities measured for the Al electrodeposition from THF under similar conditions, was at least 3 times higher than that of diethylether which suggested that Al electrodeposition occurs at a much higher rate in THF.

7 years later, in 1985, Graef investigated the electrochemical mechanism for electrodeposition of Al from AlCl₃ and LiAlH₄ in THF.⁸⁹ Contrary to the previous report by Ishibashi and Yoshio, this study was conducted in excess of LiAlH₄ rather than AlCl₃. Specifically, a 1:3 mole ratio of AlCl₃ to LiAlH₄ was used according to the following reaction¹¹⁰:



Graef also suggested that the overall electrochemical mechanism took place according to the following reaction:



According to this report and that of Daenen,¹¹¹ H^- were found to catalyze the charge transfer process which facilitates Al electrodeposition.

Motivated by the results in Graef's report, and several others that also investigated the electrochemical mechanism for Al electrodeposition from the same system at various mole ratios including Ishibashi and Yoshio,^{85,86} Galová,⁸⁸ Badawy et al.,⁹⁰ Lefebvre and Conway,⁹⁵⁻⁹⁷ we studied the reaction between $\text{Al}(\text{OTf})_3$ and LiAlH_4 at 1:3 mole ratio. Our findings not only corroborate those of Graef⁸⁹ and Daenen¹¹¹ with regards to the catalyzing role of H^- , but also demonstrate for the first time that reversible Al electrodeposition can be carried out in the absence of haloaluminate complexes, as will be discussed in chapter 4. It is worth noting that despite all efforts to reversibly electrodeposit Al from organic electrolytes, to the best of the author's knowledge, a rechargeable Al battery enabled by reversible Al electrodeposition from an organic electrolyte has not yet been reported.

Moreover, because understanding aluminum electrodeposition from organic electrolytes is essential for the development of rechargeable battery electrolytes, studying the physicochemical and electrochemical properties of AlCl_3 based organic systems is crucial. In addition to the hydride-bath previously discussed, alternative organic systems were investigated. For instance, in 1994, Legrand et al. reported several studies on the electrochemical behavior of an electrolyte consisting of AlCl_3 and LiCl in dimethylsulfone (DMSO_2).⁹¹⁻⁹⁴ Although reversible Al electrodeposition was achieved from this electrolyte, the operating temperature of the electrolyte was 130 °C which inhibits its use in a room-temperature rechargeable battery.⁹² The AlCl_3 in DMSO_2 electrolytes was investigated again in 2015 by Miyake et al.¹⁰⁰ In the same year, Nakayama et al. studied AlCl_3 in dialkylsulfones (including ethyl n-propyl sulfone (EnPS), di-n-propyl sulfone, and ethyl secondary-butyl sulfone).⁹⁹ Al speciation and electrochemistry of these mixtures were explored at various compositions and temperatures. Interestingly, the researchers successfully optimized the composition of the AlCl_3 – EnPS by using toluene as a diluent at specific mole ratios. From this electrolyte, reversible Al electrodeposition at room temperature was achieved. Additionally, the corrosivity of this system was evaluated by soaking a stainless Steel electrode in the AlCl_3 – EnPS – toluene electrolyte. While SEM imaging revealed no evidence of corrosion, this does not rule out parasitic reactions involving Cl^- which could arise during electrochemical testing.

Other types of organic systems are those comprised of AlCl_3 /glyme mixtures. Several studies on these electrolytes were reported by Kitada et al.^{98,102,105,112} Successful Al electrodeposition was carried out from diglyme but not from triglyme and tetraglyme,¹¹² probably due to stronger interaction between Al-cations and triglyme/tetraglyme molecules. It is worth emphasizing that unlike the AlCl_3 in dialkylsulfone electrolytes, where Al_2Cl_7^- is responsible for Al-plating,⁹⁹ electrodeposition from the AlCl_3 in diglyme or DMSO_2 were attributed to Al-solvent and/or Al-Cl-solvent complexes.^{112,113} More recent efforts involving AlCl_3 -based organic electrolytes is the work by Wen and other which was published in 2020.¹⁰⁶ In this study Al electrodeposition was carried out from electrolytes composed of AlCl_3 in Gamma-butyrolactone (GBL).

To induce self-ionization and study the role of polymeric AlCl_4^- complexes, excess amounts of AlCl_3 were dissolved in GBL and benzene (which was used as a diluent). While Al_2Cl_7^- species were not detected in these mixtures, NMR studies suggested the presence of a new type of polymeric AlCl_4^- species, namely, $\text{Al}_3\text{Cl}_{10}^-$. Unfortunately, AlCl_3 -based organic electrolytes are corrosive and moisture sensitive due to the presence of chlorides. This necessitates the synthesis and/or investigation of alternative Al-salts, as will be discussed in the following section.

1.4.2 Active-halide-free electrolytes

As previously mentioned, active-halide-free organic electrolytes refer to organic Al-ion systems that do not include free halogen anions (Cl^- , Br^- , F^-) or halo-aluminate complexes (such as AlCl_4^- , Al_2Cl_7^-). Excellent examples of such systems are those based on the commercially available Al-salt, Al-trifluoromethanesulfoante.

Because trifluoromethanesulfonate anions are exceptionally stable against reductive and oxidative cleavage, they do not provide free fluorides,¹¹⁴ and therefore fall under this category. For this reason, Al-triflate was chosen as the Al-salt for the studies conducted in this dissertation.

To the best of the author's knowledge, utilizing active-halide-free electrolyte of rechargeable Al batteries made its first appearance in the published literature in the same report on Al – V_2O_5 battery by Jayaprakash et al.⁴² In addition to using the AlCl_3 : [EMIm]Cl ionic liquid electrolyte, the researchers studied the electrochemical performance of V_2O_5 with an $\text{Al}(\text{OTf})_3$ in THF plus propylene carbonate (PC) organic electrolyte. It was concluded that the V_2O_5 cathode was electrochemically active in the former, yet inactive in the latter. Revisiting the cyclic voltammogram (CV) provided in their work, one can see a reductive current near 0V vs Al/Al³⁺ in the V_2O_5 - $\text{Al}(\text{OTf})_3/\text{THF}+\text{PC}$ experiment. While the reaction appears to be non-reversible and the measured currents are significantly lower than those obtained with the AlCl_3 : [EMIm]Cl ionic liquid, the observed CV profile is similar to the one we have reported for $\text{Al}(\text{OTf})_3/\text{THF}$,²⁸ which we recently confirmed to be associated with Al electrodeposition²⁹ as will be discussed in chapter 3.

In 2015, Mandai and Johansson reported a ternary electrolyte that was prepared by mixing $\text{Al}(\text{OTf})_3$ and urea in N-methylacetamide (NMA).²³ The study revealed that urea significantly enhanced the dissolution of $\text{Al}(\text{OTf})_3$ in NMA, however, unfortunately Al electrodeposition/stripping was not demonstrated.

In the same year, coinciding with their work on $\text{Al}(\text{OTf})_3/\text{diglyme}$ – Prussian blue analogue, Reed and Menke reported on the physicochemical properties of the $\text{Al}(\text{OTf})_3/\text{diglyme}$ electrolyte both computationally and experimentally.²⁴ Although the Al anode exhibited some electrochemically activity in this electrolyte, and remarkable ionic conductivities were reported (up to 25 mS/cm), reversible Al electrodeposition was not achieved, probably due to the strong chelation of the diglyme molecules to the Al-cation.

In the following year, Mandai and Johansson synthesized a series of halo-aluminate free Al salts namely, $[\text{Al}(\text{L})_6\text{X}_3]$ where L is dimethylsulfoxide (DMSO), 1-methylimidazole (MIm) or 1-butylimidazole (BIm) and X is trifluoromethanesulfonate (OTF) or bis-(trifluoromethanesulfonyl)imide (TFSI).²⁶

While the CVs reveal preliminary evidence for non-reversible electrochemical reduction of Al from the $[\text{Al}(\text{DMSO})_6][\text{TFSI}]_3$ in sulfolane, $[\text{Al}(\text{DMSO})_6][\text{OTF}]_3$ in sulfolane, and $[\text{Al}(\text{MIm})_6][\text{TFSI}]_3$ in acetonitrile electrolytes, successful Al electrodeposition was not achieved. Instead, the authors reported that decomposition of the electrolyte took place when electrodeposition from the 1-butylimidazole (BIm) based electrolyte $[\text{Al}(\text{BIm})_6][\text{TFSI}]_3$ was attempted at 80 °C.

Apart from their ubiquity in Li-ion systems,^{22,115,116} TFSI- and PF_6^- -based electrolytes have shown promise in rechargeable Mg.^{117,118} Hence, the synthesis and investigation of corresponding Al salts is of paramount significance. Perhaps it is for this reason, Chiku et al.¹⁰¹ synthesized $\text{Al}(\text{TFSI})_3$ and studied its electrochemical performance in acetonitrile using a Molybdenum working electrode. Whereas Wen et al.¹⁰⁶ synthesized aluminum hexa-fluorophosphate $\text{Al}(\text{PF}_6)_3$ and explored its electrochemistry in DMSO.

In both systems Al electrodeposition was successfully achieved, however, the electrochemical behavior of these systems, according to the CV profiles, appears to be quasi-reversible and may therefore be of limited use in a rechargeable Al battery. Nonetheless, further investigation of these Al salts in other organic solvents is crucial for understanding the role various anions play in Al electrodeposition/stripping.

1.5 Cathodes

The operation mechanisms for lithium-ion and rechargeable aluminum batteries are fundamentally distinct. In a typical Li-ion battery, Li-ions shuttle between 2 electrode materials where Li-ions are inserted/de-inserted into a graphite anode and layered Metal oxide cathode (such as LiCoO_2 , LiMnO_2 , LiNiO_2 , LiFeO_2).^{5,6,119}

On the other hand, in a rechargeable Al battery, the reaction occurring at the anode is reversible Al plating, whereas an conversion or insertion reaction occurs at the cathode.^{7,9,10,12}

The difference between the two mechanisms occurring at the cathode is that the former includes a redox reaction between Al-ions and the cathode material (typically a transition metal sulfide), while the latter involves insertion of an intercalating species (Al-ion or Al-complex) into host sites in the crystal structure of the cathode material.^{16,74}

Commonly reported insertion-type cathode materials include carbon¹²⁰ (such as graphitic-foam,⁴⁶ natural graphite,⁵⁰ and pyrolytic graphite¹²¹), V_2O_5 ,^{18,42,122} Mo_6S_8 .^{45,123,124} It is worth mentioning that intercalation into some of these materials is still debatable and the exact nature of the intercalating species and intercalation mechanisms are not fully understood.

For example, in 2016 a rechargeable Al-battery which utilizes an Al anode, a graphite cathode, and a chloroaluminate ionic liquid was reported by Lin et al.⁴⁶ Based on *Ex-situ* X-ray diffraction (XRD) and *In-situ* Raman studies, the reaction occurring at the cathode during charge/discharge was attributed to the intercalation/de-intercalation of AlCl_4^- species. However, the intercalation of Cl_2 , which was originally proposed as the intercalating species by Gifford and Palmisano in the first Al – Cl_2 battery in 1952,⁴⁰ has been overlooked.

Another controversial cathode material is the V_2O_5 . As discussed above, V_2O_5 was among the first cathode material to be evaluated in recent literature.^{18,42} As previously emphasized, Jayaprakash et al. claimed that intercalation into the V_2O_5 layers was occurring,⁴² while Reed and Menke¹⁸ suggested that a corrosion reaction was occurring between the ionic liquid electrolyte and the stainless steel current collector, which mimics the electrochemical performance of a battery. The corrosivity of the chloroaluminate ionic liquids towards various current collectors was recently highlighted.¹⁷

Furthermore, a similar study on V_2O_5 in the chloroaluminate ionic liquid electrolyte was conducted by Wang et al.¹²² In this report, however, V_2O_5 was hydrothermally deposited on a Ni current collector, and the cathodic electrochemical reaction was attributed to the V_2O_5 redox reaction. In the case of Mo_6S_8 cathode, Geng et al.⁴⁵ evaluated this cathode in ionic liquid electrolyte consisting of AlCl_3 and 1-butyl-3-methylimidazolium chloride([BMIm]Cl). Inductively coupled plasma optical emission spectroscopy (ICP-OES) and XRD studies conducted on the cathode material confirmed the presence of Al and the absence of chlorine, as a result, intercalation of Al-ions rather than chloroaluminate complexes into the host material was proposed according to the theoretical formula $\text{Al}_2\text{Mo}_6\text{S}_8$. While the intercalation process appears reversible, entrapment of the Al-ions and a significant loss in charging capacity during the first cycle was reported.

As previously mentioned, another class of materials for rechargeable Al batteries are the conversion-type cathodes such as those based on chalcogens (for example CuS ,¹²⁵ FeS_2 ,¹²⁶ Ni_3S_2 ,¹²⁷) and halogens (for example FeCl_3 ,¹²⁸ VCl_3 ,¹²⁹ NiCl_2 ,¹³⁰ and PVP-iodine.⁵¹ Although the performance of these batteries is encouraging, great efforts are still required before a practical rechargeable Al battery can be realized. Consequently, due to the severe limitations of the commonly employed chloroaluminate ionic liquids and because the electrolyte composition dictates the reactions at the electrode, special attention should be given to understanding new electrolyte systems such as the active-halide-free organic electrolytes, as will be conveyed by this dissertation.

1.6 References

- (1) Erickson, P.; Lazarus, M.; Piggot, G. Limiting Fossil Fuel Production as the next Big Step in Climate Policy. *Nat. Clim. Change* **2018**, *8* (12), 1037–1043.
- (2) Cherp, A.; Vinichenko, V.; Tosun, J.; Gordon, J. A.; Jewell, J. National Growth Dynamics of Wind and Solar Power Compared to the Growth Required for Global Climate Targets. *Nat. Energy* **2021**, *6* (7), 742–754.
- (3) Larcher, D.; Tarascon, J.-M. Towards Greener and More Sustainable Batteries for Electrical Energy Storage. *Nat. Chem.* **2015**, *7* (1), 19–29.
- (4) Goodenough, J. B. Electrochemical Energy Storage in a Sustainable Modern Society. *Energy Environ. Sci.* **2014**, *7* (1), 14–18.
- (5) Goodenough, J. B.; Park, K.-S. The Li-Ion Rechargeable Battery: A Perspective. *J. Am. Chem. Soc.* **2013**, *135* (4), 1167–1176.
- (6) Dunn, B.; Kamath, H.; Tarascon, J.-M. Electrical Energy Storage for the Grid: A Battery of Choices. *Science* **2011**, *334* (6058), 928–935.
- (7) Tu, J.; Song, W.-L.; Lei, H.; Yu, Z.; Chen, L.-L.; Wang, M.; Jiao, S. Nonaqueous Rechargeable Aluminum Batteries: Progresses, Challenges, and Perspectives. *Chem. Rev.* **2021**, *121* (8), 4903–4961.
- (8) Li, Q.; Bjerrum, N. J. Aluminum as Anode for Energy Storage and Conversion: A Review. *J. Power Sources* **2002**, *110* (1), 1–10.
- (9) Elia, G. A.; Marquardt, K.; Hoeppe, K.; Fantini, S.; Lin, R.; Knipping, E.; Peters, W.; Drillet, J.-F.; Passerini, S.; Hahn, R. An Overview and Future Perspectives of Aluminum Batteries. *Adv. Mater.* **2016**, *28* (35), 7564–7579.
- (10) Zhang, Y.; Liu, S.; Ji, Y.; Ma, J.; Yu, H. Emerging Nonaqueous Aluminum-Ion Batteries: Challenges, Status, and Perspectives. *Adv. Mater.* **2018**, *30* (38), 1706310.
- (11) Li, M.; Lu, J.; Ji, X.; Li, Y.; Shao, Y.; Chen, Z.; Zhong, C.; Amine, K. Design Strategies for Nonaqueous Multivalent-Ion and Monovalent-Ion Battery Anodes. *Nat. Rev. Mater.* **2020**, *5* (4), 276–294.
- (12) Yang, H.; Li, H.; Li, J.; Sun, Z.; He, K.; Cheng, H.-M.; Li, F. The Rechargeable Aluminum Battery: Opportunities and Challenges. *Angew. Chem. Int. Ed.* **2019**, *58* (35), 11978–11996.
- (13) Elia, G. A.; Kravchyk, K. V.; Kovalenko, M. V.; Chacón, J.; Holland, A.; Wills, R. G. An Overview and Prospective on Al and Al-Ion Battery Technologies. *J. Power Sources* **2021**, *481*, 228870.
- (14) Faegh, E.; Ng, B.; Hayman, D.; Mustain, W. E. Practical Assessment of the Performance of Aluminium Battery Technologies. *Nat. Energy* **2021**, *6* (1), 21–29.
- (15) Leung, O. M.; Schoetz, T.; Prodromakis, T.; de León, C. P. Progress in Electrolytes for Rechargeable Aluminium Batteries. *J. Electrochem. Soc.* **2021**, *168* (5), 056509.
- (16) Zafar, Z. A.; Imtiaz, S.; Razaq, R.; Ji, S.; Huang, T.; Zhang, Z.; Huang, Y.; Anderson, J. A. Cathode Materials for Rechargeable Aluminum Batteries: Current Status and Progress. *J. Mater. Chem. A* **2017**, *5* (12), 5646–5660.
- (17) Shi, J.; Zhang, J.; Guo, J. Avoiding Pitfalls in Rechargeable Aluminum Batteries Research. *ACS Energy Lett.* **2019**, *4* (9), 2124–2129.
- (18) Reed, L. D.; Menke, E. The Roles of V₂O₅ and Stainless Steel in Rechargeable Al-Ion Batteries. *J. Electrochem. Soc.* **2013**, *160* (6), A915–A917.

- (19) Wang, H.; Gu, S.; Bai, Y.; Chen, S.; Zhu, N.; Wu, C.; Wu, F. Anion-Effects on Electrochemical Properties of Ionic Liquid Electrolytes for Rechargeable Aluminum Batteries. *J. Mater. Chem. A* **2015**, *3* (45), 22677–22686.
- (20) Lai, P. K.; Skyllas-Kazacos, M. Electrodeposition of Aluminium in Aluminium Chloride/1-Methyl-3-Ethylimidazolium Chloride. *J. Electroanal. Chem. Interfacial Electrochem.* **1988**, *248* (2), 431–440.
- (21) Carlin, R. T.; Crawford, W.; Bersch, M. Nucleation and Morphology Studies of Aluminum Deposited from an Ambient-Temperature Chloroaluminate Molten Salt. *J. Electrochem. Soc.* **1992**, *139* (10), 2720.
- (22) Hu, J. J.; Long, G. K.; Liu, S.; Li, G. R.; Gao, X. P. A LiFSI–LiTFSI Binary-Salt Electrolyte to Achieve High Capacity and Cycle Stability for a Li–S Battery. *Chem. Commun.* **2014**, *50* (93), 14647–14650.
- (23) Mandai, T.; Johansson, P. Al Conductive Haloaluminate-Free Non-Aqueous Room-Temperature Electrolytes. *J. Mater. Chem. A* **2015**, *3* (23), 12230–12239.
- (24) Reed, L. D.; Arteaga, A.; Menke, E. J. A Combined Experimental and Computational Study of an Aluminum Triflate/Diglyme Electrolyte. *J. Phys. Chem. B* **2015**, *119* (39), 12677–12681.
- (25) Reed, L. D.; Ortiz, S. N.; Xiong, M.; Menke, E. J. A Rechargeable Aluminum-Ion Battery Utilizing a Copper Hexacyanoferrate Cathode in an Organic Electrolyte. *Chem. Commun.* **2015**, *51* (76), 14397–14400.
- (26) Mandai, T.; Johansson, P. Haloaluminate-Free Cationic Aluminum Complexes: Structural Characterization and Physicochemical Properties. *J. Phys. Chem. C* **2016**, *120* (38), 21285–21292.
- (27) Wen, X.; Zhang, J.; Luo, H.; Shi, J.; Tsay, C.; Jiang, H.; Lin, Y.-H.; Schroeder, M. A.; Xu, K.; Guo, J. Synthesis and Electrochemical Properties of Aluminum Hexafluorophosphate. *J. Phys. Chem. Lett.* **2021**, *12*, 5903–5908.
- (28) Slim, Z.; Menke, E. J. Comparing Computational Predictions and Experimental Results for Aluminum Triflate in Tetrahydrofuran. *J. Phys. Chem. B* **2020**, *124* (24), 5002–5008.
- (29) Slim, Z.; Menke, E. J. Aluminum Electrodeposition from Chloride-Rich and Chloride-Free Organic Electrolytes. *J. Phys. Chem. C* **2022**, *126* (5), 2365–2373.
- (30) Tommasi, D. *Traité Des Piles Électriques: Piles Hydro-Électriques Accumulateurs, Piles Thermo-Électriques et Pyro-Électriques*; George Carré, 1889.
- (31) Heise, G. W.; Schumacher, E. A.; Cahoon, N. C. A Heavy Duty Chlorine-Depolarized Cell. *J. Electrochem. Soc.* **1948**, *94* (3), 99.
- (32) Sargent, D. E. Voltaic Cell, May 22, 1951.
- (33) Samuel, R. Primary Cell, May 12, 1953.
- (34) Samuel, R. Primary Cell, February 26, 1957.
- (35) Zaromb, S. The Use and Behavior of Aluminum Anodes in Alkaline Primary Batteries. *J. Electrochem. Soc.* **1962**, *109* (12), 1125.
- (36) Faegh, E.; Shrestha, S.; Zhao, X.; Mustain, W. E. In-Depth Structural Understanding of Zinc Oxide Addition to Alkaline Electrolytes to Protect Aluminum against Corrosion and Gassing. *J. Appl. Electrochem.* **2019**, *49* (9), 895–907.
- (37) Del Duca, B. S. Electrochemical Behavior of the Aluminum Electrode in Molten Salt Electrolytes. *J. Electrochem. Soc.* **1971**, *118* (3), 405.

- (38) Holleck, G. L.; Giner, J. The Aluminum Electrode in AlCl₃-Alkali-Halide Melts. *J. Electrochem. Soc.* **1972**, *119* (9), 1161.
- (39) Holleck, G. L. The Reduction of Chlorine on Carbon in AlCl₃-KCl-NaCl Melts. *J. Electrochem. Soc.* **1972**, *119* (9), 1158.
- (40) Gifford, P. R.; Palmisano, J. B. An Aluminum/Chlorine Rechargeable Cell Employing a Room Temperature Molten Salt Electrolyte. *J. Electrochem. Soc.* **1988**, *135* (3), 650.
- (41) Paranthaman, M. P.; Brown, G.; Sun, X.-G.; Nanda, J.; Manthiram, A.; Manivannan, A. A Transformational, High Energy Density, Secondary Aluminum Ion Battery. In *ECS Meeting Abstracts*; IOP Publishing, 2010; p 314.
- (42) Jayaprakash, N.; Das, S. K.; Archer, L. A. The Rechargeable Aluminum-Ion Battery. *Chem. Commun.* **2011**, *47* (47), 12610–12612.
- (43) Wen, X.; Liu, Y.; Jadhav, A.; Zhang, J.; Borchardt, D.; Shi, J.; Wong, B. M.; Sanyal, B.; Messinger, R. J.; Guo, J. Materials Compatibility in Rechargeable Aluminum Batteries: Chemical and Electrochemical Properties between Vanadium Pentoxide and Chloroaluminate Ionic Liquids. *Chem. Mater.* **2019**, *31* (18), 7238–7247.
- (44) Abood, H. M.; Abbott, A. P.; Ballantyne, A. D.; Ryder, K. S. Do All Ionic Liquids Need Organic Cations? Characterisation of [AlCl₂·n Amide]⁺ AlCl₄⁻ and Comparison with Imidazolium Based Systems. *Chem. Commun.* **2011**, *47* (12), 3523–3525.
- (45) Geng, L.; Lv, G.; Xing, X.; Guo, J. Reversible Electrochemical Intercalation of Aluminum in Mo₆S₈. *Chem. Mater.* **2015**, *27* (14), 4926–4929.
- (46) Lin, M.-C.; Gong, M.; Lu, B.; Wu, Y.; Wang, D.-Y.; Guan, M.; Angell, M.; Chen, C.; Yang, J.; Hwang, B.-J. An Ultrafast Rechargeable Aluminium-Ion Battery. *Nature* **2015**, *520* (7547), 324–328.
- (47) Gao, T.; Li, X.; Wang, X.; Hu, J.; Han, F.; Fan, X.; Suo, L.; Pearse, A. J.; Lee, S. B.; Rubloff, G. W. A Rechargeable Al/S Battery with an Ionic-Liquid Electrolyte. *Angew. Chem.* **2016**, *128* (34), 10052–10055.
- (48) Stadie, N. P.; Wang, S.; Kravchyk, K. V.; Kovalenko, M. V. Zeolite-Templated Carbon as an Ordered Microporous Electrode for Aluminum Batteries. *ACS Nano* **2017**, *11* (2), 1911–1919.
- (49) Elia, G. A.; Hasa, I.; Greco, G.; Diemant, T.; Marquardt, K.; Hoepfner, K.; Behm, R. J.; Hoell, A.; Passerini, S.; Hahn, R. Insights into the Reversibility of Aluminum Graphite Batteries. *J. Mater. Chem. A* **2017**, *5* (20), 9682–9690.
- (50) Kravchyk, K. V.; Wang, S.; Piveteau, L.; Kovalenko, M. V. Efficient Aluminum Chloride–Natural Graphite Battery. *Chem. Mater.* **2017**, *29* (10), 4484–4492.
- (51) Tian, H.; Zhang, S.; Meng, Z.; He, W.; Han, W.-Q. Rechargeable Aluminum/Iodine Battery Redox Chemistry in Ionic Liquid Electrolyte. *ACS Energy Lett.* **2017**, *2* (5), 1170–1176.
- (52) Walter, M.; Kravchyk, K. V.; Böfer, C.; Widmer, R.; Kovalenko, M. V. Polypyrenes as High-Performance Cathode Materials for Aluminum Batteries. *Adv. Mater.* **2018**, *30* (15), 1705644.
- (53) Wang, S.; Kravchyk, K. V.; Filippin, A. N.; Müller, U.; Tiwari, A. N.; Buecheler, S.; Bodnarchuk, M. I.; Kovalenko, M. V. Aluminum Chloride-Graphite Batteries with Flexible Current Collectors Prepared from Earth-Abundant Elements. *Adv. Sci.* **2018**, *5* (4), 1700712.

- (54) Muñoz-Torrero, D.; Leung, P.; García-Quismondo, E.; Ventosa, E.; Anderson, M.; Palma, J.; Marcilla, R. Investigation of Different Anode Materials for Aluminium Rechargeable Batteries. *J. Power Sources* **2018**, *374*, 77–83.
- (55) Chen, H.; Xu, H.; Wang, S.; Huang, T.; Xi, J.; Cai, S.; Guo, F.; Xu, Z.; Gao, W.; Gao, C. Ultrafast All-Climate Aluminum-Graphene Battery with Quarter-Million Cycle Life. *Sci. Adv.* **2017**, *3* (12), eaao7233.
- (56) Yang, C.; Wang, S.; Zhang, X.; Zhang, Q.; Ma, W.; Yu, S.; Sun, G. Substituent Effect of Imidazolium Ionic Liquid: A Potential Strategy for High Coulombic Efficiency Al Battery. *J. Phys. Chem. C* **2019**, *123* (18), 11522–11528.
- (57) Kim, D. J.; Yoo, D.-J.; Otley, M. T.; Prokofjevs, A.; Pezzato, C.; Owczarek, M.; Lee, S. J.; Choi, J. W.; Stoddart, J. F. Rechargeable Aluminium Organic Batteries. *Nat. Energy* **2019**, *4* (1), 51–59.
- (58) Zhou, Q.; Wang, D.; Lian, Y.; Hou, S.; Ban, C.; Wang, Z.; Zhao, J.; Zhang, H. Rechargeable Aluminum-Ion Battery with Sheet-like MoSe₂@ C Nanocomposites Cathode. *Electrochimica Acta* **2020**, *354*, 136677.
- (59) Zhao, Q.; Zheng, J.; Deng, Y.; Archer, L. Regulating the Growth of Aluminum Electrodeposits: Towards Anode-Free Al Batteries. *J. Mater. Chem. A* **2020**, *8* (44), 23231–23238.
- (60) Xue, L.; Xin, S.; Goodenough, J. B.; Angell, C. A. An Inverse Aluminum Battery: Putting the Aluminum as the Cathode. *ACS Energy Lett.* **2017**, *2* (7), 1534–1538.
- (61) Chen, C.-Y.; Tsuda, T.; Kuwabata, S.; Hussey, C. L. Rechargeable Aluminum Batteries Utilizing a Chloroaluminate Inorganic Ionic Liquid Electrolyte. *Chem. Commun.* **2018**, *54* (33), 4164–4167.
- (62) Wang, J.; Zhang, X.; Chu, W.; Liu, S.; Yu, H. A Sub-100° C Aluminum Ion Battery Based on a Ternary Inorganic Molten Salt. *Chem. Commun.* **2019**, *55* (15), 2138–2141.
- (63) Tu, J.; Wang, J.; Zhu, H.; Jiao, S. The Molten Chlorides for Aluminum-Graphite Rechargeable Batteries. *J. Alloys Compd.* **2020**, *821*, 153285.
- (64) Wang, K.; Liu, K.; Yang, C.; Chen, Z.; Zhang, H.; Wu, Y.; Long, Y.; Jin, Y.; He, X.; Wu, H. A High-Performance Intermediate-Temperature Aluminum-Ion Battery Based on Molten Salt Electrolyte. *Energy Storage Mater.* **2022**.
- (65) Tsuda, T.; Sasaki, J.; Uemura, Y.; Kojima, T.; Senoh, H.; Kuwabata, S. Aluminum Metal Anode Rechargeable Batteries with Sulfur–Carbon Composite Cathodes and Inorganic Chloroaluminate Ionic Liquid. *Chem. Commun.* **2022**.
- (66) Angell, M.; Pan, C.-J.; Rong, Y.; Yuan, C.; Lin, M.-C.; Hwang, B.-J.; Dai, H. High Coulombic Efficiency Aluminum-Ion Battery Using an AlCl₃-Urea Ionic Liquid Analog Electrolyte. *Proc. Natl. Acad. Sci.* **2017**, *114* (5), 834–839.
- (67) Jiao, H.; Wang, C.; Tu, J.; Tian, D.; Jiao, S. A Rechargeable Al-Ion Battery: Al/Molten AlCl₃-Urea/Graphite. *Chem. Commun.* **2017**, *53* (15), 2331–2334.
- (68) Li, J.; Tu, J.; Jiao, H.; Wang, C.; Jiao, S. Ternary AlCl₃-Urea-[EMIm] Cl Ionic Liquid Electrolyte for Rechargeable Aluminum-Ion Batteries. *J. Electrochem. Soc.* **2017**, *164* (13), A3093.
- (69) Wang, C.; Li, J.; Jiao, H.; Tu, J.; Jiao, S. The Electrochemical Behavior of an Aluminum Alloy Anode for Rechargeable Al-Ion Batteries Using an AlCl₃-Urea Liquid Electrolyte. *Rsc Adv.* **2017**, *7* (51), 32288–32293.

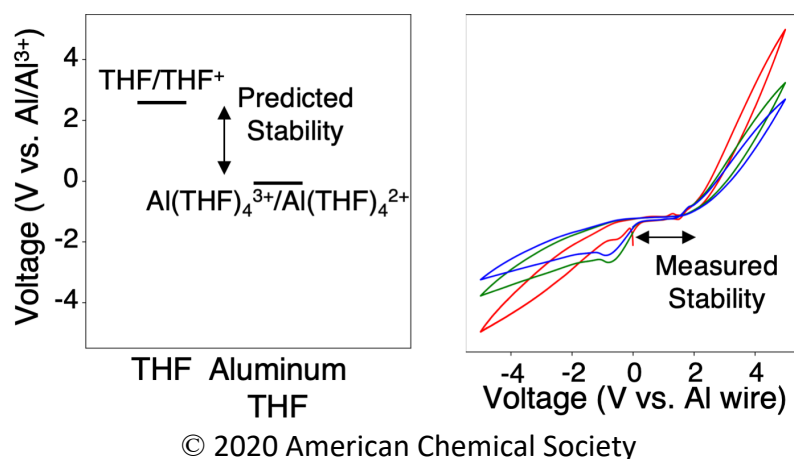
- (70) Bian, Y.; Li, Y.; Yu, Z.; Chen, H.; Du, K.; Qiu, C.; Zhang, G.; Lv, Z.; Lin, M.-C. Using an AlCl₃/Urea Ionic Liquid Analog Electrolyte for Improving the Lifetime of Aluminum-Sulfur Batteries. *ChemElectroChem* **2018**, *5* (23), 3607–3611.
- (71) Ng, K. L.; Malik, M.; Buch, E.; Glossmann, T.; Hintennach, A.; Azimi, G. A Low-Cost Rechargeable Aluminum/Natural Graphite Battery Utilizing Urea-Based Ionic Liquid Analog. *Electrochimica Acta* **2019**, *327*, 135031.
- (72) Angell, M.; Zhu, G.; Lin, M.-C.; Rong, Y.; Dai, H. Ionic Liquid Analogs of AlCl₃ with Urea Derivatives as Electrolytes for Aluminum Batteries. *Adv. Funct. Mater.* **2020**, *30* (4), 1901928.
- (73) Kao, Y.-T.; Patil, S. B.; An, C.-Y.; Huang, S.-K.; Lin, J.-C.; Lee, T.-S.; Lee, Y.-C.; Chou, H.-L.; Chen, C.-W.; Chang, Y. J. A Quinone-Based Electrode for High-Performance Rechargeable Aluminum-Ion Batteries with a Low-Cost AlCl₃/Urea Ionic Liquid Electrolyte. *ACS Appl. Mater. Interfaces* **2020**, *12* (23), 25853–25860.
- (74) Wu, F.; Yang, H.; Bai, Y.; Wu, C. Paving the Path toward Reliable Cathode Materials for Aluminum-Ion Batteries. *Adv. Mater.* **2019**, *31* (16), 1806510.
- (75) Plechkova, N. V.; Seddon, K. R. Applications of Ionic Liquids in the Chemical Industry. *Chem. Soc. Rev.* **2008**, *37* (1), 123–150.
- (76) Pena-Pereira, F.; Namieśnik, J. Ionic Liquids and Deep Eutectic Mixtures: Sustainable Solvents for Extraction Processes. *ChemSusChem* **2014**, *7* (7), 1784–1800.
- (77) Zhao, Y.; VanderNoot, T. J. Electrodeposition of Aluminium from Nonaqueous Organic Electrolytic Systems and Room Temperature Molten Salts. *Electrochimica Acta* **1997**, *42* (1), 3–13.
- (78) Hurley, F. H.; Wier, T. P. The Electrodeposition of Aluminum from Nonaqueous Solutions at Room Temperature. *J. Electrochem. Soc.* **1951**, *98* (5), 207.
- (79) Gale, R. J.; Gilbert, B.; Osteryoung, R. A. Raman Spectra of Molten Aluminum Chloride: 1-Butylpyridinium Chloride Systems at Ambient Temperatures. *Inorg. Chem.* **1978**, *17* (10), 2728–2729.
- (80) Carlin, R. T.; Osteryoung, R. A. Aluminum Anodization in a Basic Ambient Temperature Molten Salt. *J. Electrochem. Soc.* **1989**, *136* (5), 1409.
- (81) Oh, Y.; Lee, G.; Tak, Y. Stability of Metallic Current Collectors in Acidic Ionic Liquid for Rechargeable Aluminum-Ion Batteries. *ChemElectroChem* **2018**, *5* (22), 3348–3352.
- (82) Couch, D. E.; Brenner, A. A Hydride Bath for the Electrodeposition of Aluminum. *J. Electrochem. Soc.* **1952**, *99* (6), 234.
- (83) Hisano, T.; Terazawa, T.; Takeuchi, I.; Inohara, S.; Ikeda, H. The Electrodeposition of Aluminum from a Solution of Aluminum Bromide in N, N-Dimethyl Aniline. *Bull. Chem. Soc. Jpn.* **1971**, *44* (3), 599–603.
- (84) Capuano, G. A.; Davenport, W. G. Electrodeposition of Aluminum from Alkyl Benzene Electrolytes. *J. Electrochem. Soc.* **1971**, *118* (10), 1688.
- (85) Ishibashi, N.; Yoshio, M. Electrodeposition of Aluminium from the NBS Type Bath Using Tetrahydrofuran—Benzene Mixed Solvent. *Electrochimica Acta* **1972**, *17* (8), 1343–1352.
- (86) Yoshio, M.; Ishibashi, N. High-Rate Plating of Aluminium from the Bath Containing Aluminium Chloride and Lithium Aluminium Hydride in Tetrahydrofuran. *J. Appl. Electrochem.* **1973**, *3* (4), 321–325.

- (87) Peled, E.; Gileadi, E. The Electrodeposition of Aluminum from Aromatic Hydrocarbon: I. Composition of Baths and the Effect of Additives. *J. Electrochem. Soc.* **1976**, *123* (1), 15.
- (88) Galová, M. Conductometric Study of the Composition of Aluminum Chloride-Lithium Aluminum Hydride $\text{AlCl}_3\text{—LiAlH}_4$ Electrolyte in Tetrahydrofuran. *Chem. Pap.* **1982**, *36* (6), 791–797.
- (89) Graef, M. W. M. The Mechanism of Aluminum Electrodeposition from Solutions of AlCl_3 and LiAlH_4 in THF. *J. Electrochem. Soc.* **1985**, *132* (5), 1038.
- (90) Badawy, W. A.; Sabrah, B. A.; Hilal, N. H. Y. A New Bath for the Electrodeposition of Aluminium. II. Kinetics and Mechanism of the Deposition and Dissolution Processes. *J. Appl. Electrochem.* **1987**, *17* (2), 357–369.
- (91) Legrand, L.; Tranchant, A.; Messina, R. Behaviour of Aluminium as Anode in Dimethylsulfone-Based Electrolytes. *Electrochimica Acta* **1994**, *39* (10), 1427–1431.
- (92) Legrand, L.; Tranchant, A.; Messina, R. Electrodeposition Studies of Aluminum on Tungsten Electrode from DMSO 2 Electrolytes: Determination of AlIII Species Diffusion Coefficients. *J. Electrochem. Soc.* **1994**, *141* (2), 378.
- (93) Legrand, L.; Heintz, M.; Tranchant, A.; Messina, R. Sulfone-Based Electrolytes for Aluminum Electrodeposition. *Electrochimica Acta* **1995**, *40* (11), 1711–1716.
- (94) Legrand, L.; Tranchant, A.; Messina, R. Aluminium Behaviour and Stability in $\text{AlCl}_3\text{DMSO}_2$ Electrolyte. *Electrochimica Acta* **1996**, *41* (17), 2715–2720.
- (95) Lefebvre, M. C.; Conway, B. E. ^{27}Al NMR Spectroscopy Studies on Speciation of Al Complex Ions in $\text{AlCl}_3 + \text{LiAlH}_4$ Solutions in Tetrahydrofuran for Electroplating of Al. *J. Electroanal. Chem.* **1998**, *448* (2), 217–227.
- (96) Lefebvre, M. C.; Conway, B. E. Nucleation and Morphologies in the Process of Electrocrystallization of Aluminium on Smooth Gold and Glassy-Carbon Substrates. *J. Electroanal. Chem.* **2000**, *480* (1–2), 46–58.
- (97) Lefebvre, M. C.; Conway, B. E. Elementary Steps and Mechanism of Electrodeposition of Al from Complex Hydride Ions in Tetrahydrofuran Baths. *J. Electroanal. Chem.* **2000**, *480* (1–2), 34–45.
- (98) Kitada, A.; Nakamura, K.; Fukami, K.; Murase, K. AlCl_3 -Dissolved Diglyme as Electrolyte for Room-Temperature Aluminum Electrodeposition. *Electrochemistry* **2014**, *82* (11), 946–948.
- (99) Nakayama, Y.; Senda, Y.; Kawasaki, H.; Koshitani, N.; Hosoi, S.; Kudo, Y.; Morioka, H.; Nagamine, M. Sulfone-Based Electrolytes for Aluminium Rechargeable Batteries. *Phys. Chem. Chem. Phys.* **2015**, *17* (8), 5758–5766.
- (100) Miyake, M.; Fujii, H.; Hirato, T. Electroplating of Al on Mg Alloy in a Dimethyl Sulfone–Aluminum Chloride Bath. *Surf. Coat. Technol.* **2015**, *277*, 160–164.
- (101) Chiku, M.; Matsumura, S.; Takeda, H.; Higuchi, E.; Inoue, H. Aluminum Bis (Trifluoromethanesulfonyl) Imide as a Chloride-Free Electrolyte for Rechargeable Aluminum Batteries. *J. Electrochem. Soc.* **2017**, *164* (9), A1841.
- (102) Kitada, A.; Kato, Y.; Fukami, K.; Murase, K. Room Temperature Electrodeposition of Flat and Smooth Aluminum Layers from An AlCl_3 /Diglyme Bath. *J. Surf. Finish. Soc. Jpn.* **2018**, *69* (7), 310–311.

- (103) Zhang, B.; Shi, Z.; Shen, L.; Liu, A.; Xu, J.; Hu, X. Electrodeposition of Al, Al-Li Alloy, and Li from an Al-Containing Solvate Ionic Liquid under Ambient Conditions. *J. Electrochem. Soc.* **2018**, *165* (9), D321.
- (104) Yitzhack, N.; Tereschuk, P.; Sezin, N.; Starosvetsky, D.; Natan, A.; Ein-Eli, Y. Aluminum Electrodeposition from a Non-Aqueous Electrolyte—a Combined Computational and Experimental Study. *J. Solid State Electrochem.* **2020**, *24*, 2833–2846.
- (105) Zhang, Z.; Kitada, A.; Gao, S.; Fukami, K.; Tsuji, N.; Yao, Z.; Murase, K. A Concentrated AlCl₃–Diglyme Electrolyte for Hard and Corrosion-Resistant Aluminum Electrodeposits. *ACS Appl. Mater. Interfaces* **2020**, *12* (38), 43289–43298.
- (106) Wen, X.; Liu, Y.; Xu, D.; Zhao, Y.; Lake, R. K.; Guo, J. Room-Temperature Electrodeposition of Aluminum via Manipulating Coordination Structure in AlCl₃ Solutions. *J. Phys. Chem. Lett.* **2020**, *11* (4), 1589–1593.
- (107) Peters, W.; Duong, H. T.; Lee, S.; Drillet, J.-F. Investigation of Al (TfO) 3-Based Deep Eutectic Solvent Electrolytes for Aluminium-Ion Batteries. Part I: Understanding the Positively Charged Al Complex Formation. *Phys. Chem. Chem. Phys.* **2021**, *23* (38), 21923–21933.
- (108) Brenner, A. Electrolysis of Organic Solvents with Reference to the Electrodeposition of Metals. *J. Electrochem. Soc.* **1959**, *106* (2), 148.
- (109) Connor, J. H.; Brenner, A. Electrodeposition of Metals from Organic Solutions: II. Further Studies on the Electrodeposition of Aluminum from a Hydride Bath. *J. Electrochem. Soc.* **1956**, *103* (12), 657.
- (110) Finholt, A. E.; Bond Jr, A. C.; Schlesinger, H. I. Lithium Aluminum Hydride, Aluminum Hydride and Lithium Gallium Hydride, and Some of Their Applications in Organic and Inorganic Chemistry. *J. Am. Chem. Soc.* **1947**, *69* (5), 1199–1203.
- (111) Daenen, T. E. G. Cyclic Reaction Mechanism in the Electrodeposition of Aluminium. *Nature* **1979**, *280* (5721), 378–380.
- (112) Kitada, A.; Nakamura, K.; Fukami, K.; Murase, K. Electrochemically Active Species in Aluminum Electrodeposition Baths of AlCl₃/Glyme Solutions. *Electrochimica Acta* **2016**, *211*, 561–567.
- (113) Legrand, L.; Tranchant, A.; Messina, R.; Romain, F.; Lautie, A. Raman Study of Aluminum Chloride- Dimethylsulfone Solutions. *Inorg. Chem.* **1996**, *35* (5), 1310–1312.
- (114) Howells, R. D.; Mc Cown, J. D. Trifluoromethanesulfonic Acid and Derivatives. *Chem. Rev.* **1977**, *77* (1), 69–92.
- (115) Yang, H.; Zhuang, G. V.; Ross Jr, P. N. Thermal Stability of LiPF₆ Salt and Li-Ion Battery Electrolytes Containing LiPF₆. *J. Power Sources* **2006**, *161* (1), 573–579.
- (116) Younesi, R.; Veith, G. M.; Johansson, P.; Edström, K.; Vegge, T. Lithium Salts for Advanced Lithium Batteries: Li–Metal, Li–O₂, and Li–S. *Energy Environ. Sci.* **2015**, *8* (7), 1905–1922.
- (117) Ha, S.-Y.; Lee, Y.-W.; Woo, S. W.; Koo, B.; Kim, J.-S.; Cho, J.; Lee, K. T.; Choi, N.-S. Magnesium (II) Bis (Trifluoromethane Sulfonyl) Imide-Based Electrolytes with Wide Electrochemical Windows for Rechargeable Magnesium Batteries. *ACS Appl. Mater. Interfaces* **2014**, *6* (6), 4063–4073.
- (118) Keyzer, E. N.; Glass, H. F.; Liu, Z.; Bayley, P. M.; Dutton, S. E.; Grey, C. P.; Wright, D. S. Mg (PF₆) 2-Based Electrolyte Systems: Understanding Electrolyte–Electrode

- Interactions for the Development of Mg-Ion Batteries. *J. Am. Chem. Soc.* **2016**, *138* (28), 8682–8685.
- (119) Manthiram, A. A Reflection on Lithium-Ion Battery Cathode Chemistry. *Nat. Commun.* **2020**, *11* (1), 1–9.
- (120) Mckerracher, R. D.; Holland, A.; Cruden, A.; Wills, R. G. A. Comparison of Carbon Materials as Cathodes for the Aluminium-Ion Battery. *Carbon* **2019**, *144*, 333–341.
- (121) Greco, G.; Tatchev, D.; Hoell, A.; Krumrey, M.; Raoux, S.; Hahn, R.; Elia, G. A. Influence of the Electrode Nano/Microstructure on the Electrochemical Properties of Graphite in Aluminum Batteries. *J. Mater. Chem. A* **2018**, *6* (45), 22673–22680.
- (122) Wang, H.; Bai, Y.; Chen, S.; Luo, X.; Wu, C.; Wu, F.; Lu, J.; Amine, K. Binder-Free V₂O₅ Cathode for Greener Rechargeable Aluminum Battery. *ACS Appl. Mater. Interfaces* **2015**, *7* (1), 80–84.
- (123) Lee, B.; Lee, H. R.; Yim, T.; Kim, J. H.; Lee, J. G.; Chung, K. Y.; Cho, B. W.; Oh, S. H. Investigation on the Structural Evolutions during the Insertion of Aluminum Ions into Mo₆S₈ Chevrel Phase. *J. Electrochem. Soc.* **2016**, *163* (6), A1070.
- (124) Tong, Y.; Gao, A.; Zhang, Q.; Gao, T.; Yue, J.; Meng, F.; Gong, Y.; Xi, S.; Lin, Z.; Mao, M. Cation-Synergy Stabilizing Anion Redox of Chevrel Phase Mo₆S₈ in Aluminum Ion Battery. *Energy Storage Mater.* **2021**, *37*, 87–93.
- (125) Wang, S.; Jiao, S.; Wang, J.; Chen, H.-S.; Tian, D.; Lei, H.; Fang, D.-N. High-Performance Aluminum-Ion Battery with CuS@C Microsphere Composite Cathode. *ACS Nano* **2017**, *11* (1), 469–477.
- (126) Mori, T.; Orikasa, Y.; Nakanishi, K.; Kezheng, C.; Hattori, M.; Ohta, T.; Uchimoto, Y. Discharge/Charge Reaction Mechanisms of FeS₂ Cathode Material for Aluminum Rechargeable Batteries at 55° C. *J. Power Sources* **2016**, *313*, 9–14.
- (127) Wang, S.; Yu, Z.; Tu, J.; Wang, J.; Tian, D.; Liu, Y.; Jiao, S. A Novel Aluminum-Ion Battery: Al/AlCl₃-[EMIm] Cl/Ni₃S₂@ Graphene. *Adv. Energy Mater.* **2016**, *6* (13), 1600137.
- (128) Donahue, F. M.; Mancini, S. E.; Simonsen, L. Secondary Aluminium-Iron (III) Chloride Batteries with a Low Temperature Molten Salt Electrolyte. *J. Appl. Electrochem.* **1992**, *22* (3), 230–234.
- (129) Suto, K.; Nakata, A.; Murayama, H.; Hirai, T.; Yamaki, J.; Ogumi, Z. Electrochemical Properties of Al/Vanadium Chloride Batteries with AlCl₃-1-Ethyl-3-Methylimidazolium Chloride Electrolyte. *J. Electrochem. Soc.* **2016**, *163* (5), A742.
- (130) Nakaya, K.; Nakata, A.; Hirai, T.; Ogumi, Z. Oxidation of Nickel in AlCl₃-1-Butylpyridinium Chloride at Ambient Temperature. *J. Electrochem. Soc.* **2014**, *162* (1), D42.

Chapter 2: Comparing Computational Predictions and Experimental Results for Aluminum Triflate in Tetrahydrofuran



2.1 Introduction

A green and energy sustainable society can be achieved through the development of non-fossil fuel energy storage devices. Finding reliable, post-lithium secondary battery chemistries is a major challenge in terms of energy conversion and storage.¹ Lithium ion batteries have dominated the mobile electronics market ever since they were made commercially available by Sony in the early 1990's. However, The limited availability of lithium (Li), the primary component in Li-ion batteries, and its uneven distribution in the earth's crust, raises concerns about its ability to meet the future energy needs.² As a result, aluminum ion batteries have been proposed as a promising candidate capable of replacing the state of the art lithium ion batteries.^{3,4} Significant efforts for the development of cathode materials and electrolytes for aluminum ion batteries have been motivated by the abundance, low cost (~1.4 USD/Kg), high theoretical volumetric charge density (8042 mAh/ml), and the trivalent nature of aluminum.^{5,6}

To take advantage of these attributes of aluminum, it is necessary to have an electrolyte that enables aluminum electrodeposition. The most widely explored electrolytes for Al-ion batteries are room temperature ionic liquids. Notable examples of such systems are mixtures of AlCl_3 and 1-ethyl-3-methylimidazolium chloride [EMIM]Cl or 1-butyl-3-methylimidazolium chloride [BMIM]Cl.⁶ In these electrolytes, reversible electrochemical behavior (deposition/stripping) of aluminum has only been associated with acidic electrolytes where the dominating species are Al_2Cl_7^- rather than AlCl_4^- .^{7,8} Unfortunately, these electrolytes exhibit high reactivity and corrosivity towards cathode materials, limiting their usefulness in practical devices.^{9,10}

Considering non-ionic liquid electrolytes, ethers have shown promise as possible organic solvents for non-aqueous electrolyte systems due to their strong Lewis basicity and high donor numbers. Ever since Couch and Brenner revealed the possibility of electrodepositing metallic aluminum from a hydride bath that consisted of a mixture of AlCl_3 and LiAlH_4 in 1952,¹¹ there has been considerable efforts to electrodeposit aluminum from organic solvents.^{12,13,14} In addition, significant ionic conductivities of such systems have been reported making ethereal electrolytes an important candidate for aluminum ion batteries.^{15,16,17}

The present study builds on this and investigates the experimental and DFT-derived physicochemical properties of aluminum trifluoromethanesulfonate (Al-triflate) in tetrahydrofuran (THF). Electrochemical activity of aluminum ions was revealed by cyclic voltammetry measurements on glassy carbon and gold working electrodes at various concentrations and compared to the redox properties predicted by DFT. Spectroscopic measurements in agreement with computational predictions suggest the presence of a concentration dependent behavior for the triflate/Al-complex with the presence of Al-triflate bond in the most concentrated solutions. Furthermore, electrochemical impedance spectroscopy measurements demonstrate the room temperature ionic conductivity profile as a function of molar concentrations, where an increase in ionic conductivity is observed up to the point of saturation.

2.2 Materials and Methods

2.2.1 Density functional theory calculations

All calculations were done using the Gaussian 09 suite of electronic structure program.¹⁸ The B3PW91 density functional was employed using the unrestricted spin-formalism for all open-shell cases along with the 6-311+G(d) basis set.^{19,20} Geometry optimizations were carried out using standard methods and all nature of the stationery points on the potential energy surfaces were confirmed using second-derivative calculations.²¹ A solvation model density (SMD) continuum solvation model was used to evaluate the solvation free energies based on the self-consistent reaction field (SCRF) approach and THF was used for all SMD calculations.²² In all cases, the stability of the SCF solution was verified.^{23,24}

2.2.2 Experimental details

Aluminum triflate and THF were purchased from Sigma-Aldrich. The aluminum triflate was used without further purification, while the THF was purified in a commercial purification system and transferred to a glove box under argon. All chemical preparations and electrochemical measurements were carried out in an argon-filled VAC glovebox with water and oxygen levels held below 1.5 ppm and 0.5 ppm respectively, and water content in the electrolytes was measured by Karl Fischer titration to be between 30 and 60 ppm. The solutions described below were prepared by dissolving appropriate amounts of Al-Triflate in THF. Complete dissolution was achieved by stirring overnight.

Cyclic voltammetry measurements were performed using a Gamry potentiostat. The electrochemical cells for cyclic voltammetry measurements consisted of either a gold or carbon working electrode, an aluminum wire counter electrode and an aluminum wire pseudoreference electrode set up in a standard three electrode cell configuration. A scan rate of 10 mV/s was used.

Ionic conductivity measurements were performed using a ParStat 2273 by means of electrochemical impedance spectroscopy. A 10 mV ac signal with a 0V dc offset was used over a 0.1-4 kHz frequency range. The impedance cell was prepared in the lab and consisted of two platinum wires encased in flint glass tubing that was polished with 0.3 μm alumina. The cell was calibrated using a 0.01M KCl standard solution at 20 °C.

FTIR spectra were measured using Vertex 70 spectrometer using a KBr window and 64 scans. Resolutions of 4 cm^{-1} were used for concentrated solutions and 1 cm^{-1} for the most dilute. The spectra were normalized and smoothed using Spectragryph software.²⁵

2.3 Results and Discussion

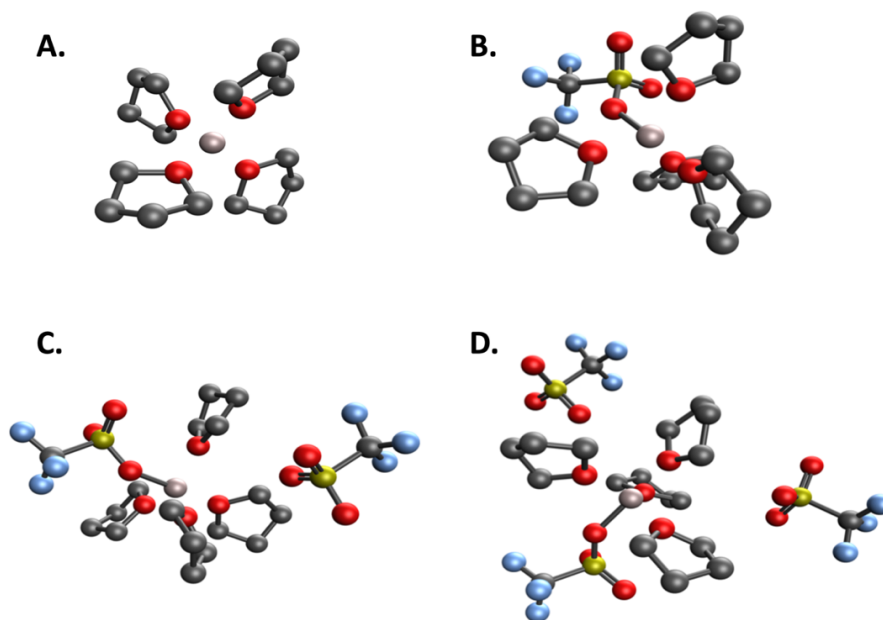


Figure 2.1 Optimized structures (hydrogens not shown) of (A) $\text{Al}(\text{THF})_4^{3+}$, (B) $[\text{Al}(\text{THF})_4(\text{Triflate})]^{2+}$, (C) $[\text{Al}(\text{THF})_4(\text{Triflate})][\text{Triflate}]^+$, and (D) $[\text{Al}(\text{THF})_4(\text{Triflate})][\text{Triflate}]_2$. Pink: Al, black: carbon, red: oxygen, blue: fluorine, gold: sulfur. © 2020 American Chemical Society.

2.3.1 Coordination structures

DFT calculations were performed to determine the coordination structures of solvent-phase Al^{3+} -THF complexes. The theoretical Gibbs free energy of the reactions resulting in an Al^{3+} cation coordinated by 3, 4 and 5 THF molecules has been evaluated.



While the reactions producing $\text{Al}(\text{THF})_4^{3+}$ and $\text{Al}(\text{THF})_5^{3+}$ were shown to be the most thermodynamically favorable with a calculated solvent phase Gibbs free energy of -1700 kJ/mol, we expect the $\text{Al}(\text{THF})_4^{3+}$ complex to be the more important due to the entropic factors, which the calculations do not account for, and so we have focused our computational efforts on this $\text{Al}(\text{THF})_4^{3+}$ complex.

To evaluate the effect imposed by triflate anions on the geometry and the spectroscopic features of the $\text{Al}(\text{THF})_4^{3+}$, we performed DFT calculation on $\text{Al}(\text{THF})_4^{3+}$ with a different number of coordinating anions.

The optimized geometries of complexes are shown in figure 2.1. DFT calculations indicate that all the geometries revealed in figure 2.1A-D are stable. As evident by the Al-core geometries revealed in figure 2.1B-D, contact ion pairing between $\text{Al}(\text{THF})_4^{3+}$ and triflate anion is present. Based on these results, ion-pairing in the Al-triflate/THF electrolytes can be divided into two classes; one where the triflate anion is bound to the $\text{Al}(\text{THF})_4^{3+}$ complex, and another where the triflate anion is directly bound to the Al^{3+} core. Interestingly, among all the optimized geometries, only one triflate was directly bound to the aluminum cation as a result of steric effects. The bond occurring between the Al-core and the oxygen atom of the triflate anion demonstrated in the optimized geometries in figure 2.1B-D has a length of 1.8Å. Consequently, the presence of Al-triflate bond in these electrolytes and the distinct ionic environments of the triflate anions allow for a detailed discussion of the anion dependent physicochemical properties as will be seen later on.

2.3.2 Determination of ionic association between aluminum and triflate in THF using infrared spectroscopy

Table 2.1 Measured and computed vibrational frequencies (cm^{-1}) of CF_3 symmetric deformation, SO_3 symmetric and antisymmetric stretching modes. © 2020 American Chemical Society.

Species Mode	Free triflate		Contact ion pair		Bound triflate	
	Computed	Measured	Computed	Measured	Computed	Measured
CF_3 symmetric deformation	746.63	-	750.44	757-764	767.30	766-767
SO_3 symmetric stretch	989.60	1027-1032	989.88	1070	-	-
SO_3 antisymmetric stretch	1222.44 1222.88	-	1238.28	1236-1246	1319.50	1307-1308

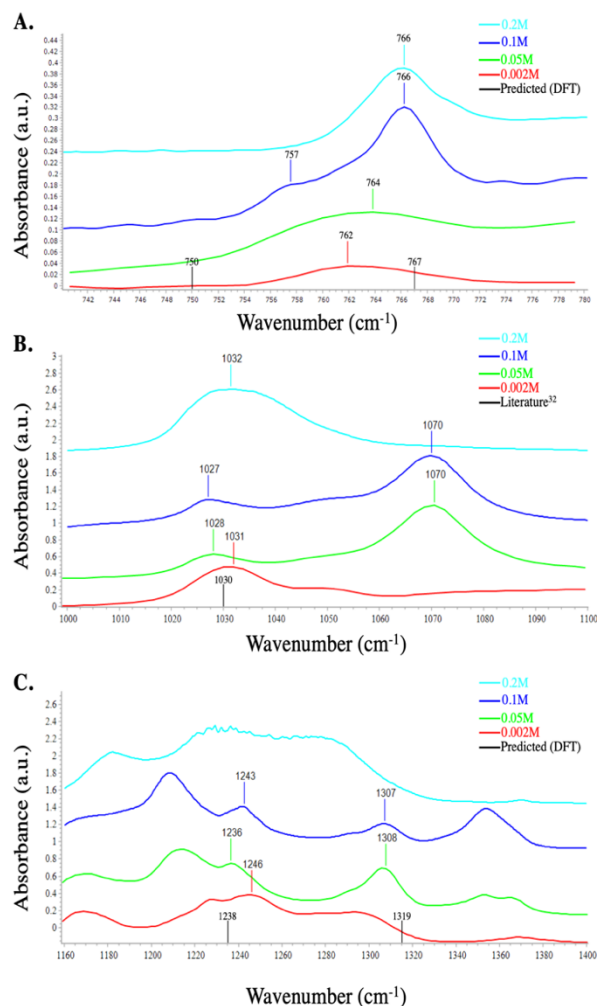


Figure 2.2 FTIR spectra of Al-triflate/THF solutions showing (A) CF₃ symmetric deformation region, (B) SO₃ symmetric stretch region and (C) SO₃ antisymmetric stretch region. © 2020 American Chemical Society.

In the course of establishing a conductive environment capable of transporting Al³⁺ ions, ionic association is a key factor to be considered. In order to understand ionic association and complex ion formation, infrared spectra was collected on solutions with varying concentrations of aluminum triflate, and compared with DFT calculations on free triflate and Al(THF)₄³⁺ complexes. The results of these measurements and calculations are summarized in table 2.1. Well known characteristic IR-bands for electrolytes comprising of triflate anions have been extensively studied by Frech and Huang.²⁶⁻³¹ Bands observed within 750-775 cm⁻¹ region of the IR-spectra correspond to vibrational frequencies of the C-S stretch coupled with a C-F bending mode of the triflate anion, also known as the CF₃ symmetric deformation mode, $\delta_s(\text{CF}_3)$.²⁷

Figure 2.2A reveals the absorption bands of the $\delta_s(\text{CF}_3)$ for four different concentrations. Spectral characterization reveals two distinct regimes for the behavior of triflate anions. The lower intensity bands observed at 762, 764, and the shoulder peak at 757 cm^{-1} are attributed to complex-bound triflates. Similarly, higher intensity peaks observed at 766 cm^{-1} in the most concentrated solutions, i.e. 0.1 and 0.2M, correspond to $\delta_s(\text{CF}_3)$ mode of Al-bound triflate anions.

These results are well represented by the predicted IR-Spectra obtained through DFT calculations on the $[\text{Al}(\text{THF})_4(\text{Triflate})][\text{Triflate}]_1^+$ and $[\text{Al}(\text{THF})_4(\text{Triflate})][\text{Triflate}]_2^-$, both complexes exhibit vibrational frequencies around 752 and 767 cm^{-1} corresponding to the $\delta_s(\text{CF}_3)$ vibrational mode of the complex-bound and the Al-bound triflates respectively. Qualitatively similar frequencies were reported by Reed and others,¹⁵ for the $\delta_s(\text{CF}_3)$ vibrational frequencies of triflate anions in solutions comprising of Al-triflate in 2-methoxyethyl ether, with the exception of free triflate at 751 cm^{-1} corresponding to the CF_3 vibrational frequency of free triflate. This peak was absent in all the IR measurements of the Al-trif/THF solutions reported in this study, suggesting that the $\text{Al}(\text{THF})_4^{3+}$ complex is more readily accessible to the triflate anion than the aluminum-diglyme complex previously reported. In the interest of comparison, the vibrational frequencies of a free triflate anion in THF was also acquired through DFT calculations, revealing a CF_3 vibrational frequency of 747 cm^{-1} . The shift in frequency upon complexation of the triflate anion with the $\text{Al}(\text{THF})_4^{3+}$ complex arises from the charge redistribution on the triflate anion due to the perturbation of the charge density of the triflate molecules by the highly charged Al-cation.^{15,26} Additionally, the origin of the changes in the frequencies were traced by comparing the C-S and S-O bond lengths of free triflate to that of complex and Al-bound triflate, which decrease as the triflate anions are positioned in closer proximity to the Al-core, altering the internal force constants of various constituents that contribute to the $\delta_s(\text{CF}_3)$ mode.

Moreover, as noted earlier, vibrational frequencies corresponding to the CF_3 symmetric deformation mode were absent within the region of $750\text{-}775\text{ cm}^{-1}$. However, it is important to note that this does not necessarily indicate the absence of free triflate anions in these solutions. As shown in the spectral profile revealed by figure 2.2B, the band observed around 1027 cm^{-1} can be assigned to the non-degenerate symmetric stretch of the SO_3 for free triflates, $\nu_s\text{SO}_3$.³² This observation can be supported by the fact that the band positions seems to be relatively unaffected by the changes in concentration. Similar band positions have been observed for monovalent,^{26,33} divalent,³² and lanthanide-based systems.³⁴ The higher frequency band centered around 1070 cm^{-1} in the 0.05 and 0.1 M solutions can be attributed to contact ion pairs and/or ion aggregates.³⁴

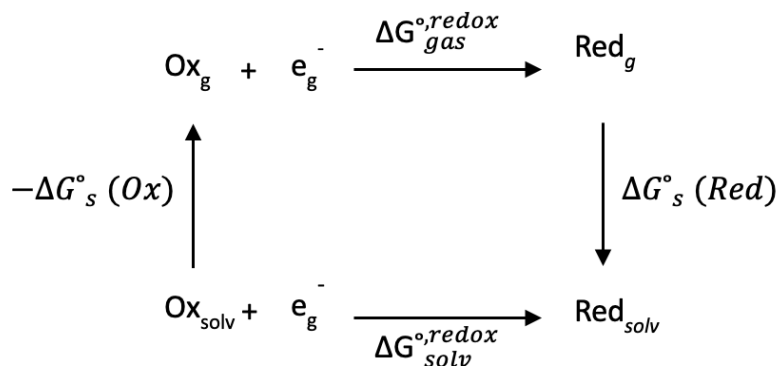
Furthermore, a better representation of the strength of ionic association can be inferred by examining the $1200\text{-}1400\text{ cm}^{-1}$ region of the IR-spectrum, shown in figure 2.2C. For instance, previous reports on the ionic interaction present in solutions prepared by dissolving lithium and tetrabutylammonium triflate salts in various solvents revealed that solutions comprising of Li-triflate in tetrahydrofuran, triethylene glycol dimethyl ether, acetone, and acetonitrile exhibit a splitting in the doubly degenerate antisymmetric SO_3 mode, $\nu_{as}\text{SO}_3$ into two components, and the degree of band splitting can be used to demonstrate the strength of ionic association, $\Delta\nu_{as}(\text{SO}_3)$.

The frequency separation for Li-triflate in THF was reported to be 54 cm⁻¹, with the two components detected at 1254 and 1308 cm⁻¹.²⁷

Comparatively, the split components shown in figure 2.2C, designated by the peaks positioned at 1238 and 1309 cm⁻¹ with a $\Delta\nu_{\text{as}}(\text{SO}_3)$ of around 71cm⁻¹. The discrepancy between band widths for Li-triflate/THF and Al-triflate/THF can be associated to the higher charge density of the Al-cation compared to that of lithium.

Surprisingly, the computational results for [Al(THF)₄(Triflate)][Triflate]⁺ indicate that the bands positioned at 1238 and 1309 cm⁻¹ correspond to the two distinct environments of triflate discussed earlier, rather than the splitting of the doubly-degenerate $\Delta\nu_{\text{s}}(\text{SO}_3)$ previously proposed by Frech and Huang.²⁶⁻³¹

2.3.3 Stability predictions and electrochemical profiling



Scheme 2.1 Born-Haber cycle used to calculate the changes in the standard solvation Gibbs Free Energy. © 2020 American Chemical Society.

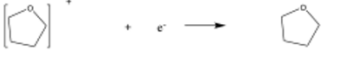

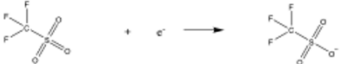
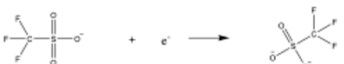
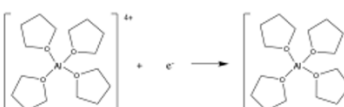
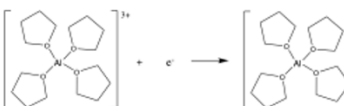
$$\Delta G_{\text{solv}}^{\circ, \text{redox}} = -\Delta G_{\text{s}}^{\circ}(\text{Ox}) + \Delta G_{\text{gas}}^{\circ, \text{redox}} + \Delta G_{\text{s}}^{\circ}(\text{Red}) \quad (1)$$

To provide a rationale for understanding the electrochemical behavior of Al³⁺ in THF, the following approach was carried out. The one electron reduction process represented by the Born-Haber cycle in scheme 1^{35,36,37} was used to calculate the absolute redox potentials, $E_{\text{calc}}^{\text{abs}}$ of the species of interest i.e triflate, THF, and Al(THF)₄³⁺. Equation (1) was applied to obtain the standard solvent-phase Gibbs free energy change, $\Delta G_{\text{solv}}^{\circ, \text{redox}}$ by computing the solvation free energies of the oxidized species, $\Delta G_{\text{s}}^{\circ}(\text{Ox})$, reduced species, $\Delta G_{\text{s}}^{\circ}(\text{Red})$, and the gas phase standard Gibbs free Energies $\Delta G_{\text{gas}}^{\circ, \text{redox}}$.

$$E_{\text{calc}}^{\text{abs}} = -\frac{\Delta G_{\text{solv}}^{\circ, \text{redox}}}{nF} \quad (2)$$

E_{calc}^{abs} was then calculated using equation (2), where n is the number of electrons involved in the reduction reaction, and F is Faraday's constant. Consequently, estimates of the electrochemical window of the aforementioned species and predictions on the stability of the Al-trif/THF electrolyte can thus be made. Table 2.2 summarizes the results of these calculations:

Table 2.2 Gibbs Free Energies and absolute reduction potentials of solvent, anion and complexes. © 2020 American Chemical Society.

Reaction	$\Delta G_s^{(Ox)}$ (kcal/mol)	ΔG_{gas}^{redox} (kcal/mol)	$\Delta G_s^{(Red)}$ (kcal/mol)	E_{calc}^{abs} (V)	E_{calc} (V vs. Al/Al ³⁺)
	-56.9	-210.4	-3.9	6.82	2.54
	-3.9	-29.1	-33.9	0.04	-4.24
	-3.2	-117.0	-44.3	6.86	2.58
	-44.3	109.9	-143.0	-0.49	-4.77
	-508.9	-444.3	-296.7	10.07	5.79
	-296.7	-257.6	-137.7	4.28	0

The electrochemical windows of THF, triflate, and Al(THF)₄³⁺ as predicted from these calculations are approximately 6.8V, 7.3V and 5.8V respectively. These results suggest that the stability of this electrolyte is governed by two reactions, the oxidation of THF and the reduction of Al(THF)₄³⁺, which results in an expected electrochemical window of around 2.5V.^{15, 37} Furthermore, because an aluminum wire was used as a pseudo-reference electrode for all cyclic voltammetry measurements, and on the basis of the results shown in table 2.2, the electrochemical reduction of Al(THF)₄³⁺ is expected to be present at 0V vs the aluminum wire, and the oxidation of THF at 2.5V vs. the aluminum wire.

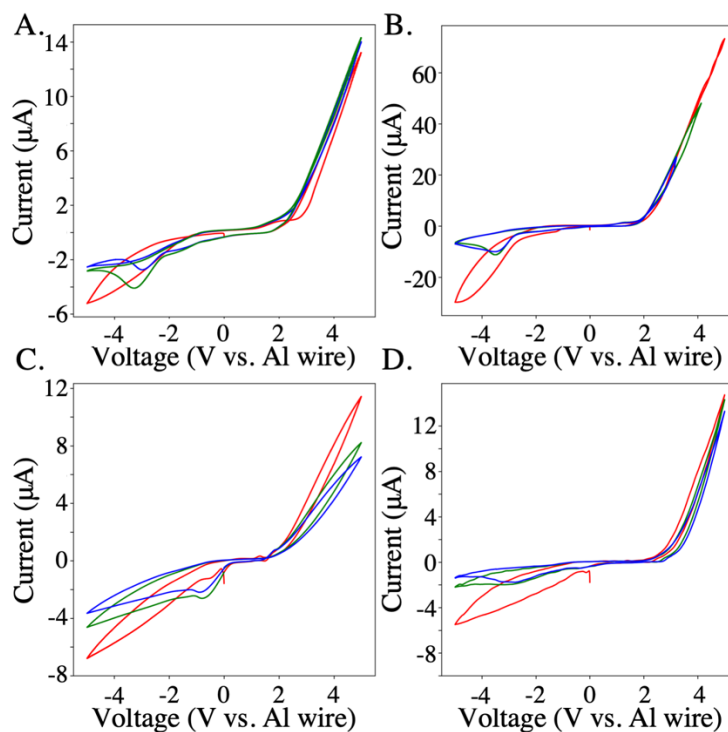


Figure 2.3 Displays the first three cycles of cyclic voltammograms for Al-triflate/THF electrolytes at different concentrations with a sweep rate of 10mV/s: (A) 0.05M on glassy carbon WE. (B) 0.1M concentration glassy carbon WE. (C) 0.01M on gold WE. (D) 0.1M on gold WE. The first scan is red, the second blue and the third is green. © 2020 American Chemical Society.

To test these predictions, cyclic voltammetry was performed using a glassy carbon working electrode and a gold working electrode. Examination of the I-V polarization curves on a glassy carbon electrode, shown in figure 2.3A and B, and on a gold electrode, shown in figure 2.3C and D, reveal an oxidation near 2.5 V, relatively independent of concentration, which is in good agreement with our predictions and so we assign to the oxidation of THF. However, the onset potentials for the reduction reactions of the 0.05M and 0.1M solutions on the glassy carbon electrode are around -1 and -2V respectively, well below the predicted value of 0V vs aluminum for the $\text{Al}(\text{THF})_4^{3+}$ reduction, but well above the predicted value of either THF or triflate reduction. On the contrary, cyclic voltammograms measured on a gold working electrode are shown in figure 2.3C and D and reveal electrochemical activity around 0V which we attribute to the electrochemical reduction of $\text{Al}(\text{THF})_4^{3+}$. Our hypothesis is that this reduction is going all the way to aluminum metal, and that the reduction potential dependence on electrode material are due to changes in wetting energy between aluminum on carbon and aluminum on gold. This hypothesis is consistent with our observation of a color change of the gold electrode from gold to silver in color.

Furthermore, the lack of an oxidation current due to aluminum stripping is likely due to the lack of a strong Lewis base in this electrolyte, consistent with previous work by Graef,¹⁴ where the mechanism for reversibly depositing/dissolving aluminum from an $\text{AlCl}_3\text{-LiAlH}_4\text{/THF}$ bath was proposed. A key finding was that a chloride-rich environment was necessary for the formation of stable aluminum chloride ligands without which, the activation overpotential for the dissolution of aluminum would not be realized. However, this hypothesis requires further investigation and is outside the focus of this work.

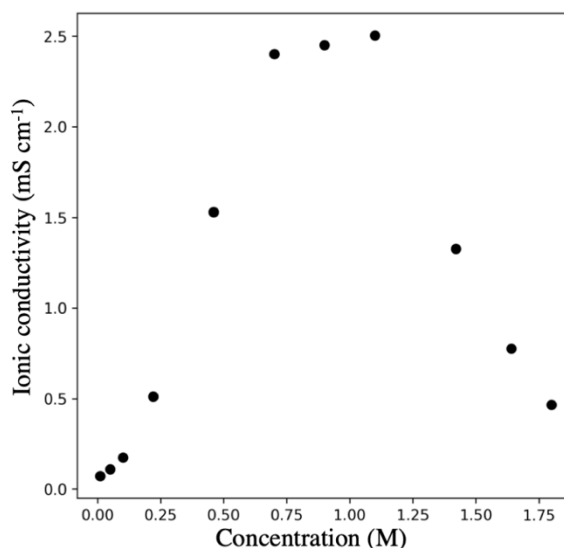


Figure 2.4 Ionic conductivity of the solution as a function of aluminum triflate concentration. © 2020 American Chemical Society.

To further examine the effect of increasing the concentration on the electrochemical properties of the electrolyte, electrochemical impedance spectroscopy was conducted to measure the ionic conductivities for different molar concentrations at room temperature. Figure 2.4 shows that the ionic conductivities for these electrolytes increases as a function of concentration up to the point of saturation around 0.8M, with conductivities as high as a 2.5mS/cm, before the ionic conductivity starts to decrease around 1.2M, which may be attributed to an increase in viscosity and ion pairing following the trend reported elsewhere.¹⁵

2.4 Conclusions

In summary, we have investigated the physicochemical aspects of Al-trif/THF electrolytes. DFT calculations were performed at the B3PW91/6311+G(d) level of theory to predict the structural, spectroscopic and electrochemical features of ionic species present. Complementary to the DFT-predicted vibrational frequencies, FTIR spectra of several Al-triflate concentrations were measured. Peaks within the 750-780 cm^{-1} region of the spectral profiles reveal corroborating evidence for the presence of two distinct ionic environments for triflate anion contact ion pairs. Al-bound triflates with an Al-O bond length of 1.8 Å, and outer-shell ligands. In addition to contact ion pairs, peaks centered around 1030 cm^{-1} confirm the presence of free triflate anions in all concentrations.

Cyclic voltammetry measurements provide insight into electrochemical behavior of Al-ions on gold and carbon working electrodes. Oxidation was observed on both gold and glassy carbon electrodes around 2.5 V, while reduction was observed near 0 V on gold and -2 V on glassy carbon, consistent with THF oxidation and $\text{Al}(\text{THF})_4^{3+}$ reduction predicted by theory. Finally, the ionic conductivity of these electrolytes follows an expected trend, with a maximum of 2.5 mS/cm^{-1} near saturation.

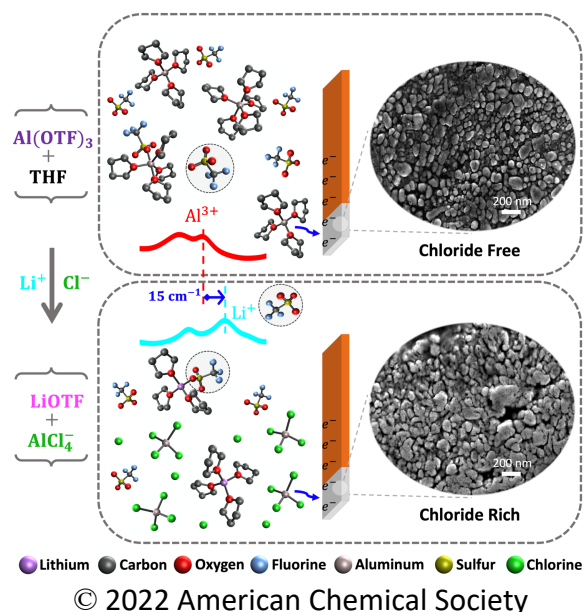
2.5 References

- (1) Armand, M.; Tarascon, J. M., Building better batteries. *Nature* **2008**, *451* (7179), 652-657.
- (2) Nishi, Y., 2 - Past, Present and Future of Lithium-Ion Batteries: Can New Technologies Open up New Horizons? In *Lithium-Ion Batteries*, Pistoia, G., Ed. Elsevier: Amsterdam, 2014; pp 21-39.
- (3) Gao, X.-P.; Yang, H.-X., Multi-electron reaction materials for high energy density batteries. *Energy & Environmental Science* **2010**, *3* (2), 174-189.
- (4) Zu, C.-X.; Li, H., Thermodynamic analysis on energy densities of batteries. *Energy & Environmental Science* **2011**, *4* (8), 2614-2624.
- (5) Hu, Y.; Sun, D.; Luo, B.; Wang, L., Recent progress and future trends of aluminum batteries. *Energy Technology* **2019**, *7* (1), 86-106.
- (6) Elia, G. A.; Marquardt, K.; Hoepfner, K.; Fantini, S.; Lin, R.; Knipping, E.; Peters, W.; Drillet, J.-F.; Passerini, S.; Hahn, R., An overview and future perspectives of aluminum batteries. *Advanced Materials* **2016**, *28* (35), 7564-7579.
- (7) Gale, R. J.; Osteryoung, R. A., Potentiometric investigation of dialuminum heptachloride formation in aluminum chloride-1-butylpyridinium chloride mixtures. *Inorganic Chemistry* **1979**, *18* (6), 1603-1605.
- (8) Jiang, T.; Chollier Brym, M. J.; Dubé, G.; Lasia, A.; Brisard, G. M., Electrodeposition of aluminium from ionic liquids: Part I—electrodeposition and surface morphology of aluminium from aluminium chloride (AlCl_3)–1-ethyl-3-methylimidazolium chloride ([EMIm]Cl) ionic liquids. *Surface and Coatings Technology* **2006**, *201* (1), 1-9.
- (9) Reed, L. D.; Menke, E., The roles of V_2O_5 and stainless steel in rechargeable Al-ion batteries. *Journal of the Electrochemical Society* **2013**, *160* (6), A915-A917.

- (10) Tseng, C.-H.; Chang, J.-K.; Chen, J.-R.; Tsai, W. T.; Deng, M.-J.; Sun, I. W., Corrosion behaviors of materials in aluminum chloride–1-ethyl-3-methylimidazolium chloride ionic liquid. *Electrochemistry Communications* **2010**, *12* (8), 1091-1094.
- (11) Couch, D. E.; Brenner, A., A hydride bath for the electrodeposition of aluminum. *Journal of the Electrochemical Society* **1952**, *99* (6), 234.
- (12) Garai, T., Electro-deposition of aluminium in non-aqueous solvents. *Materials Chemistry and Physics* **1983**, *8* (5), 399-434.
- (13) Ishibashi, N.; Yoshio, M., Electrodeposition of aluminium from the NBS type bath using tetrahydrofuran—benzene mixed solvent. *Electrochimica Acta* **1972**, *17* (8), 1343-1352.
- (14) Graef, M. W. M., The mechanism of aluminum electrodeposition from solutions of AlCl₃ and LiAlH₄ in THF. *Journal of the Electrochemical Society* **1985**, *132* (5), 1038.
- (15) Reed, L. D.; Arteaga, A.; Menke, E. J., A combined experimental and computational study of an aluminum triflate/diglyme electrolyte. *The Journal of Physical Chemistry B* **2015**, *119* (39), 12677-12681.
- (16) Reed, L. D.; Ortiz, S. N.; Xiong, M.; Menke, E. J., A rechargeable aluminum-ion battery utilizing a copper hexacyanoferrate cathode in an organic electrolyte. *Chemical Communications* **2015**, *51* (76), 14397-14400.
- (17) Kitada, A.; Nakamura, K.; Fukami, K.; Murase, K., AlCl₃-dissolved diglyme as electrolyte for room-temperature aluminum electrodeposition. *Electrochemistry* **2014**, *82* (11), 946-948.
- (18) Frisch, M. J.; Trucks, G. W.; Schlegel, H. B.; Scuseria, G. E.; Robb, M. A.; Cheeseman, J. R.; Scalmani, G.; Barone, V.; Mennucci, B.; Petersson, G. A., et al. *Gaussian 09*, Gaussian, Inc.: Wallingford, CT, USA, 2009.
- (19) Becke, A. D., Density-functional thermochemistry. III. The role of exact exchange. *The Journal of Chemical Physics* **1993**, *98* (7), 5648-5652.
- (20) Krishnan, R.; Binkley, J. S.; Seeger, R.; Pople, J. A., Self-consistent molecular orbital methods. XX. A basis set for correlated wave functions. *The Journal of Chemical Physics* **1980**, *72* (1), 650-654.
- (21) Hratchian, H. P.; Schlegel, H. B., Chapter 10 - Finding Minima, Transition States, and Following Reaction Pathways on Ab Initio Potential Energy Surfaces. In *Theory and Applications of Computational Chemistry*, Dykstra, C. E.; Frenking, G.; Kim, K. S.; Scuseria, G. E., Eds. Elsevier: Amsterdam, 2005; pp 195-249.
- (22) Marenich, A. V.; Cramer, C. J.; Truhlar, D. G., Universal solvation model based on solute electron density and on a continuum model of the solvent defined by the bulk dielectric constant and atomic surface tensions. *The Journal of Physical Chemistry B* **2009**, *113* (18), 6378-6396.
- (23) Bauernschmitt, R.; Ahlrichs, R., Stability analysis for solutions of the closed shell Kohn–Sham equation. *The Journal of Chemical Physics* **1996**, *104* (22), 9047-9052.
- (24) Seeger, R.; Pople, J. A., Self-consistent molecular orbital methods. XVIII. Constraints and stability in Hartree–Fock theory. *The Journal of Chemical Physics* **1977**, *66* (7), 3045-3050.
- (25) Menges, F. *Spectragryph optical spectroscopy software*, 2016.

- (26) Huang, W.; Frech, R.; Wheeler, R. A., Molecular structures and normal vibrations of trifluoromethane sulfonate (CF₃SO₃⁻) and its lithium ion pairs and aggregates. *The Journal of Physical Chemistry* **1994**, *98* (1), 100-110.
- (27) Frech, R.; Huang, W., Anion-solvent and anion-cation interactions in lithium and tetrabutylammonium trifluoromethanesulfonate solutions. *Journal of Solution Chemistry* **1994**, *23* (4), 469-481.
- (28) Frech, R.; Huang, W.; Dissanayake, M. A. K. L., Ionic association of lithium triflate in glymes, model solvents, and high molecular weight poly(ethylene oxide). *MRS Proceedings* **1994**, *369*, 523.
- (29) Huang, W.; Frech, R., Dependence of ionic association on polymer chain length in poly(ethylene oxide)-lithium triflate complexes. *Polymer* **1994**, *35* (2), 235-242.
- (30) Bernson, A.; Lindgren, J.; Huang, W.; Frech, R., Coordination and conformation in PEO, PEGM and PEG systems containing lithium or lanthanum triflate. *Polymer* **1995**, *36* (23), 4471-4478.
- (31) Frech, R.; Huang, W., Ionic association in poly (propylene oxide) complexed with divalent metal trifluoromethanesulfonate salts. *Solid State Ionics* **1993**, *66* (1), 183-188.
- (32) Wendsjö, Å.; Lindgren, J.; Thomas, J. O.; Farrington, G. C., The effect of temperature and concentration on the local environment in the system M(CF₃SO₃)₂PEOn for M=Ni, Zn and Pb. *Solid State Ionics* **1992**, *53-56*, 1077-1082.
- (33) Schantz, S.; Sandahl, J.; Börjesson, L.; Torell, L. M.; Stevens, J. R., Ion pairing in polymer electrolytes; A comparative Raman study of NaCF₃SO₃ complexed in poly(propylene-glycol) and dissolved in acetonitrile. *Solid State Ionics* **1988**, *28-30*, 1047-1053.
- (34) Bernson, A.; Lindgren, J., Ion aggregation and morphology for poly (ethylene oxide)-based polymer electrolytes containing rare earth metal salts. *Solid State Ionics* **1993**, *60* (1), 31-36.
- (35) Roy, L. E.; Jakubikova, E.; Guthrie, M. G.; Batista, E. R., Calculation of one-electron redox potentials revisited. Is it possible to calculate accurate potentials with density functional methods? *The Journal of Physical Chemistry A* **2009**, *113* (24), 6745-6750.
- (36) Konezny, S. J.; Doherty, M. D.; Luca, O. R.; Crabtree, R. H.; Soloveichik, G. L.; Batista, V. S., Reduction of systematic uncertainty in DFT redox potentials of transition-metal complexes. *The Journal of Physical Chemistry C* **2012**, *116* (10), 6349-6356.
- (37) Shao, N.; Sun, X.-G.; Dai, S.; Jiang, D.-e., Electrochemical windows of sulfone-based electrolytes for high-voltage Li-ion batteries. *The Journal of Physical Chemistry B* **2011**, *115* (42), 12120-12125.

Chapter 3: Aluminum Electrodeposition from Chloride-Rich and Chloride-Free Organic Electrolytes



3.1 Introduction

The pursuit of high energy density for electrification of the transportation system and the demand for intermittent grid storage along with the significant uncertainty in material supplies for lithium-ion batteries^{1,2} are propelling research efforts towards multivalent ion battery technologies, including those based on magnesium (Mg), calcium (Ca) and aluminum (Al).^{3,4} Among post-lithium(Li) ion batteries, Al is of particular interest because of its superior theoretical volumetric capacity and low-cost compared to Li and other post-Li battery metals on account of its trivalency and high abundance.^{5,6} However, making use of Al's remarkable capacity is challenging due to its relatively small ionic radius and high charge density, which inevitably leads to the formation of Al-ion complexes rather than "free" Al-ions in commonly employed chloroaluminate ionic liquids, diminishing the expected capacities of rechargeable Al batteries.⁷ In spite of the recent advances in developing cathode materials,^{8,9} and electrolytes,^{6,10} the rechargeable Al battery remains in its infancy.¹¹ Accordingly, breaking new ground in Al-ion electrolyte chemistries for rechargeable Al batteries is of utmost significance.

Due to their ability to electrodeposit/strip Al, chloroaluminate ionic liquids based on aluminum trichloride (AlCl_3) are often investigated as electrolytes for rechargeable Al batteries.^{12–28} Nevertheless, their integration into a practical rechargeable Al battery is hindered by severe drawbacks including the instability of cathode materials in these electrolytes leading to rapid capacity fading,²⁰ high corrosivity towards Al anodes²⁹ and stainless steel current collectors,¹³ and side reactions that generate Cl_2 gas.^{30,31} Moreover, considering that molten salts are often limited to high operating temperatures,⁶ organic solvents present an appealing choice for room temperature rechargeable Al battery application. The development of an organic electrolyte, however, is a challenging task that requires a fundamental understanding of the solute/solvent ion-dipole and coulombic interactions.³²

Tremendous efforts have been dedicated to electrodeposit Al from a plethora of organic systems including AlCl_3 and lithium hydride (LiH) in diethyl ether,³³ AlCl_3 and lithium aluminum hydride (LiAlH_4) in tetrahydrofuran (THF) and benzene mixture,³⁴ AlCl_3 and LiAlH_4 in THF and toluene,³⁵ AlCl_3 and LiAlH_4 in THF,^{36–39} aluminum tribromide (AlBr_3) in aromatic hydrocarbons,^{40,41} AlBr_3 in *N,N*-dimethylaniline,⁴² AlBr_3 and potassium bromide (KBr) in ethylbenzene,⁴³ AlCl_3 in sulfones,^{44–49} AlCl_3 in glycol ethers (glymes),^{50–53} AlCl_3 in ethylene carbonate,⁵⁴ and AlCl_3 in gamma-butyrolactone (GBL).⁵⁵

Unfortunately, these electrolytes are inherently corrosive and the prospects of practically implementing rechargeable Al batteries as electrochemical energy storage devices is contingent upon active chloride-free systems.⁵⁶ It is therefore imperative to investigate organic electrolytes based on alternative Al-salts. Inspired by the aforementioned challenges associated with Al-halides, researchers have sought to synthesize novel chloride-free Al-salts including; aluminum hexa-dimethyl sulfoxide trifluoromethanesulfonate $[\text{Al}(\text{DMSO})_6][\text{OTF}]_3$, aluminum hexa-dimethyl sulfoxide bis(trifluoromethylsulfonyl)imide $[\text{Al}(\text{DMSO})_6][\text{TFSI}]_3$, aluminum hexa-methylimidazole bis(trifluoromethylsulfonyl)imide $[\text{Al}(\text{MIm})_6][\text{TFSI}]_3$,⁵⁷ $\text{Al}(\text{TFSI})_3$ in acetonitrile,⁵⁸ and aluminum hexafluorophosphate ($\text{Al}(\text{PF}_6)_3$) in DMSO,⁵⁹ as well as explore the commercially available aluminum trifluoromethanesulfonate ($\text{Al}(\text{OTF})_3$) in propylene carbonate and THF mixture,¹² 2-methoxy ethyl ether (diglyme),^{60,61} *N*-methyl acetamide,⁶² and THF.⁶³ It is worth noting that employing $\text{Al}(\text{OTF})_3$ as a potential Al-salt for rechargeable Al batteries has not been restricted to organic solvents, with its application in aqueous systems^{64,65} and ionic liquids⁶⁶ having already been demonstrated. Despite these endeavors, the role free chlorides (Cl^-) play in Al-ion organic electrolyte chemistry, and a clear demonstration of Al electrodeposition using $\text{Al}(\text{OTF})_3$, has not yet been established.

In chapter 2, we explored the ionic speciation and the electrochemical activity of Al-complexes in $\text{Al}(\text{OTF})_3/\text{THF}$ computationally and experimentally. Density functional theory (DFT) calculations coupled with Fourier transform infrared spectroscopy (FTIR) suggested that Al exists in these solutions as fully solvated Al-complexes, in addition to the presence of inner-sphere and outer-sphere trifluoromethanesulfonate anions (OTF^-).⁶³ Further investigation at higher concentrations ($>0.1\text{M}$), presented herein, reveals that these solutions are dominated by $[\text{Al}(\text{THF})_2(\text{OTF})_2]^+$.

The structure evolution of these species is depicted in (Figure 3.1a-c). In light of these findings and to ascertain the effect of Cl^- on the electrochemical behavior of Al-ions, we report here evidence for the electrochemical reduction of Al-ions to Al-metal from THF through a comparative study that reveals the electrochemical behavior and ionic speciation of Al-complexes in three electrolyte systems: $\text{Al}(\text{OTF})_3/\text{THF}$, $\text{Al}(\text{OTF})_3 + \text{LiCl}/\text{THF}$, and AlCl_3/THF .

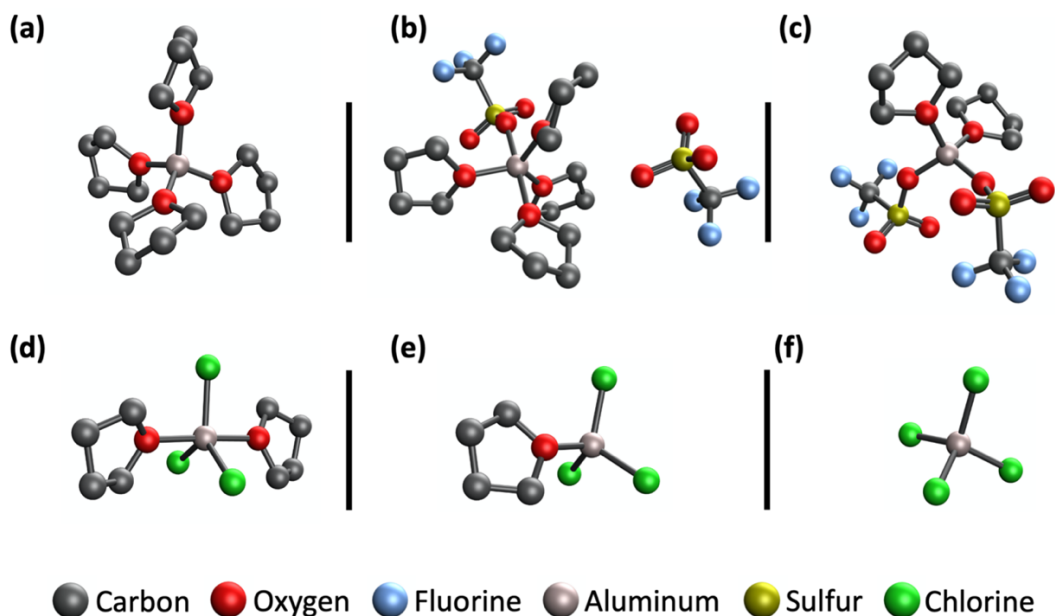


Figure 3.1 Optimized structures (hydrogens not shown) of (a) $\text{Al}(\text{THF})_4^{3+}$, (b) $[\text{Al}(\text{THF})_4(\text{OTF})][(\text{OTF})]^+$, (c) $[\text{Al}(\text{THF})_2(\text{OTF})_2]^+$, (d) $\text{AlCl}_3(\text{THF})_2$, (e) $\text{AlCl}_3(\text{THF})$, and (f) AlCl_4^- . © 2022 American Chemical Society.

In this study, lithium chloride (LiCl) was chosen as an additive due to its ability to provide free Cl^- in THF, a result of the ionic character of the $\text{Li} - \text{Cl}$ bond in LiCl compared to the more covalent nature of the $\text{Al} - \text{Cl}$ bonds in AlCl_3 . To examine the effect of Cl^- on Al speciation, a comprehensive investigation of computed versus measured vibrational frequencies was undertaken, with a summary of the DFT results provided in the (Supporting Information, see Table 3.1). Our findings on the AlCl_3/THF solutions complement those of Derouault et al.,⁶⁷ where the major species in these solutions were found to be charge neutral $\text{AlCl}_3(\text{THF})_2$ and $\text{AlCl}_3(\text{THF})$ (shown in Figure 3.1d,e). The spectral features of the $\text{Al}(\text{OTF})_3/\text{THF}$ and AlCl_3/THF solutions at various concentrations are then used to elucidate the reactions involving $\text{Al}(\text{OTF})_3$ and LiCl in THF. Our results suggest that this electrolyte is dominated by AlCl_4^- (Figure 3.1f) at $\text{Al}(\text{OTF})_3 : \text{LiCl}$ mole ratios equal to or above 1:3, in addition to the ionic association between Li^+ and OTF^- in this electrolyte. The striking dissimilarities in the spectroscopic and electrochemical attributes for the Cl^- rich environments i.e. AlCl_3/THF and $\text{Al}(\text{OTF})_3 + \text{LiCl}/\text{THF}$, provide insight into the role of particular Cl^- containing Al-complexes in Al electrodeposition/stripping behavior in THF.

3.2 Materials and Methods

3.2.1 Density functional theory calculations

All density functional theory (DFT) calculations were done using the Gaussian 09 suite of electronic structure program.⁶⁸ The B3PW91 density functional was employed using the unrestricted spin-formalism. All structures were fully optimized in the solvent phase incorporating tetrahydrofuran (THF) using a solvation model density (SMD) continuum solvation model based on the self-consistent reaction field (SCRF) approach. Chloride containing calculations were carried out using the aug-cc-(PVTZ) basis set. For all other calculations the 6311+G(d) basis set was used. Vibrational analyses were performed to obtain harmonic vibrational frequencies. In all cases, the optimized structures were found to be a local minima on the potential energy surfaces by confirming the absence of any imaginary frequencies.

3.2.2 Experimental details

99.9% Aluminum trifluoromethanesulfonate ($\text{Al}(\text{OTf})_3$), 99% lithium chloride (LiCl), 99.995% lithium triflate (LiOTf), ultrapure 99.99% aluminum trichloride (AlCl_3), and 99.9% tetrahydrofuran (THF) were purchased from Sigma-Aldrich. LiCl was weighed and dried overnight in a vacuum oven at 120 °C, all other chemicals were used without further purification. All chemical preparations and electrochemical measurements were conducted in an argon-filled glovebox. All electrolytes were prepared by dissolving appropriate amounts of each salt in 5 ml of THF. To ensure complete dissolution, the solutions were stirred overnight. It is important to note that $\text{Al}(\text{OTf})_3$ salt is highly hygroscopic, and trace amounts of moisture can significantly inhibit its dissolution in organic solvents. Copper (Cu) foil substrates were purchased from McMaster-Carr.

At low concentrations the $\text{Al}(\text{OTf})_3/\text{THF}$ solutions are transparent, at high concentrations the electrolytes become turbid and yellowish in color. The $\text{Al}(\text{OTf})_3 + \text{LiCl}/\text{THF}$ are transparent solution and highly hygroscopic turning white in color when trace amounts of moisture is present. The reaction between AlCl_3 and THF is a very violent reaction, and so AlCl_3 was slowly added to THF. At low concentrations the solutions are transparent turning dark brown/reddish in color at higher concentrations.

Attenuated total reflectance (ATR) Fourier transform infrared (FTIR) spectroscopy was carried out using a Vertex 70 spectrometer. Samples of each electrolyte were packed in glass cells, sealed under argon and transferred to FTIR spectrometer to ensure minimal interaction with air. A 4 cm^{-1} resolution and 120 scans were used.

The concentration of aluminum was set to 0.1M for all electrochemical measurements, including the various mole ratios of $\text{Al}(\text{OTf})_3$ & LiCl. For example a 1:2 $\text{Al}(\text{OTf})_3$: LiCl solution is comprised of 0.1M $\text{Al}(\text{OTf})_3 + 0.2\text{M LiCl} / 5\text{ ml of THF}$. Electrochemical measurements were conducted using a potentiostat (Gamry). A standard three electrode set up was used for both cyclic voltammetry (CV) and chronoamperometry experiments. CV's were obtained using a gold working electrode, an Al wire pseudoreference, an Al wire counter electrode and a scan rate of 50 mV/s.

Chronoamperometry was carried out using a Cu substrate as the working electrode, an Al wire pseudoreference and an Al wire counter electrode. The potential was set to 0V (with a pre-step initial voltage of -0.1V) for the Al(OTF)₃/THF electrolyte and +0.25 V for both the AlCl₃/THF and 1:3 Al(OTF)₃ + LiCl/THF electrolytes. Before and after the chronoamperometry experiments, the Cu electrodes were rinsed with acetone and dried in a vacuum oven for at least 30 minutes. Electron microscopy was conducted with a field emission scanning electron microscope (Zeiss Gemini SEM 500). X-ray photoelectron spectroscopy (XPS) measurements were carried out using Nexsa spectrometer. The sample for the XPS analysis was prepared by holding the potential of a Cu substrate at 0V vs. the Al wire for 72 hours in a 0.1M Al(OTF)₃/THF electrolyte followed by rinsing the Cu substrate with acetone.

3.3 Results and Discussion

A series of electrolyte solutions were prepared by dissolving appropriate amounts of Al-salt (Al(OTF)₃, AlCl₃) and/or Li-salt (LiOTF, LiCl) in THF. FTIR spectra were collected and are shown in (Figure 3.2). Initially, it was crucial to examine the spectral regions corresponding to the complex-ion formation in the Al(OTF)₃/THF electrolyte at various concentrations (Figure 3.2a).

Characteristic peaks attributed to free and coordinated OTF⁻ have been extensively studied by Frech and Huang.⁶⁹⁻⁷³ In accordance with these reports, we revealed in our previous investigation of the Al(OTF)₃/THF electrolytes that the peak at 1028 cm⁻¹ is associated with symmetric stretch (ν_s SO₃) of free OTF⁻ and that the 1200-1400 cm⁻¹ region of the spectra displays bands assigned to the asymmetric stretch of the OTF⁻ anions (ν_{as} SO₃) for two types of contact ion pairs, outer sphere and inner sphere OTF⁻, referred to here as SSIP (for Solvent-Separated Ion Pair) and Agg (for Aggregates), respectively.⁶³ Re-examining this region, we find that the broad peak centered at 1210 cm⁻¹ is likely a combination of two spectral components, a peak at 1220 cm⁻¹, SSIP, assigned to ν_{as} SO₃, another, Agg, at 1210 cm⁻¹ assigned to ν C – S coupled with ν_s SO₃ of OTF⁻ (Supporting Information Table 3.1). Upon access of an additional OTF⁻ to the inner solvation sphere of the Al-cation, a new peak appears both computationally and experimentally at ~1350 cm⁻¹. We attribute this peak to a new type of Agg, represented by the following species; [Al(THF)₂(OTF)₂]⁺ and [Al(THF)₃(OTF)₂]⁺. Although the predicted reaction energies for both complexes are similar (Table 3.2), entropic factors are not accounted for in these calculations. As a result, we attribute the peak at ~1350 cm⁻¹ to the tetrahedral complex [Al(THF)₂(OTF)₂]⁺.

Moreover, comparing the Al(OTF)₃/THF spectra to that of pure solvent (THF), we find that the peak at 1068 cm⁻¹ becomes broader as the concentration increases, suggesting that this band is not only associated with THF but also Al-Agg.^{63,74}

The peak emerging at 883 cm⁻¹, as supported by our DFT calculations, can be assigned to ν (Al – O) coupled with τ CH₂ of Al – THF bond. (Table 3.1. in Supporting Information) Finally, the peak observed at 1048 cm⁻¹ is more prominent at concentrations >0.3M which suggest that this peak may be associated with ionic aggregates of Al(OTF)₃.

Based on these results the following dissociation reactions for $\text{Al}(\text{OTf})_3$ in THF can be proposed, corresponding to the structures shown in Figure 3.1a-c:

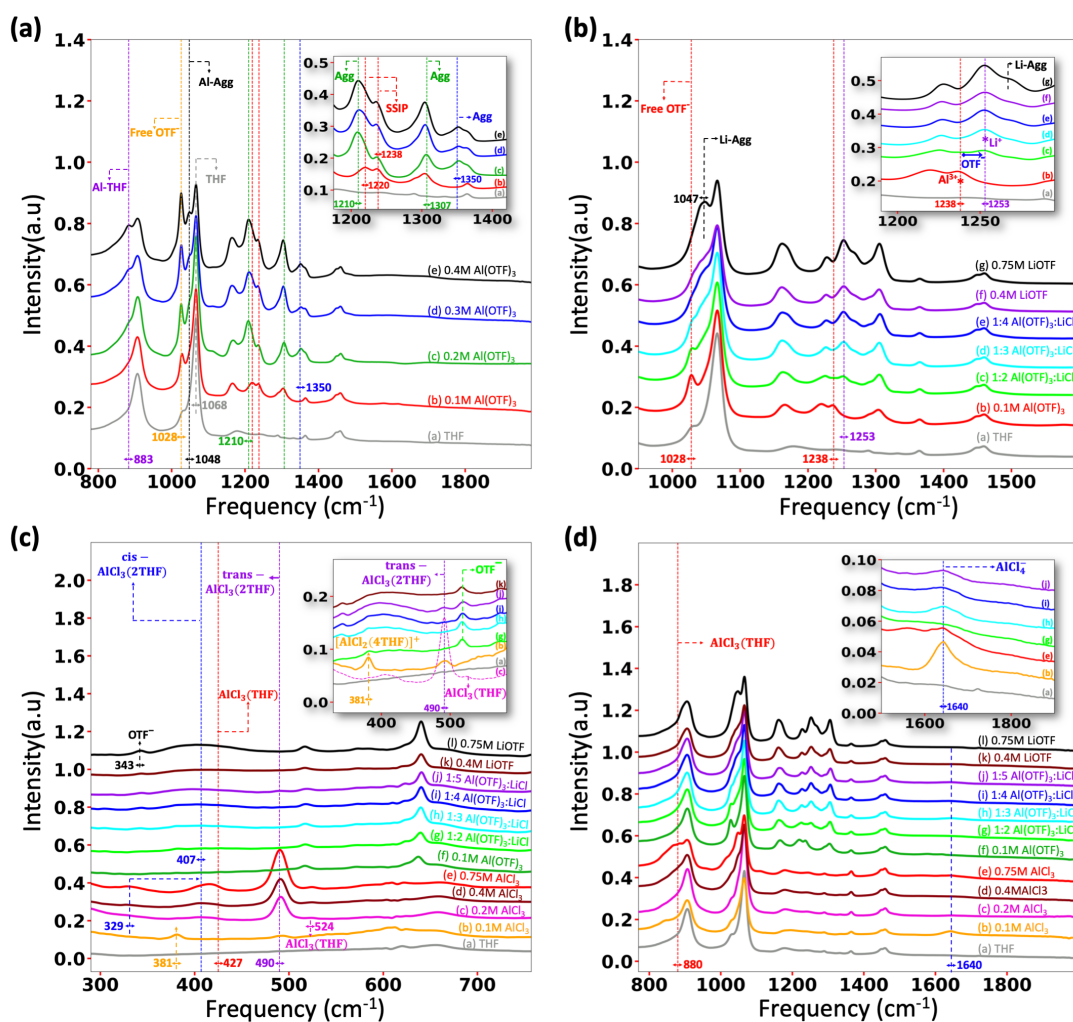
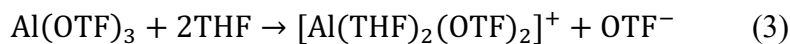
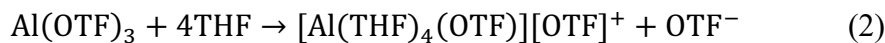
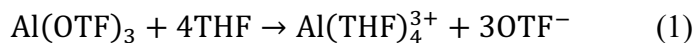


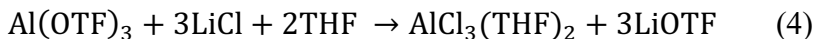
Figure 3.2 FTIR spectra of various concentrations of Al and/or Li salts in THF. OTF⁻: trifluoromethanesulfonate anion, SSIP: solvent separated ion pair, Agg: aggregate. © 2022 American Chemical Society.

With considerable knowledge of the $\text{Al}(\text{OTF})_3/\text{THF}$ spectroscopic features in hand, the reaction between $\text{Al}(\text{OTF})_3$ and LiCl in THF can now be studied. The progress of this reaction is depicted in the inset of Figure 3.2b (See also Supporting Information Figure 3.5). As LiCl is introduced to a 0.1M $\text{Al}(\text{OTF})_3$ solution at mole ratios equal to or above 1:2, a transfer of the OTF^- from Al- to Li-ions is evident. This is illustrated by the peak shift from 1238 to 1253 cm^{-1} , which, according to our DFT calculations, may be assigned to Al –SSIP and Li – CIP (Contact Ion Pair), respectively. At 1:3 mole ratios, this region of the spectrum is identical to that of a solution of 0.4M LiOTF in THF. Thus, one may infer that a double displacement reaction between $\text{Al}(\text{OTF})_3$ and LiCl takes place at 1:3 mole ratio according to reaction 4. While Li cations have OTF^- in their vicinity, the formation of LiOTF ionic aggregates can be excluded from the 1:3 electrolyte due to the absence of the peak at 1047 cm^{-1} , which is typically attributed to LiOTF aggregates,⁷² and the shoulder peak at 1269 cm^{-1} , observed only in the 0.75M LiOTF/THF solution.

After establishing that the 1:3 electrolytes are primarily comprised of AlCl_3 and LiOTF , inspecting ionic species previously reported for AlCl_3/THF solutions is crucial. Alves et al. investigated AlCl_3/THF solutions by Raman spectroscopy and deduced that these electrolytes were dominated by AlCl_4^- in dilute systems whereas $\text{AlCl}_3(\text{THF})_3$ are favored at higher concentrations.⁷⁵ On the other hand, Derouault et al. investigated Al-halide (AlCl_3 or AlBr_3) in THF by FTIR and NMR spectroscopy,⁶⁷ and the results were compared to the FTIR and Raman spectra of solid Al-halide complexes.⁷⁶ The latter concluded that dissolving AlCl_3 in THF produced mainly $\text{AlCl}_3(\text{THF})$, cis- and trans- isomers of $\text{AlCl}_3(\text{THF})_2$, and AlCl_4^- and $[\text{AlCl}_2(\text{THF})_4]^+$ which resulted from slight dissociation of $\text{AlCl}_3(\text{THF})_2$ according to a proposed equilibria which is provided in the (Supporting Information). We note that our FTIR spectra for AlCl_3/THF appear identical to those of Derouault et al.⁶⁷ The spectra comparison with the $\text{Al}(\text{OTF})_3 + \text{LiCl}/\text{THF}$ solution is shown in (Figure 3.2c and d). The distinct broad-band centered around 490 cm^{-1} , observed for all measured concentrations of the AlCl_3/THF solutions, has been assigned to the $\nu(\text{Al} - \text{Cl})$ of $\text{AlCl}_3(\text{THF})_2$ and AlCl_4^- at 490 cm^{-1} and 494 cm^{-1} , respectively.⁶⁷ Comparatively, our DFT calculations suggest a peak for the $\nu_{\text{as}}(\text{Al} - \text{Cl})$ at 476 and 488 cm^{-1} for the trans- $\text{AlCl}_3(\text{THF})_2$ and a peak for the triply degenerate $\nu_{\text{as}}(\text{Al} - \text{Cl})$ of AlCl_4^- at 477 cm^{-1} . Surprisingly, these peaks are absent in the 1:3 and 1:4 electrolytes, yet a weak-intensity peak is observed at 490 cm^{-1} for the 1:5 electrolyte. These intriguing disparities suggest that the peak at 490 cm^{-1} is attributed to $\text{AlCl}_3(\text{THF})_2$ rather than AlCl_4^- . The absence of a peak at 477 cm^{-1} associated with AlCl_4^- is probably due to the strong perturbation of the tetrahedral symmetry of AlCl_4^- caused by the presence of excess amounts of Li^+ , a phenomenon which has previously been reported for LiAlCl_4 melts.⁷⁷

Additionally, DFT calculations suggest that the most thermodynamically favored reaction is that of AlCl_3 and Cl^- to produce AlCl_4^- (Table 3.3). To confirm the presence of AlCl_4^- in these electrolytes, the 800-1800 cm^{-1} regions of the spectra shown in Figure 3.2d were examined. A broad peak $\sim 1640 \text{ cm}^{-1}$ emerges at 1:3 mole ratios, this peak is also present in dilute (0.1M) and concentrated (0.75M) AlCl_3/THF solutions. A similar band has been reported for AlCl_4^- analogs,⁷⁸ which supports assigning this peak to AlCl_4^- .

In accordance with these findings, we propose the following dissociation mechanisms for the reaction between $\text{Al}(\text{OTF})_3$ and LiCl in THF at 1:3 mole ratio:



Only when the amount of LiCl added to a 0.1M $\text{Al}(\text{OTF})_3/\text{THF}$ solution exceeded a 1:4 molar ratio, a peak appeared at 490 cm^{-1} , indicating that an equilibrium exists between $\text{AlCl}_3(\text{THF})_2$ and AlCl_4^- with the former being produced only when substantial amounts of AlCl_4^- have formed. This observation can be supported by the fact that THF is a much weaker Lewis base than Cl^- .

Moreover, the weak-intensity peak observed at $\sim 381 \text{ cm}^{-1}$ in the 1:2 solutions, concealed by an overlapping broad-band from LiOTF at higher mole ratios, is probably associated with $[\text{AlCl}_2(\text{THF})_4]^+$, previously reported $\sim 360 \text{ cm}^{-1}$.⁶⁷ The broad peak at 407 cm^{-1} is attributed to $\nu(\text{Al} - \text{O})$ ⁶⁷ as supported by our DFT calculations for $\text{AlCl}_3(\text{THF})$ (Table 3.1). Other bands attributed to this complex according to our DFT calculations are the peak at $\sim 524 \text{ cm}^{-1}$ (Figure 3.2c) associated with $\nu_{\text{as}}(\text{Al} - \text{Cl})$, and the peak at 880 cm^{-1} (Figure 3.2d) associated with $\nu(\text{Al} - \text{O})$ coupled with $\tau(\text{CH}_2)$ (Table 3.1).

Finally, the vibrational frequencies of polymeric AlCl_4^- , namely Al_2Cl_7^- and $\text{Al}_3\text{Cl}_{10}^-$ were calculated using DFT. Our results indicate that both species would have bands in the 200-600 cm^{-1} region. Although several peaks are observed at various concentrations in said region, it's highly unlikely that these peaks are attributable to polymeric AlCl_4^- . The only report of such species in similar systems, to our knowledge, is that of AlCl_3/GBL solutions where the presence of $\text{Al}_3\text{Cl}_{10}^-$ was proposed at considerably high concentrations.⁵⁵ Thus, polymerization of AlCl_4^- in THF, although possible, is unlikely to occur in dilute solutions (<1M), such as those studied here.

To evaluate the electrochemical behavior of these electrolytes, cyclic voltammetry (CV) experiments were performed for 0.1M $\text{Al}(\text{OTF})_3/\text{THF}$, 1:3 $\text{Al}(\text{OTF})_3 + \text{LiCl}/\text{THF}$ and 0.1M AlCl_3/THF using a gold working electrode in a standard three electrode setup, the results of which are shown in (Figure 3.3). The CV for 0.1M $\text{Al}(\text{OTF})_3/\text{THF}$ electrolyte (Figure 3.3a) reveals the electrochemical reduction of Al-ions with an onset reduction potential ca. +0.15V (vs. Al/Al^{3+}). The addition of LiCl at a 1:3 mole ratio (Figure 3.3b) results in a shift in reduction potential to ca. +0.4V along with a dramatic increase in current, suggesting more facile Al electrodeposition in Cl^- rich environment, similar to shifts observed in the magnesium aluminum chloride complex electrolyte.⁷⁹

This electrolyte also exhibits a broad cathodic wave that extends beyond -1V, possibly due to co-deposition of Li which is expected around this potential versus the Al wire. CV measurements for the 1:2 mole solution were hindered by the formation of a gas bubble on the surface of the gold electrode, whereas the 1:4 and 1:5 solutions exhibited a similar CV profile to that of the 1:3 electrolyte (Supporting Information Figure 3.7).

In contrast, the AlCl_3/THF electrolyte exhibits a non-diffusion controlled electrochemical reduction ca. 0V for the 0.1M solution (Figure 3.3c) while a drastic shift in reduction potential is evident at higher concentrations (0.75M) (inset of Figure 3.3c). Two adjoint cathodic waves are observed ca. +0.25V, which we attribute to the electrochemical reduction of Al-ions. The shift in electrochemical activity as a function of increasing AlCl_3/THF concentration is shown in (Supporting Information Figure 3.6). While the CVs appear to demonstrate underpotential deposition (UPD) in all three electrolytes, this is likely an artifact stemming from using a pseudoreference electrode (an aluminum wire with an uncontrolled/unknown surface) rather than true UPD. However, the positive shift in reduction potential for the AlCl_3/THF and 1:3 electrolyte clearly reveals that electrochemical reduction of Cl^- containing Al species is less energy demanding suggesting that Cl^- significantly enhance the electrochemical activity of Al-ions.

Additionally, an anodic peak is evident ca. +0.8V in the most concentrated AlCl_3/THF solutions, this oxidative feature may have arisen as a result of partial Al-stripping caused by the increased acidity of the solution, likely due to the formation of $\text{AlCl}_3(\text{THF})$ as we have previously revealed by DFT/FTIR analyses.

To further understand the nature of the acidic environment causing these immense differences in electrochemical behavior of Al-ions in the Cl^- rich environments (1:3 electrolyte and 0.75M AlCl_3/THF), a clear description of the ionic profile of both electrolytes is necessary. According to previously discussed spectroscopy analyses, the electrochemically active Al species in the 1:3 electrolyte is likely the anionic species AlCl_4^- arising from ligand transfer which is promoted by excess amounts of LiCl. In this system, AlCl_4^- is associated with Li – OTF CIP. Comparatively, Al speciation in AlCl_3/THF is much more diverse, and the origin of AlCl_4^- is intricate. It is well known that AlCl_3 dimers may undergo symmetric and/or asymmetric cleavage when dissolved in ethereal organic solvents.^{57,80} While DFT calculations revealed that both processes are equally plausible in THF,⁸¹ experimental evidence repeatedly corroborates that these solutions are dominated by $\text{AlCl}_3(\text{THF})_2$.^{79,82}

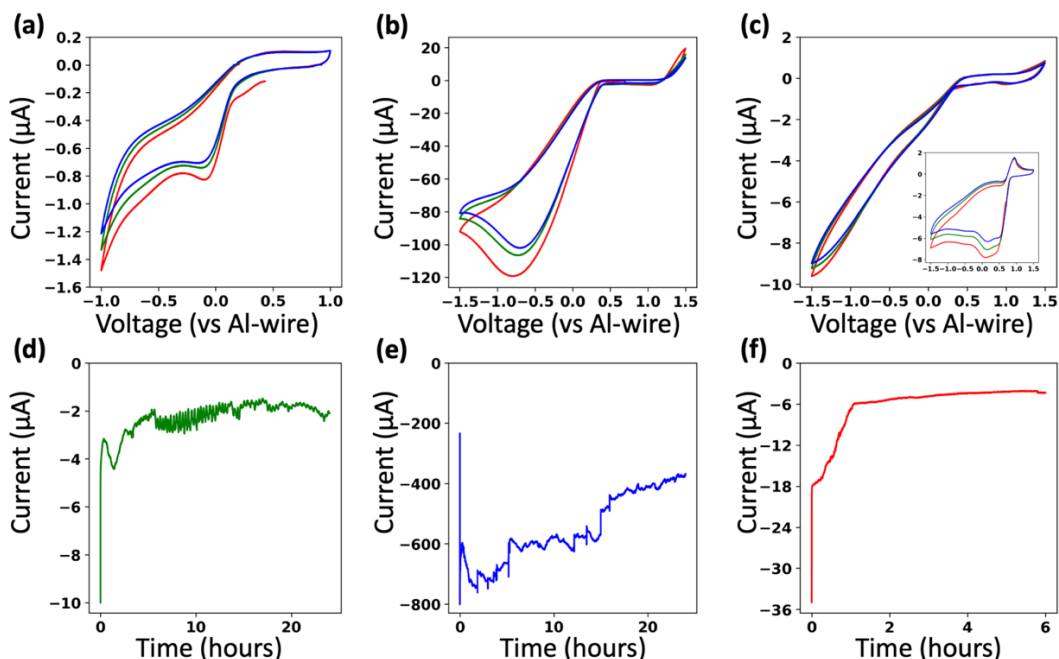


Figure 3.3 Cyclic voltammograms (first scan is red, second is green, and third is blue) on gold working electrode at 50 mV/s scan rate for (a) 0.1M Al(OTF)₃/THF, (b) 1:3 Al(OTF)₃:LiCl/THF and (c) 0.1M AlCl₃/THF with inset showing 0.75M AlCl₃/THF corresponding chronoamperograms on Cu-substrate of (d) 0.1M Al(OTF)₃/THF at 0V, (e) 1:3 Al(OTF)₃:LiCl/THF at +0.25V and (f) 0.1M AlCl₃/THF at +0.25V (vs. Al/Al³⁺). © 2022 American Chemical Society.

Interestingly, temperature dependant NMR spectroscopy for this system suggested that AlCl₃(THF)₂ undergoes self ionization to produce [AlCl₄⁻][AlCl₂⁺(THF)₄].^{67,83} Hence, the acidic character of the AlCl₃/THF solution is perhaps also due to ionic association of the AlCl₄⁻ to the highly acidic [AlCl₂⁺(THF)₄] rather than the charge neutral Li – OTF CIP.

To gauge the likelihood of aluminum deposition, chronoamperometry was carried out on these three systems, in dilute solutions ([Al]=0.1M) using a Cu foil substrate in a standard three electrode setup. Chronoamperograms corresponding to Al-plating from 0.1M Al(OTF)₃/THF, 1:3 Al(OTF)₃:LiCl/THF and 0.1M AlCl₃/THF are shown in (Figure 3.3d, e and f), respectively. The potential for the Al(OTF)₃/THF electrolyte was set to 0V vs. (Al/Al³⁺), whereas the potential for the AlCl₃/THF and 1:3 electrolyte was set to +0.25V (vs. Al/Al³⁺). Over the course of these chronoamperometry experiment, a cathodic current was obtained for all three electrolytes. Despite the significantly lower electrodeposition potential of the 1:3 electrolyte, the measured current in this electrolyte is at least 2 orders of magnitudes higher than that of the Al(OTF)₃/THF electrolyte. The total charge passed was calculated by integrating the chronoamperometry curves, and was found to be -196.3 mC, -47.47 C, and -134.2 mC for the Al(OTF)₃/THF, 1:3 Al(OTF)₃ + LiCl/THF and AlCl₃/THF electrolytes, respectively.

The oscillations in the reductive currents observed only in the 0.1M Al(OTF)₃/THF and 1:3 Al(OTF)₃:LiCl/THF are probably associated with the reductive decomposition of free anionic ligands (OTF⁻, Cl⁻) which are absent from the AlCl₃/THF electrolyte.

A similar observation occurring during potentiostatic zinc (Zn) deposition from $\text{Zn}(\text{TFSI})_2$ and ZnCl_2 electrolytes has been reported.⁸⁴ Furthermore, the gradual decrease in current in the 1:3 $\text{Al}(\text{OTF})_3$: LiCl/THF is likely attributed to the decrease in active surface area of the Cu substrate and/or depletion of Al cations due to more facile Al deposition from this electrolyte.

To confirm that the reductive processes observed in cyclic voltammetry and chronoamperometry plots correspond to electrochemical reduction of Al-ions to Al-metal, a scanning electron microscope (SEM) was used to evaluate the surface morphology of the Cu substrates. (Figure 3.4) shows a series of SEM images of an untreated Cu substrate (a,b), Al deposits obtained from $\text{Al}(\text{OTF})_3/\text{THF}$ (c,d), 1:3 electrolyte (e,f), and AlCl_3/THF (g-h). Low magnification SEM images (Supporting Information Figure 3.9) show that the 1:3 electrolyte exhibits high corrosivity as evident by the dark pits on the surface of the Al/Cu. High magnification SEM imaging for the Al deposits obtained from $\text{Al}(\text{OTF})_3/\text{THF}$ reveal that these deposits undergo structural rearrangement during deposition to form streaks of nanoparticle agglomerates as shown in (Supporting Information Figure 3.10) probably due to the non-homogenous surface of the Cu substrates.

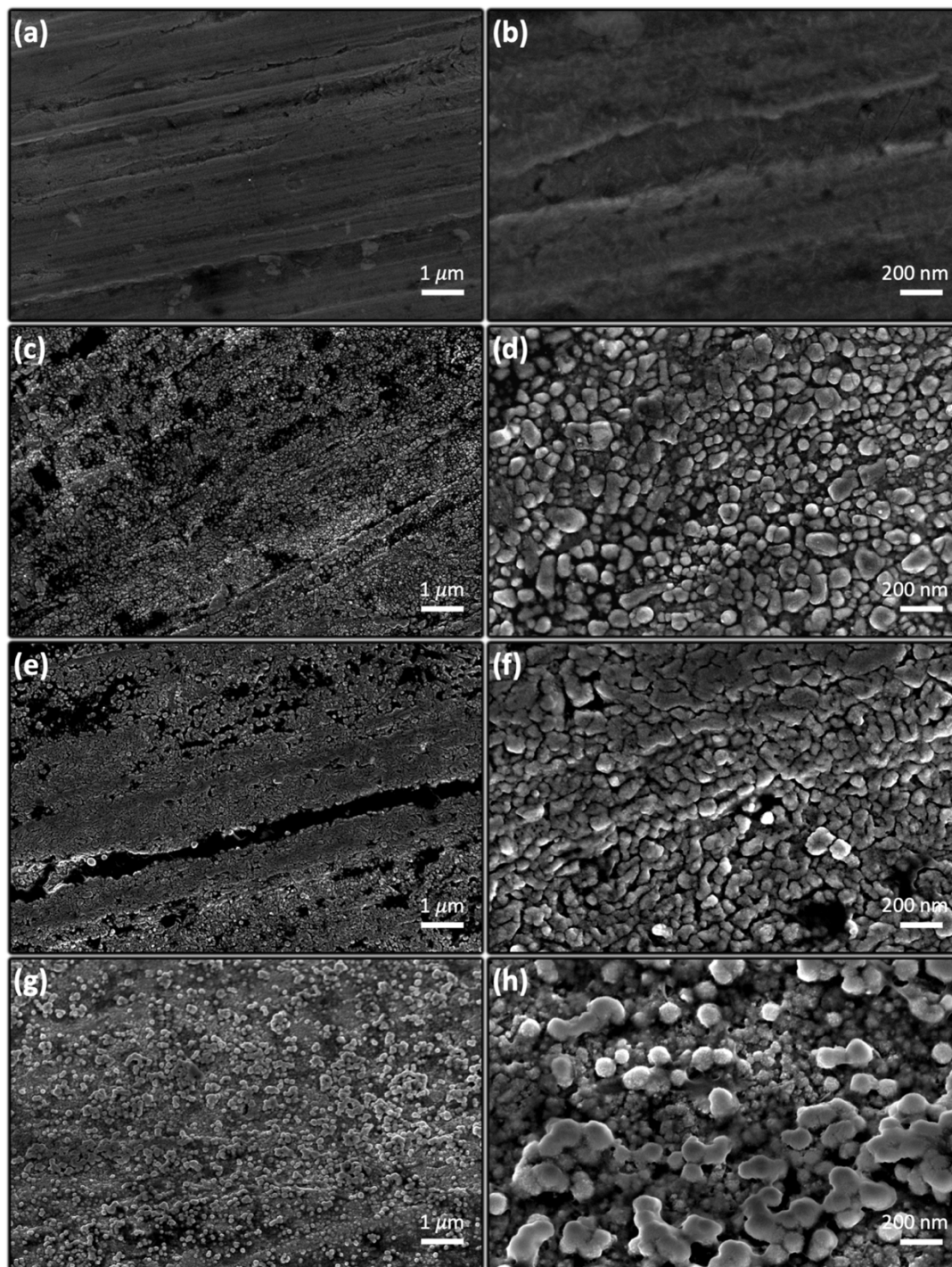


Figure 3.4 SEM images of (a-b) untreated Cu substrate, Al electrodeposits on Cu-substrate (vs. Al/Al^{3+}) obtained from (c-d) 0.1M $Al(OTf)_3/THF$ at 0V for 24 hours, (e-f) 1:3 $Al(OTf)_3:LiCl/THF$ at +0.25V for 24 hours and (g-h) 0.1M $AlCl_3/THF$ at +0.25V for 6 hours. © 2022 American Chemical Society.

3.4 Conclusion

In summary, FTIR measurements complemented by DFT calculations provided unique insight into Al complex ion formation in Cl^- free ($\text{Al}(\text{OTF})_3/\text{THF}$) and Cl^- rich (AlCl_3/THF and $\text{Al}(\text{OTF})_3 + \text{LiCl}/\text{THF}$) environments. The spectral features associated with the OTF^- anion were highlighted for the purpose of measuring the effect of Cl^- on Al-ion speciation and subsequently, the electrochemical behavior of Al-ions. At the cost of high corrosivity, Cl^- significantly enhances the electrochemical activity of Al-ions. Spectral analyses coupled with CV measurements for the Cl^- rich systems suggest that a sufficiently acidic ionic environment may enable stripping of Al in THF. Finally, Al nanoparticles were deposited potentiostatically from dilute solutions ($[\text{Al}]=0.1\text{M}$) of all three systems.

3.5 Outlook

Organic electrolytes for rechargeable Al battery application are generally overlooked due to their volatility and high flammability. However, operational organic electrolytes typically comprise of concentrated electrolytes where the effect of free solvent is diminished leading to low volatility.⁵³ With regards to the flammability of these systems, this hurdle may be overcome by exploring additives that inhibit flammability via routes similar to those investigated for Li-ion⁸⁵ and Na-ion⁸⁶ electrolytes. We speculate that Al can be electrochemically deposited from organic solvents of similar properties using $\text{Al}(\text{OTF})_3$. Extending this work to other systems while exploring numerous additives may provide profound understanding of Al-anion and Al-solvent interactions which could potentially lead to an optimized, non-corrosive and safe organic electrolyte for practical rechargeable Al battery application.

3.6 Supporting Information

Table 3.1 Measured and computed vibrational frequencies of aluminum complexes. ν = bond stretch, τ = twisting, δ = group angle deformation, subscript s = symmetric, subscript as = asymmetric, $\text{OTF}^- = \text{CF}_3\text{SO}_3^-$.

Species	Mode	Computed (cm^{-1})	Measured (cm^{-1})	Literature
$[\text{Al}(\text{THF})_5]^{3+}$	$\nu(\text{Al} - \text{O})$ $+ \tau(\text{CH}_2)$	885.49	883	This work
$[\text{Al}(\text{THF})_4(\text{OTF})]^{2+}$	$\nu(\text{Al} - \text{O})$ $+ \tau(\text{CH}_2)$	885.72	883	This work
	Inner sphere $\nu(\text{C} - \text{S}) + \nu_s\text{SO}_3$	1214.78	1210	This work
$[\text{Al}(\text{THF})_4(\text{OTF})][(\text{OTF})]^{1+}$	$\nu(\text{Al} - \text{O})$ $+ \tau(\text{CH}_2)$	886.00	883	This work
	Inner sphere $\nu(\text{C} - \text{S}) + \nu_s\text{SO}_3$	1210.21	1210	This work
	Outer sphere $\nu_{as}\text{SO}_3$	1238.28	1238	This work and our previous work ⁶³
	Inner sphere $\nu_{as}\text{SO}_3$	1319.50	1307	This work and our previous work ⁶³
$[\text{Al}(\text{THF})_4(\text{OTF})][(\text{OTF})_2]$	$\nu(\text{Al} - \text{O})$ $+ \tau(\text{CH}_2)$	880.20	883	This work
	Outer sphere $\nu(\text{C} - \text{S}) + \nu_s\text{SO}_3$	1218.82 1219.14	1220	This work
$[\text{Al}(\text{THF})_3(\text{OTF})_2]^{1+}$	$\nu(\text{Al} - \text{O})$ $+ \tau(\text{CH}_2)$	886.78	883	This work
		888.64		
	Inner sphere $\nu(\text{C} - \text{S}) + \nu_s\text{SO}_3$	1211.99	1210	This work
		1216.32		
Inner sphere $\nu_{as}\text{SO}_3$	1343.23	1350		

		1316.50	1307	
$[Al(THF)_2(OTF)_2]^{1+}$	$\nu(Al - O)$ $+ \tau(CH_2)$	898.45	883	This work
	Inner sphere $\nu(C - S) + \nu_s SO_3$	1214.35	1210	
		1216.12		
	Inner sphere $\nu_{as} SO_3$	1351.58	1350	This work
1357.27				
Mixed Speciation	$\nu_{as}(CF_3)$ of free OTF^- (peak is independent of concentration), Inner sphere & outer sphere OTF^-	1172.00 – 1198.78	1164 (broad peak)	This work
Free OTF^-	$\nu_s SO_3$	-	1028	This work and our previous work ⁶³
$Al(OTF)_3$ Aggregate	-	-	1048	This work
$Li(THF)_3(OTF)$	Inner sphere $\nu_{as} SO_3$	1252.60	1253	This work
$Li - OTF$ contact ion pair	$\nu_{as} SO_3$	-	1254	Ref ⁷⁰
$Li - OTF$ Aggregate	-	-	1047	This work and ref ⁷³
	-	-	1269	This work
$AlCl_2^+(THF)_3$	$\nu_{as}(Al - Cl)$	524.29	524	This work
$AlCl_3(THF)$	$\nu(Al - O)$	427.01	417 (broad peak)	This work and ref ⁶⁷

	$\nu_{as}(Al - Cl)$	527.38	524	This work
	$\nu(Al - O)$ $+ \tau(CH_2)$	880.01	880	This work
<i>cis</i> - $AlCl_3(THF)_2$	-	-	329	Ref ⁶⁷
			407 (Broad peak)	
<i>trans</i> - $AlCl_3(THF)_2$	$\nu_{as}(Al - Cl)$	487.86	490	This work
		476.34		
	$\nu(Al - Cl)$	-	490	Ref ⁴
$AlCl_4^-$	$\nu_{as}(Al - Cl)$ Triply degenerate	477.45	-	This work
	$\nu(Al - Cl)$	-	494	Ref ⁶⁷
	-	-	1640	This work and ref ⁷⁸
$[AlCl_2^+(THF)_4]$	-	-	381	This work
	-	-	360	Ref ⁶⁷

Table 3.2 Predicted reaction energies from DFT calculations (OTF).

Reaction	Predicted Solvent Phase Reaction Energies(kJ/mol)
$Al^{3+} + 2THF + 2OTF \rightarrow Al(THF)_2(OTF)_2$	-1975
$Al^{3+} + 3THF + 2OTF \rightarrow Al(THF)_3(OTF)_2$	-1968

Table 3.3 Predicted reaction energies from DFT calculations (chloride)

Reaction	Predicted Solvent Phase Reaction Energies(kJ/mol)
$AlCl_3 + Cl^- \rightarrow AlCl_4^-$	-166
$AlCl_4^- + Cl^- \rightarrow AlCl_5^{2-}$	+91
$AlCl_3 + 2Cl^- \rightarrow AlCl_5^{2-}$	-75
$AlCl_4^- + THF \rightarrow AlCl_4^-(THF)$	+96
$AlCl_3 + 2THF \rightarrow AlCl_3(THF)_2$	-46
$AlCl_3 + THF \rightarrow AlCl_3THF$	-91
$Al_2Cl_6 + AlCl_4^- \rightarrow Al_3Cl_{10}^-$	+10
$2AlCl_3 + AlCl_4^- \rightarrow Al_3Cl_{10}^-$	-28
$AlCl_3 + AlCl_4^- \rightarrow Al_2Cl_7^-$	-25
$Al_2Cl_6 + Cl^- \rightarrow Al_2Cl_7^-$	-153
$AlCl_3 + AlCl_3 \rightarrow Al_2Cl_6$	-38
$AlCl_2^+(THF)_3 + Cl^- \rightarrow AlCl_3 + 3THF$	-77
$AlCl_2^+(THF)_2 + Cl^- \rightarrow AlCl_3 + 2THF$	-41
$Al_2Cl_6 + 4THF \rightarrow 2AlCl_3(THF)_2$	-54
$Al_2Cl_6 + 3THF \rightarrow AlCl_2^+(THF)_3 + AlCl_4^-$	-50
$Al_2Cl_6 + 2THF \rightarrow AlCl_2^+(THF)_2 + AlCl_4^-$	-86

Note: For both Tables 3.2 and 3.3 the predicted solvent phase reaction energies were calculated by subtracting the “sum of electronic and thermal free energies” of the reactants from that of the products for each reaction. Energies for all chloride containing molecules in table 3.3 were calculated in a similar manner to those of table 3.2. Positive values for predicted energies indicates a thermodynamically unstable species.

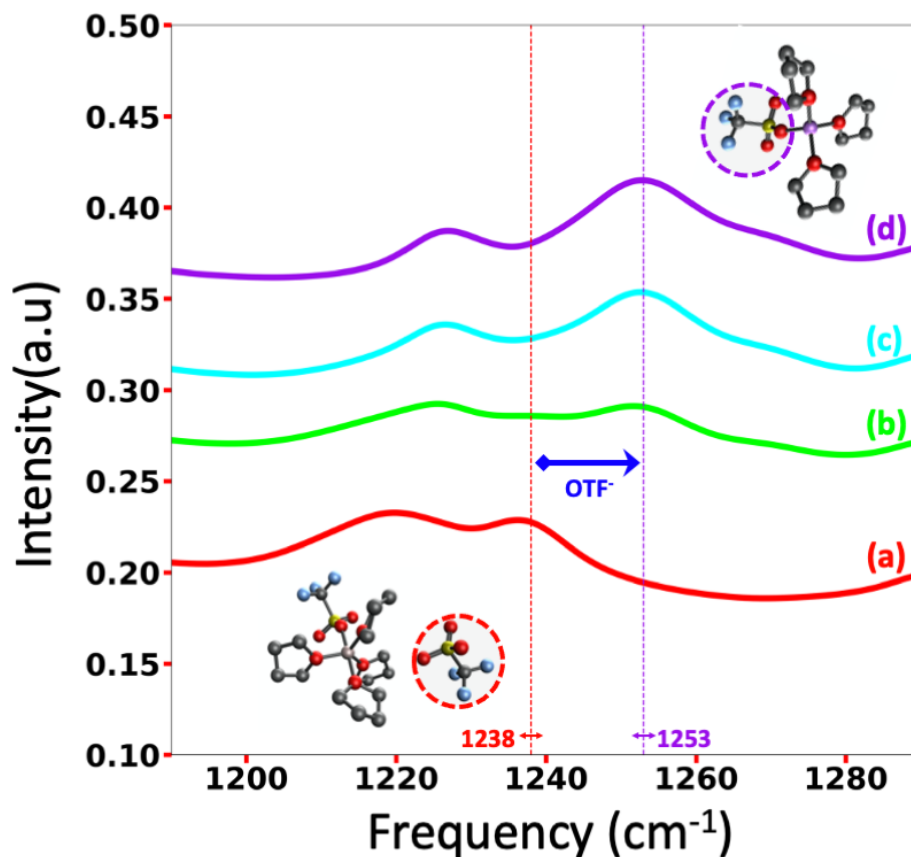


Figure 3.5 Illustration of OTF⁻ transfer from Al-cation to Li-cation. Illustration of measured and computed, $\nu_{as}SO_3$ peak shifting upon transfer of OTF⁻ from Al-cation to Li-cation due to the addition of LiCl to a 0.1M Al(OTF)₃/THF electrolyte. (a) 0.1M Al(OTF)₃/THF, (b) 1:2 Al(OTF)₃:LiCl/THF, (c) 1:3 Al(OTF)₃:LiCl/THF, and (d) 0.4M LiOTF/THF.

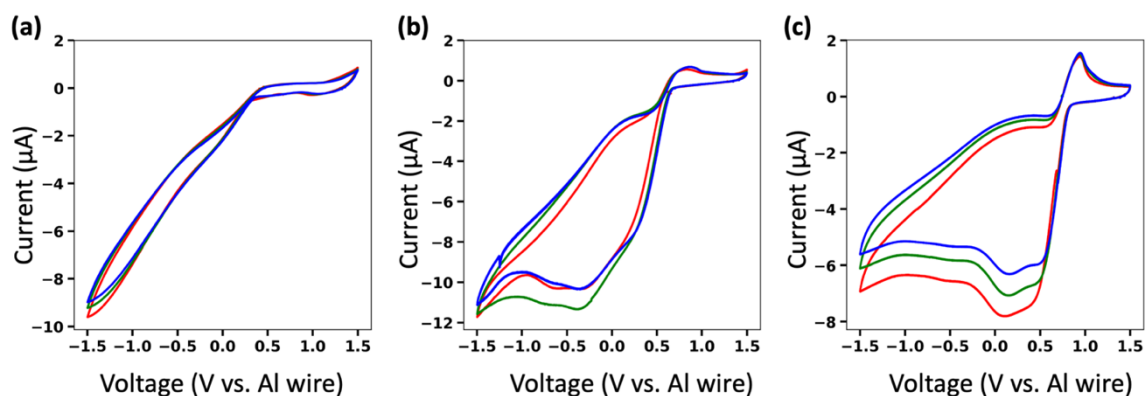


Figure 3.6 Cyclic voltammogram shift as function of increasing concentration of AlCl₃ in THF Showing the shift in onset of electrochemical reduction potential as concentration is increased (a) 0.1M, (b) 0.4M, and (c) 0.75M.

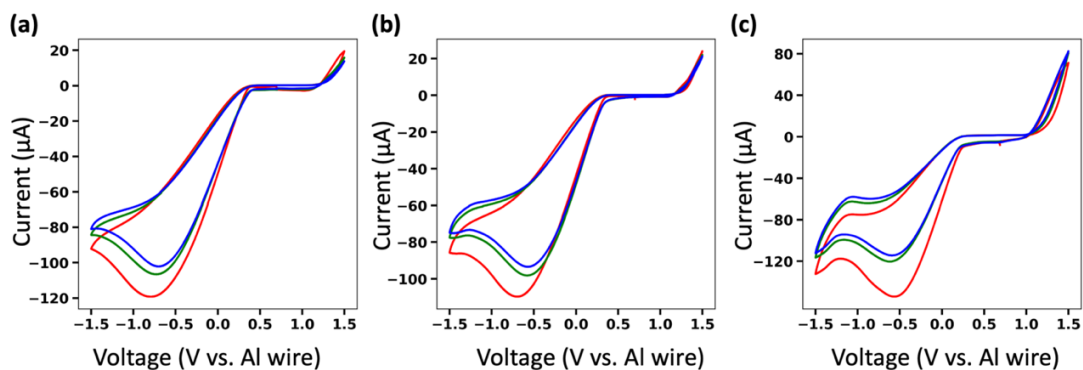


Figure 3.7 Cyclic voltammogram of $\text{Al}(\text{OTF})_3$ and LiCl in THF at various mole ratios Showing the similarity in CV profiles for (a) 1:3 $\text{Al}(\text{OTF})_3$: LiCl , (b) 1:4 $\text{Al}(\text{OTF})_3$: LiCl , and (c) 1:5 $\text{Al}(\text{OTF})_3$: LiCl electrolytes.

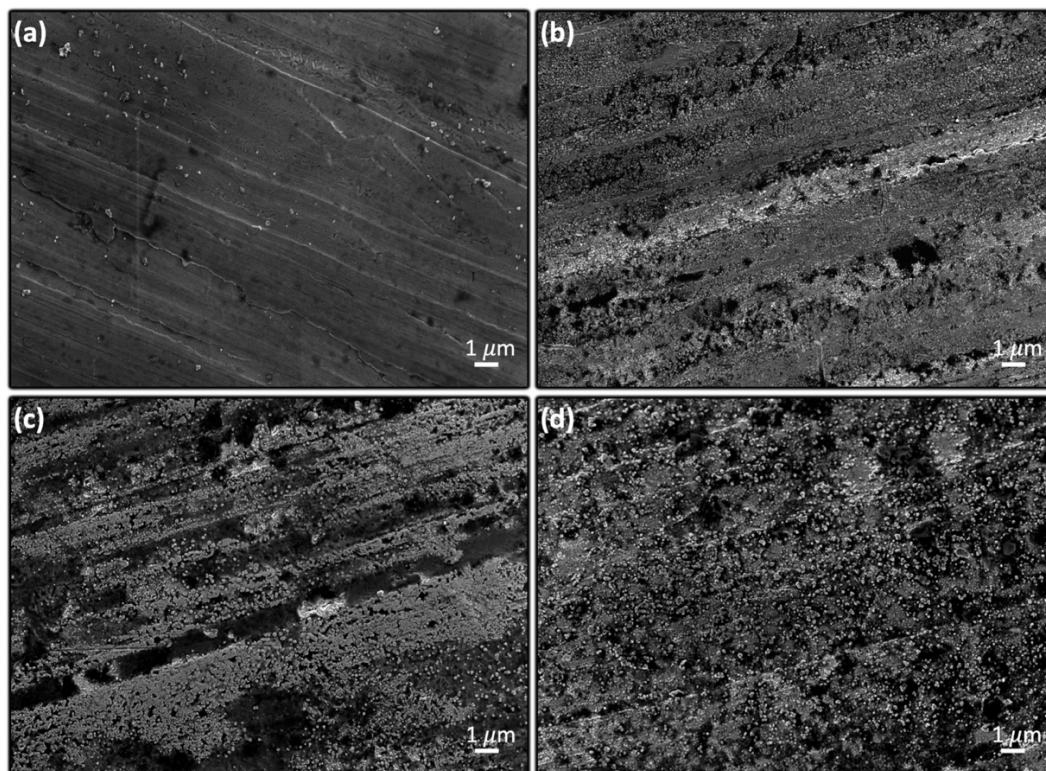


Figure 3.8 Low magnification SEM images (a) Untreated Cu substrate, Al electrodeposits on Cu-substrate (vs. Al/Al^{3+}) obtained from (b) 0.1M $\text{Al}(\text{OTF})_3/\text{THF}$ at 0V for 24 hours, (c) 1:3 $\text{Al}(\text{OTF})_3$: LiCl/THF at +0.25V for 24 hours, (d) 0.1M AlCl_3/THF at +0.25V for 6 hours.

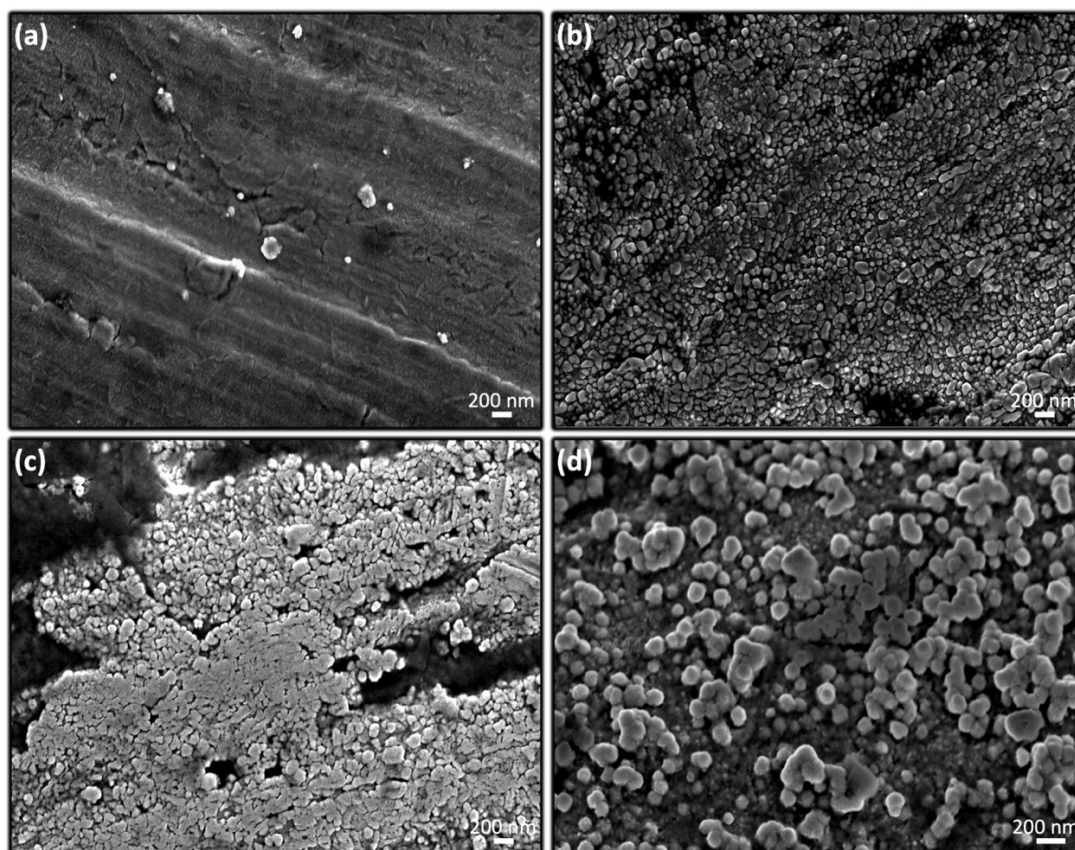


Figure 3.9 High magnification SEM images of Al nanodeposits. (a) Untreated Cu substrate, Al electrodeposits on Cu-substrate (vs. Al/Al^{3+}) obtained from (b) 0.1 M $\text{Al}(\text{OTf})_3/\text{THF}$ at 0V for 24 hours, (c) 1:3 $\text{Al}(\text{OTf})_3:\text{LiCl}/\text{THF}$ at +0.25V for 24 hours, (d) 0.1 M AlCl_3/THF at +0.25V for 6 hours.

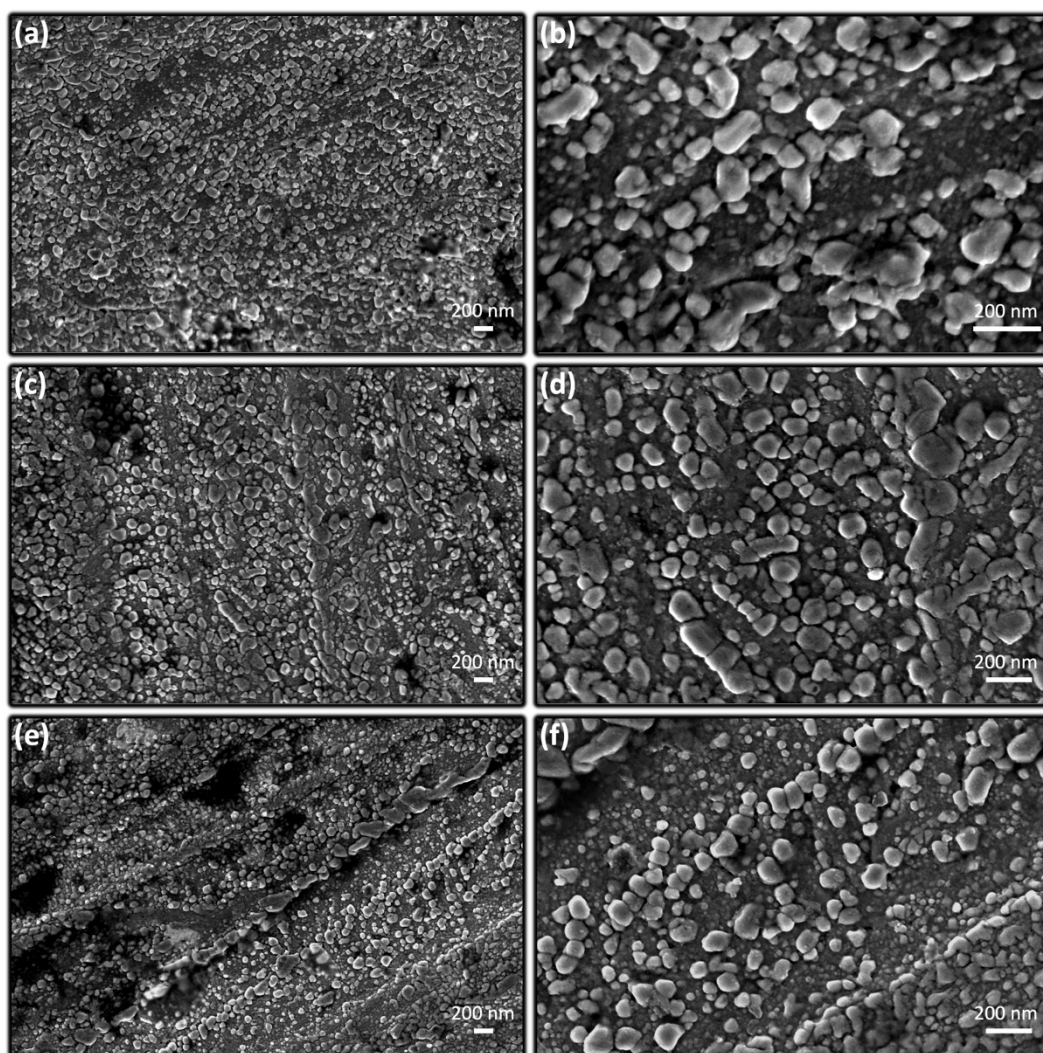


Figure 3.10 SEM images of chloride-free Al electrodeposits from 0.1M solution. Showing low magnification (a, c, and e) and corresponding high magnification (b, d, and f) SEM images of electrochemically deposited aluminum nanoparticles from the 0.1M $\text{Al}(\text{OTf})_3/\text{THF}$ on the Cu-substrate.

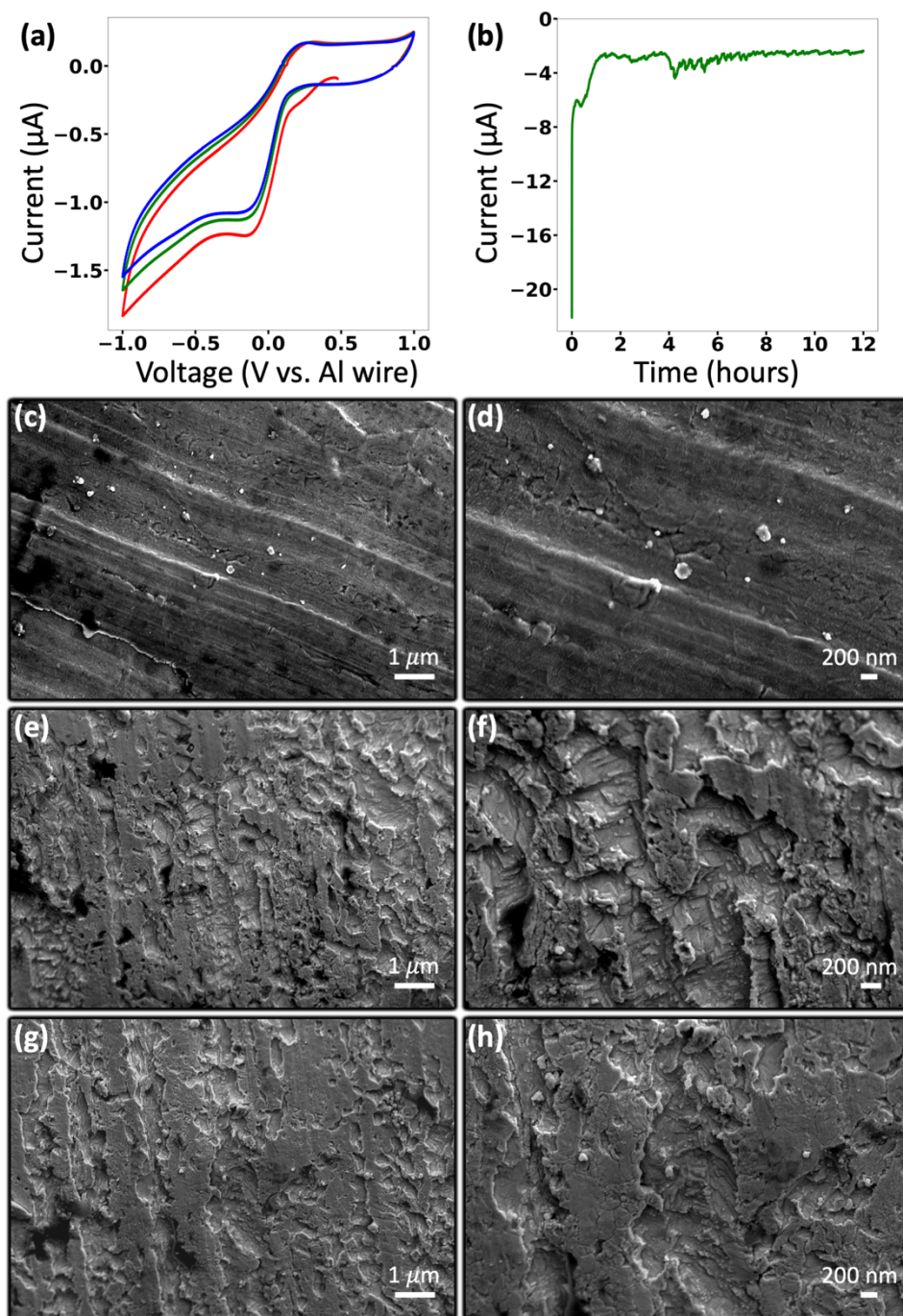


Figure 3.11 Chloride-free aluminum electroplating from 0.2M solution. Showing (a) cyclic voltammogram on gold working electrode at 50 mV/s scan rate for 0.2M $\text{Al}(\text{OTF})_3/\text{THF}$, corresponding (b) chronoamperogram on a Cu-substrate at -0.1V vs. $(\text{Al}/\text{Al}^{3+})$ for 12 hours. Low (c) and high (d) magnification SEM images of untreated

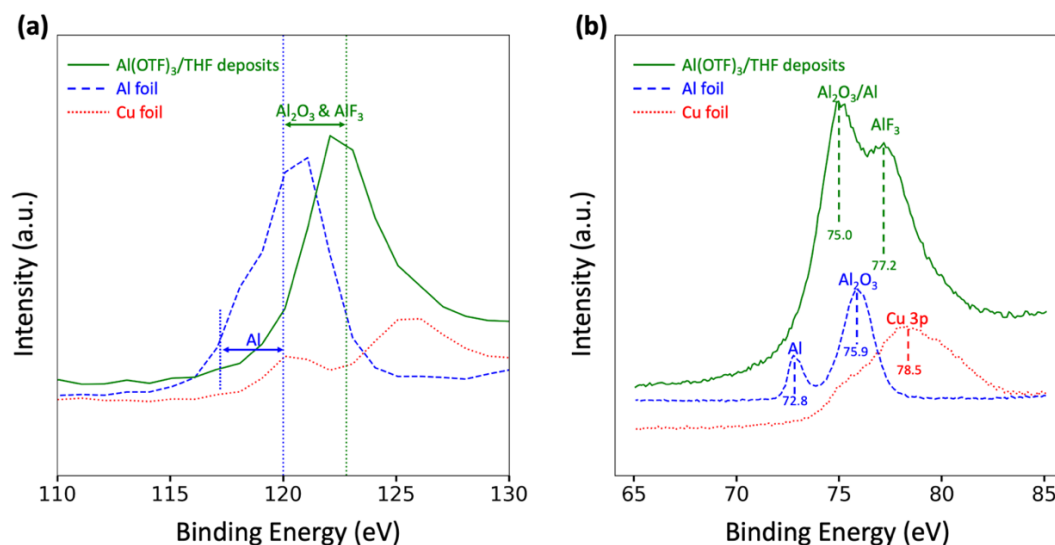
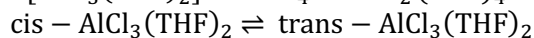
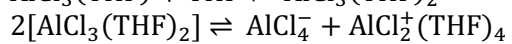


Figure 3.12 X-ray photoelectron spectroscopy (XPS) spectra of Al-deposits from $\text{Al}(\text{OTF})_3$ Electrolyte. Showing (a) Al (2s) and (b) Al (2p) XPS regions for: Al deposit obtained by electrodeposition of Al from a 0.1M $\text{Al}(\text{OTF})_3/\text{THF}$ electrolyte at 0 V vs. Al wire for 72 hours (green line curve), control Al foil (blue dashed curve), and untreated Cu substrate (red dotted curve).

Table 3.4 Comparison of measured Al (2p) binding energies (eV) to literature values

This work	Ref. ⁵⁹
72.8	72.6 (Al metal)
75.0	74.8 ($\text{Al}_2\text{O}_3/\text{Al}$)
75.9	75.8 (Al_2O_3)
77.2	77.0 (AlF_3)
78.5 (Cu3p)	-

Dissociation mechanism proposed by Derouault *et al.*⁶⁷



3.7 References

- (1) Jaffe, S. Vulnerable Links in the Lithium-Ion Battery Supply Chain. *Joule* **2017**, *1* (2), 225–228.
- (2) Olivetti, E. A.; Ceder, G.; Gaustad, G. G.; Fu, X. Lithium-Ion Battery Supply Chain Considerations: Analysis of Potential Bottlenecks in Critical Metals. *Joule* **2017**, *1* (2), 229–243.
- (3) Liang, Y.; Dong, H.; Aurbach, D.; Yao, Y. Current Status and Future Directions of Multivalent Metal-Ion Batteries. *Nat. Energy* **2020**, *5* (9), 646–656.
- (4) Li, M.; Lu, J.; Ji, X.; Li, Y.; Shao, Y.; Chen, Z.; Zhong, C.; Amine, K. Design Strategies for Nonaqueous Multivalent-Ion and Monovalent-Ion Battery Anodes. *Nat. Rev. Mater.* **2020**, *5* (4), 276–294.
- (5) Muldoon, J.; Bucur, C. B.; Gregory, T. Quest for Nonaqueous Multivalent Secondary Batteries: Magnesium and Beyond. *Chem. Rev.* **2014**, *114* (23), 11683–11720.
- (6) Tu, J.; Song, W.-L.; Lei, H.; Yu, Z.; Chen, L.-L.; Wang, M.; Jiao, S. Nonaqueous Rechargeable Aluminum Batteries: Progresses, Challenges, and Perspectives. *Chem. Rev.* **2021**, *121* (8), 4903–4961.
- (7) Faegh, E.; Ng, B.; Hayman, D.; Mustain, W. E. Practical Assessment of the Performance of Aluminium Battery Technologies. *Nat. Energy* **2021**, *6* (1), 21–29.
- (8) Zafar, Z. A.; Imtiaz, S.; Razaq, R.; Ji, S.; Huang, T.; Zhang, Z.; Huang, Y.; Anderson, J. A. Cathode Materials for Rechargeable Aluminum Batteries: Current Status and Progress. *J. Mater. Chem. A* **2017**, *5* (12), 5646–5660.
- (9) Wu, F.; Yang, H.; Bai, Y.; Wu, C. Paving the Path toward Reliable Cathode Materials for Aluminum-Ion Batteries. *Adv. Mater.* **2019**, *31* (16), 1806510.
- (10) Leung, O. M.; Schoetz, T.; Prodromakis, T.; de León, C. P. Progress in Electrolytes for Rechargeable Aluminium Batteries. *J. Electrochem. Soc.* **2021**, *168* (5), 056509.
- (11) Zhang, Y.; Liu, S.; Ji, Y.; Ma, J.; Yu, H. Emerging Nonaqueous Aluminum-Ion Batteries: Challenges, Status, and Perspectives. *Adv. Mater.* **2018**, *30* (38), 1706310.
- (12) Jayaprakash, N.; Das, S. K.; Archer, L. A. The Rechargeable Aluminum-Ion Battery. *Chem. Commun.* **2011**, *47* (47), 12610–12612.
- (13) Reed, L. D.; Menke, E. The Roles of V₂O₅ and Stainless Steel in Rechargeable Al-Ion Batteries. *J. Electrochem. Soc.* **2013**, *160* (6), A915–A917.
- (14) Geng, L.; Lv, G.; Xing, X.; Guo, J. Reversible Electrochemical Intercalation of Aluminum in Mo₆S₈. *Chem. Mater.* **2015**, *27* (14), 4926–4929.
- (15) Lin, M.-C.; Gong, M.; Lu, B.; Wu, Y.; Wang, D.-Y.; Guan, M.; Angell, M.; Chen, C.; Yang, J.; Hwang, B.-J.; Dai, H. An Ultrafast Rechargeable Aluminium-Ion Battery. *Nature* **2015**, *520* (7547), 324–328.
- (16) Gao, T.; Li, X.; Wang, X.; Hu, J.; Han, F.; Fan, X.; Suo, L.; Pearse, A. J.; Lee, S. B.; Rubloff, G. W.; Gaskell, K. J. A Rechargeable Al/S Battery with an Ionic-Liquid Electrolyte. *Angew. Chem., Int. Ed.* **2016**, *128* (34), 10052–10055.
- (17) Stadie, N. P.; Wang, S.; Kravchyk, K. V.; Kovalenko, M. V. Zeolite-Templated Carbon as an Ordered Microporous Electrode for Aluminum Batteries. *ACS Nano* **2017**, *11* (2), 1911–1919.
- (18) Elia, G. A.; Hasa, I.; Greco, G.; Diemant, T.; Marquardt, K.; Hoepfner, K.; Behm, R. J.; Hoell, A.; Passerini, S.; Hahn, R. Insights into the Reversibility of Aluminum Graphite Batteries. *J. Mater. Chem. A* **2017**, *5* (20), 9682–9690.

- (19) Kravchyk, K. V.; Wang, S.; Piveteau, L.; Kovalenko, M. V. Efficient Aluminum Chloride–Natural Graphite Battery. *Chem. Mater.* **2017**, *29* (10), 4484–4492.
- (20) Tian, H.; Zhang, S.; Meng, Z.; He, W.; Han, W.-Q. Rechargeable Aluminum/Iodine Battery Redox Chemistry in Ionic Liquid Electrolyte. *ACS Energy Lett.* **2017**, *2* (5), 1170–1176.
- (21) Walter, M.; Kravchyk, K. V.; Böfer, C.; Widmer, R.; Kovalenko, M. V. Polypyrenes as High-Performance Cathode Materials for Aluminum Batteries. *Adv. Mater.* **2018**, *30* (15), 1705644.
- (22) Wang, S.; Kravchyk, K. V.; Filippin, A. N.; Müller, U.; Tiwari, A. N.; Buecheler, S.; Bodnarchuk, M. I.; Kovalenko, M. V. Aluminum Chloride-Graphite Batteries with Flexible Current Collectors Prepared from Earth-Abundant Elements. *Adv. Sci.* **2018**, *5* (4), 1700712.
- (23) Muñoz-Torrero, D.; Leung, P.; García-Quismondo, E.; Ventosa, E.; Anderson, M.; Palma, J.; Marcilla, R. Investigation of Different Anode Materials for Aluminium Rechargeable Batteries. *J. Power Sources* **2018**, *374*, 77–83.
- (24) Chen, H.; Xu, H.; Wang, S.; Huang, T.; Xi, J.; Cai, S.; Guo, F.; Xu, Z.; Gao, W.; Gao, C. Ultrafast All-Climate Aluminum-Graphene Battery with Quarter-Million Cycle Life. *Sci. Adv.* **2017**, *3* (12), eaao7233.
- (25) Yang, C.; Wang, S.; Zhang, X.; Zhang, Q.; Ma, W.; Yu, S.; Sun, G. Substituent Effect of Imidazolium Ionic Liquid: A Potential Strategy for High Coulombic Efficiency Al Battery. *J. Phys. Chem. C* **2019**, *123* (18), 11522–11528.
- (26) Kim, D. J.; Yoo, D.-J.; Otley, M. T.; Prokofjevs, A.; Pezzato, C.; Owczarek, M.; Lee, S. J.; Choi, J. W.; Stoddart, J. F. Rechargeable Aluminium Organic Batteries. *Nat. Energy* **2019**, *4* (1), 51–59.
- (27) Zhou, Q.; Wang, D.; Lian, Y.; Hou, S.; Ban, C.; Wang, Z.; Zhao, J.; Zhang, H. Rechargeable Aluminum-Ion Battery with Sheet-like MoSe₂@ C Nanocomposites Cathode. *Electrochim. Acta* **2020**, *354*, 136677.
- (28) Zhao, Q.; Zheng, J.; Deng, Y.; Archer, L. Regulating the Growth of Aluminum Electrodeposits: Towards Anode-Free Al Batteries. *J. Mater. Chem. A* **2020**, *8* (44), 23231–23238.
- (29) Wang, H.; Gu, S.; Bai, Y.; Chen, S.; Zhu, N.; Wu, C.; Wu, F. Anion-Effects on Electrochemical Properties of Ionic Liquid Electrolytes for Rechargeable Aluminum Batteries. *J. Mater. Chem. A* **2015**, *3* (45), 22677–22686.
- (30) Lai, P. K.; Skyllas-Kazacos, M. Electrodeposition of Aluminium in Aluminium Chloride/1-Methyl-3-Ethylimidazolium Chloride. *J. Electroanal. Chem* **1988**, *248* (2), 431–440.
- (31) Carlin, R. T.; Crawford, W.; Bersch, M. Nucleation and Morphology Studies of Aluminum Deposited from an Ambient-Temperature Chloroaluminate Molten Salt. *J. Electrochem. Soc.* **1992**, *139* (10), 2720.
- (32) Yang, H.; Li, H.; Li, J.; Sun, Z.; He, K.; Cheng, H.-M.; Li, F. The Rechargeable Aluminum Battery: Opportunities and Challenges. *Angew. Chem., Int. Ed.* **2019**, *58* (35), 11978–11996.
- (33) Couch, D. E.; Brenner, A. A Hydride Bath for the Electrodeposition of Aluminum. *J. Electrochem. Soc.* **1952**, *99* (6), 234.

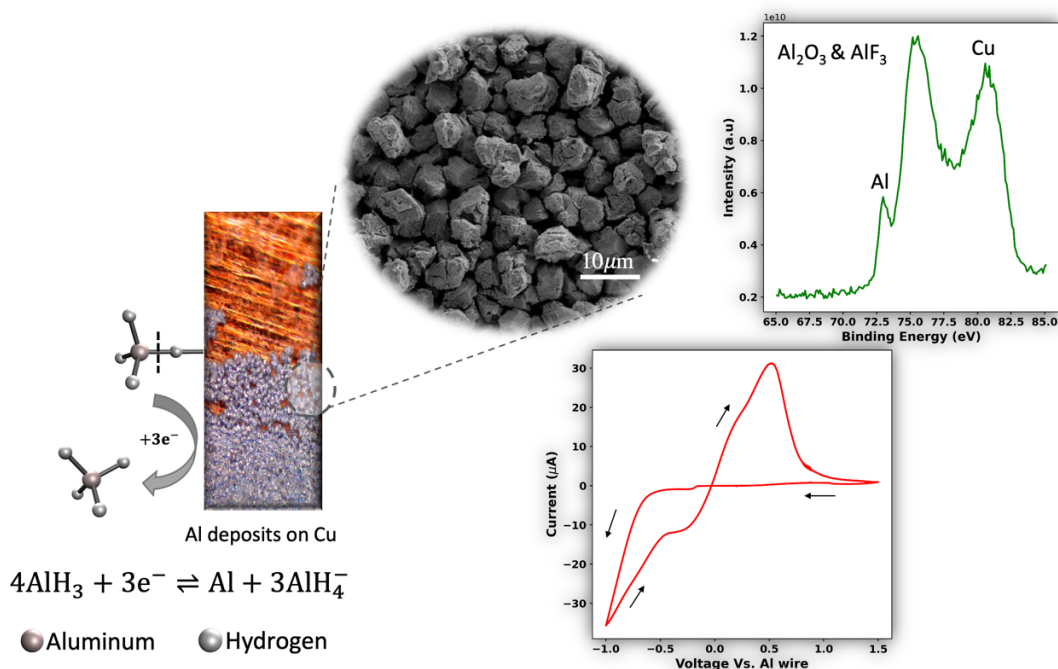
- (34) Ishibashi, N.; Yoshio, M. Electrodeposition of Aluminium from the NBS Type Bath Using Tetrahydrofuran—Benzene Mixed Solvent. *Electrochim. Acta* **1972**, *17* (8), 1343–1352.
- (35) Badawy, W. A.; Sabrah, B. A.; Hilal, N. H. Y. A New Bath for the Electrodeposition of Aluminium. II. Kinetics and Mechanism of the Deposition and Dissolution Processes. *J. Appl. Electrochem.* **1987**, *17* (2), 357–369.
- (36) Yoshio, M.; Ishibashi, N. High-Rate Plating of Aluminium from the Bath Containing Aluminium Chloride and Lithium Aluminium Hydride in Tetrahydrofuran. *J. Appl. Electrochem.* **1973**, *3* (4), 321–325.
- (37) Graef, M. W. M. The Mechanism of Aluminum Electrodeposition from Solutions of AlCl_3 and LiAlH_4 in THF. *J. Electrochem. Soc.* **1985**, *132* (5), 1038.
- (38) Lefebvre, M. C.; Conway, B. E. Elementary Steps and Mechanism of Electrodeposition of Al from Complex Hydride Ions in Tetrahydrofuran Baths. *J. Electroanal. Chem.* **2000**, *480* (1–2), 34–45.
- (39) Lefebvre, M. C.; Conway, B. E. Nucleation and Morphologies in the Process of Electrocrystallization of Aluminium on Smooth Gold and Glassy-Carbon Substrates. *J. Electroanal. Chem.* **2000**, *480* (1–2), 46–58.
- (40) Capuano, G. A.; Davenport, W. G. Electrodeposition of Aluminum from Alkyl Benzene Electrolytes. *J. Electrochem. Soc.* **1971**, *118* (10), 1688.
- (41) Peled, E.; Gileadi, E. The Electrodeposition of Aluminum from Aromatic Hydrocarbon: I. Composition of Baths and the Effect of Additives. *J. Electrochem. Soc.* **1976**, *123* (1), 15.
- (42) Hisano, T.; Terazawa, T.; Takeuchi, I.; Inohara, S.; Ikeda, H. The Electrodeposition of Aluminum from a Solution of Aluminum Bromide in N, N-Dimethyl Aniline. *Bull. Chem. Soc. Jpn.* **1971**, *44* (3), 599–603.
- (43) Yitzhac, N.; Tereschuk, P.; Sezin, N.; Starosvetsky, D.; Natan, A.; Ein-Eli, Y. Aluminum Electrodeposition from a Non-Aqueous Electrolyte—a Combined Computational and Experimental Study. *J. Solid State Electrochem* **2020**, *24*, 2833–2846.
- (44) Legrand, L.; Tranchant, A.; Messina, R. Behaviour of Aluminium as Anode in Dimethylsulfone-Based Electrolytes. *Electrochim. Acta* **1994**, *39* (10), 1427–1431.
- (45) Legrand, L.; Tranchant, A.; Messina, R. Electrodeposition Studies of Aluminum on Tungsten Electrode from DMSO 2 Electrolytes: Determination of AlIII Species Diffusion Coefficients. *J. Electrochem. Soc.* **1994**, *141* (2), 378.
- (46) Legrand, L.; Heintz, M.; Tranchant, A.; Messina, R. Sulfone-Based Electrolytes for Aluminum Electrodeposition. *Electrochim. Acta* **1995**, *40* (11), 1711–1716.
- (47) Legrand, L.; Tranchant, A.; Messina, R. Aluminium Behaviour and Stability in $\text{AlCl}_3\text{DMSO}_2$ Electrolyte. *Electrochim. Acta* **1996**, *41* (17), 2715–2720.
- (48) Nakayama, Y.; Senda, Y.; Kawasaki, H.; Koshitani, N.; Hosoi, S.; Kudo, Y.; Morioka, H.; Nagamine, M. Sulfone-Based Electrolytes for Aluminium Rechargeable Batteries. *Phys. Chem. Chem. Phys.* **2015**, *17* (8), 5758–5766.
- (49) Miyake, M.; Fujii, H.; Hirato, T. Electroplating of Al on Mg Alloy in a Dimethyl Sulfone–Aluminum Chloride Bath. *Surf. Coat. Technol.* **2015**, *277*, 160–164.
- (50) Kitada, A.; Nakamura, K.; Fukami, K.; Murase, K. AlCl_3 -Dissolved Diglyme as Electrolyte for Room-Temperature Aluminum Electrodeposition. *Electrochemistry* **2014**, *82* (11), 946–948.

- (51) Kitada, A.; Nakamura, K.; Fukami, K.; Murase, K. Electrochemically Active Species in Aluminum Electrodeposition Baths of AlCl₃/Glyme Solutions. *Electrochim. Acta* **2016**, *211*, 561–567.
- (52) Kitada, A.; Kato, Y.; Fukami, K.; Murase, K. Room Temperature Electrodeposition of Flat and Smooth Aluminum Layers from An AlCl₃/Diglyme Bath. *J. Surf. Finish. Soc. of Jpn.* **2018**, *69* (7), 310–311.
- (53) Zhang, Z.; Kitada, A.; Gao, S.; Fukami, K.; Tsuji, N.; Yao, Z.; Murase, K. A Concentrated AlCl₃-Diglyme Electrolyte for Hard and Corrosion-Resistant Aluminum Electrodeposits. *ACS Appl. Mater. Interfaces* **2020**, *12* (38), 43289–43298.
- (54) Zhang, B.; Shi, Z.; Shen, L.; Liu, A.; Xu, J.; Hu, X. Electrodeposition of Al, Al-Li Alloy, and Li from an Al-Containing Solvate Ionic Liquid under Ambient Conditions. *J. Electrochem. Soc.* **2018**, *165* (9), D321.
- (55) Wen, X.; Liu, Y.; Xu, D.; Zhao, Y.; Lake, R. K.; Guo, J. Room-Temperature Electrodeposition of Aluminum via Manipulating Coordination Structure in AlCl₃ Solutions. *J. Phys. Chem. Lett.* **2020**, *11* (4), 1589–1593.
- (56) Shi, J.; Zhang, J.; Guo, J. Avoiding Pitfalls in Rechargeable Aluminum Batteries Research. *ACS Energy Lett.* **2019**, *4* (9), 2124–2129.
- (57) Mandai, T.; Johansson, P. Haloaluminate-Free Cationic Aluminum Complexes: Structural Characterization and Physicochemical Properties. *J. Phys. Chem. C* **2016**, *120* (38), 21285–21292.
- (58) Chiku, M.; Matsumura, S.; Takeda, H.; Higuchi, E.; Inoue, H. Aluminum Bis (Trifluoromethanesulfonyl) Imide as a Chloride-Free Electrolyte for Rechargeable Aluminum Batteries. *J. Electrochem. Soc.* **2017**, *164* (9), A1841.
- (59) Wen, X.; Zhang, J.; Luo, H.; Shi, J.; Tsay, C.; Jiang, H.; Lin, Y.-H.; Schroeder, M. A.; Xu, K.; Guo, J. Synthesis and Electrochemical Properties of Aluminum Hexafluorophosphate. *J. Phys. Chem. Lett.* **2021**, *12*, 5903–5908.
- (60) Reed, L. D.; Ortiz, S. N.; Xiong, M.; Menke, E. J. A Rechargeable Aluminum-Ion Battery Utilizing a Copper Hexacyanoferrate Cathode in an Organic Electrolyte. *Chem. Commun.* **2015**, *51* (76), 14397–14400.
- (61) Reed, L. D.; Arteaga, A.; Menke, E. J. A Combined Experimental and Computational Study of an Aluminum Triflate/Diglyme Electrolyte. *J. Phys. Chem. B* **2015**, *119* (39), 12677–12681.
- (62) Mandai, T.; Johansson, P. Al Conductive Haloaluminate-Free Non-Aqueous Room-Temperature Electrolytes. *J. Mater. Chem. A* **2015**, *3* (23), 12230–12239.
- (63) Slim, Z.; Menke, E. J. Comparing Computational Predictions and Experimental Results for Aluminum Triflate in Tetrahydrofuran. *J. Phys. Chem. B* **2020**, *124* (24), 5002–5008.
- (64) Wu, C.; Gu, S.; Zhang, Q.; Bai, Y.; Li, M.; Yuan, Y.; Wang, H.; Liu, X.; Yuan, Y.; Zhu, N.; Wu, F. Electrochemically Activated Spinel Manganese Oxide for Rechargeable Aqueous Aluminum Battery. *Nat. Commun* **2019**, *10* (1), 1–10.
- (65) Yan, C.; Lv, C.; Wang, L.; Cui, W.; Zhang, L.; Dinh, K. N.; Tan, H.; Wu, C.; Wu, T.; Ren, Y. Architecting a Stable High-Energy Aqueous Al-Ion Battery. *J. Am. Chem. Soc.* **2020**, *142* (36), 15295–15304.

- (66) Wang, H.; Gu, S.; Bai, Y.; Chen, S.; Wu, F.; Wu, C. High-Voltage and Noncorrosive Ionic Liquid Electrolyte Used in Rechargeable Aluminum Battery. *ACS Appl. Mater. Interfaces* **2016**, *8* (41), 27444–27448.
- (67) Derouault, J.; Granger, P.; Forel, M. T. Spectroscopic Investigation of Aluminum Trihalides-Tetrahydrofuran Complexes. 2. Solutions of Aluminum Chloride or Bromide in Tetrahydrofuran and in (Tetrahydrofuran-Dichloromethane). *Inorg. Chem.* **1977**, *16* (12), 3214–3218.
- (68) Frisch, M. J.; Trucks, G. W.; Schlegel, H. B.; Scuseria, G. E.; Robb, M. A.; Cheeseman, J. R.; Scalmani, G.; Barone, V.; Mennucci, B.; Petersson, G. A. *Gaussian 09*; Gaussian, Inc, Wallingford, CT, 2009.
- (69) Frech, R.; Huang, W. Ionic Association in Poly (Propylene Oxide) Complexed with Divalent Metal Trifluoromethanesulfonate Salts. *Solid State Ion.* **1993**, *66* (1–2), 183–188.
- (70) Frech, R.; Huang, W. Anion-Solvent and Anion-Cation Interactions in Lithium and Tetrabutylammonium Trifluoromethanesulfonate Solutions. *J. Solution Chem.* **1994**, *23* (4), 469–481.
- (71) Huang, W.; Frech, R. Dependence of Ionic Association on Polymer Chain Length in Poly (Ethylene Oxide)-Lithium Triflate Complexes. *Polymer* **1994**, *35* (2), 235–242.
- (72) Huang, W.; Frech, R.; Wheeler, R. A. Molecular Structures and Normal Vibrations of Trifluoromethane Sulfonate (CF₃SO₃⁻) and Its Lithium Ion Pairs and Aggregates. *J. Phys. Chem.* **1994**, *98* (1), 100–110.
- (73) Bernson, A.; Lindgren, J.; Huang, W.; Frech, R. Coordination and Conformation in PEO, PEGM and PEG Systems Containing Lithium or Lanthanum Triflate. *Polymer* **1995**, *36* (23), 4471–4478.
- (74) Bernson, A.; Lindgren, J. Ion Aggregation and Morphology for Poly (Ethylene Oxide)-Based Polymer Electrolytes Containing Rare Earth Metal Salts. *Solid State Ion.* **1993**, *60* (1–3), 31–36.
- (75) Alves, C. C.; Campos, T. B.; Alves, W. A. FT-Raman Spectroscopic Analysis of the Most Probable Structures in Aluminum Chloride and Tetrahydrofuran Solutions. *Spectrochim. Acta A* **2012**, *97*, 1085–1088.
- (76) Derouault, J.; Forel, M. T. Spectroscopic Investigation of Aluminum Trihalides-Tetrahydrofuran Complexes. 1. Structure and Force Fields of the 1: 1 and 1: 2 Solid Compounds Formed by Aluminum Chloride or Bromide. *Inorg. Chem.* **1977**, *16* (12), 3207–3213.
- (77) Gale, R. J.; Osteryoung, R. A. Infrared Spectral Investigations of Room-Temperature Aluminum Chloride-1-Butylpyridinium Chloride Melts. *Inorg. Chem.* **1980**, *19* (8), 2240–2242.
- (78) Kore, R.; Kelley, S. P.; Aduri, P.; Rogers, R. D. Mixed Metal Double Salt Ionic Liquids Comprised of [HN 222] 2 [ZnCl 4] and AlCl 3 Provide Tunable Lewis Acid Catalysts Related to the Ionic Environment. *Dalton Trans.* **2018**, *47* (23), 7795–7803.
- (79) See, K. A.; Liu, Y.-M.; Ha, Y.; Barile, C. J.; Gewirth, A. A. Effect of Concentration on the Electrochemistry and Speciation of the Magnesium Aluminum Chloride Complex Electrolyte Solution. *ACS Appl. Mater. Interfaces* **2017**, *9* (41), 35729–35739.
- (80) Cowley, A. H.; Cushner, M. C.; Davis, R. E.; Riley, P. E. Crystal and Molecular Structure of the 1: 2 Aluminum Trichloride-Tetrahydrofuran Complex AlCl₃. 2THF. *Inorg. Chem.* **1981**, *20* (4), 1179–1181.

- (81) Moss, J. B. Computational and Experimental Studies on Energy Storage Materials and Electrocatalysts. MS Thesis, Utah State University, 2019.
- (82) Lefebvre, M. C.; Conway, B. E. ^{27}Al NMR Spectroscopy Studies on Speciation of Al Complex Ions in $\text{AlCl}_3 + \text{LiAlH}_4$ Solutions in Tetrahydrofuran for Electroplating of Al. *J. Electroanal. Chem.* **1998**, *448* (2), 217–227.
- (83) Nöth, H.; Rurländer, R.; Wolfgardt, P. An Investigation of AlCl_3 Solutions in Ethers by ^{27}Al NMR Spectroscopy. *Zeitschrift für Naturforschung B* **1982**, *37* (1), 29–37.
- (84) Wang, Y.-S.; Yeh, H.-W.; Tang, Y.-H.; Kao, C.-L.; Chen, P.-Y. Voltammetric Study and Electrodeposition of Zinc in Hydrophobic Room-Temperature Ionic Liquid 1-Butyl-1-Methylpyrrolidinium Bis ((Trifluoromethyl) Sulfonyl) Imide ([BMP][TFSI]): A Comparison between Chloride and TFSI Salts of Zinc. *J. Electrochem. Soc.* **2016**, *164* (2), D39.
- (85) Deng, K.; Zeng, Q.; Wang, D.; Liu, Z.; Wang, G.; Qiu, Z.; Zhang, Y.; Xiao, M.; Meng, Y. Nonflammable Organic Electrolytes for High-Safety Lithium-Ion Batteries. *Energy Storage Mater.* **2020**, *32*, 425–447.
- (86) Yu, Y.; Che, H.; Yang, X.; Deng, Y.; Li, L.; Ma, Z.-F. Non-Flammable Organic Electrolyte for Sodium-Ion Batteries. *Electrochem. Commun.* **2020**, *110*, 106635.

Chapter 4:Hydride-Enhanced Plating and Stripping of Aluminum from Triflate-Based Organic Electrolytes



4.1 Introduction

The rechargeable aluminum (Al) battery is a likely candidate for next-generation energy storage systems due to Al's unmatched theoretical volumetric capacity, abundant resources, and considerably low cost.^{1,2} Most research on rechargeable Al batteries employ chloroaluminate ionic liquids as the electrolyte.³⁻²¹ While these systems demonstrate impressive cycleability with certain cathode materials,^{8,10,11,14,15,17,19,21} they suffer from high corrosivity and reactivity towards battery components,^{5,20,22,23} and side reactions involving toxic chlorine (Cl_2).^{24,25} One approach to overcome these challenges is through the development of active-halide-free organic electrolytes.²⁶

Thus far, only a handful of active-halide-free organic electrolytes have been reported.²⁷⁻³⁴ A timeline showing the progress in organic electrolyte development for rechargeable Al battery is shown in Chapter 1 Figure 1.2. Early work on active-halide-free electrolytes involved aluminum trifluoromethanesulfonate ($\text{Al}(\text{OTF})_3$) and urea in N-methyl acetamide (NMA),²⁹ and $\text{Al}(\text{OTF})_3$ in 2-methoxy ethyl ether (diglyme).^{27,28} Unfortunately, from both systems, Al electrodeposition could not be carried out. Following their work on $\text{Al}(\text{OTF})_3$ and urea in NMA, Mandai and Johansson introduced an interesting strategy for the development of active-halide-free electrolytes.³⁰

Several promising electrolyte systems were reported, including aluminum *hexa*-dimethylsulfoxide trifluoromethanesulfonate $[\text{Al-DMSO}]_6[\text{OTF}]_3$ in sulfolane, aluminum *hexa*-dimethyl sulfoxide bis(trifluoromethanesulfonyl)imide $[\text{Al-DMSO}]_6[\text{TFSI}]_3$ in sulfolane, aluminum *hexa*-methylimidazole bis(trifluoromethanesulfonyl)imide $[\text{Al(MIm)}]_6[\text{TFSI}]_3$ in acetonitrile (MeCN), and aluminum *hexa*-butylimidazole bis(trifluoromethanesulfonyl)imide $[\text{Al(BIm)}]_6[\text{TFSI}]_3$.

Al electrodeposition was attempted from $[\text{Al(BIm)}]_6[\text{TFSI}]_3$ at 80 °C, however, the Al electrodeposition process was accompanied by severe electrolyte decomposition.

While considerable progress has been made, only two systems have shown promising reversible Al electrochemistry. Notable work on the synthesis of Al(TFSI)_3 and aluminum hexa-fluorophosphate ($\text{Al(PF}_6)_3$) salts was conducted by Chiku et al.³¹ and Xiaoyu et al.,³³ respectively. Although evidence for Al electrodeposition was reported for the $\text{Al(TFSI)}_3/\text{MeCN}$ electrolyte, the demonstrated reversibility of this process was unclear, and therefore requires further investigation.³¹ On the other hand, quasi-reversible Al plating/stripping along with a side reaction involving the reductive generation of dimethyl sulfide was demonstrated from $\text{Al(PF}_6)_3/\text{DMSO}$. Surprisingly, however, the Al plating and stripping potentials were of unusually low-energy efficiency, with a reduction and oxidation potentials of -1V and +0.5V (vs Al/Al^{3+}), respectively.³³

In the case of Al(OTF)_3 , as mentioned earlier, Reed et al. investigated this salt in diglyme. Although Al electrodeposition from the $\text{Al(OTF)}_3/\text{diglyme}$ was not achieved,²⁸ reversible intercalation/deintercalation behavior was demonstrated with a Prussian blue analogue cathode.²⁷ Unlike the $\text{Al(OTF)}_3/\text{diglyme}$ electrolyte, however, non-reversible Al electrodeposition can be carried out from Al(OTF)_3 in tetrahydrofuran (THF) electrolytes, as we have revealed in our previous reports.^{32,34}

To highlight the role of hydrides (H^-) in the Al plating/stripping process, in this report, we demonstrate room-temperature reversible Al plating/stripping from an active-halide-free organic electrolyte based on $\text{Al(OTF)}_3/\text{THF}$ facilitated by a lithium aluminum hydride (LiAlH_4) additive. The spectroscopic and electrochemical aspects of the trifluoromethanesulfonate (OTF^-)-based electrolyte were evaluated and compared to the well-known chloride (Cl^-)-based system.³⁵⁻⁴⁴ This comparison revealed that the H^- species not only catalyzes the Al plating/stripping process in the Cl^- -based electrolytes as previously proposed by Daenen³⁸ and Graef,⁴⁰ but also allows for this process to be carried out in the absence of any haloaluminate species. Density functional theory (DFT) calculations along with Fourier transform infrared spectroscopy (FTIR) analyses reveal remarkably dissimilar Al-hydride speciation in these two systems. Unambiguous evidence for Al deposition is demonstrated using an optical microscope, a scanning electron microscope (SEM) and X-ray diffraction (XRD) spectroscopy. Characterization by means of X-ray photoelectron spectroscopy (XPS) indicates that the deposits from the OTF^- -based electrolyte comprise metallic Al, aluminum trifluoride (AlF_3) and aluminum oxide (Al_2O_3), whereas the deposits from the Cl^- -based electrolyte comprise mainly aluminum trichloride (AlCl_3) and Al_2O_3 . Depth profile XPS analyses of the Al films from either the OTF^- -based or Cl^- -based electrolytes suggest that during the plating process, freshly deposited Al reacts with the electrolyte components to form Al_2O_3 and either AlF_3 (from the OTF^- -based) or AlCl_3 (from the Cl^- -based).

4.2 Materials and Methods

4.2.1 Density functional theory calculations

All density functional theory (DFT) calculations were carried out using Gaussian 09 suite of electronic structure program. All results were obtained using the unrestricted spin-formalism employing the B3PW91 density functional and the 6311+G(d) basis set. All structures were fully optimized using the solvation model density (SMD) continuum solvation model based on the self-consistent reaction field (SCRF) approach, and tetrahydrofuran (THF) was used as the solvent for all calculations. All structures were found to be local minima on the potential energy by confirming the absence of any imaginary frequencies.

4.2.2 Electrolyte preparation

All chemical preparations were conducted in an argon-filled glovebox. 99.9% aluminum trifluoromethanesulfonate ($\text{Al}(\text{OTf})_3$), 99.99% aluminum trichloride (AlCl_3), 97% lithium aluminum hydride (LiAlH_4), 99.9% tetrahydrofuran (THF), were all purchased from Sigma-Aldrich and used as received. To prepare the OTF-based electrolyte, a 1:3 mole ratio of $\text{Al}(\text{OTf})_3$ to LiAlH_4 was used. Initially, 0.2 g of LiAlH_4 were dissolved in 3.5 mL of THF. Similarly, a 0.83 g of $\text{Al}(\text{OTf})_3$ were dissolved in 3.5 mL in THF. Both solutions were stirred separately for at least 30 minutes to ensure complete dissociation. The LiAlH_4 /THF solution was slowly added drop-wise to the $\text{Al}(\text{OTf})_3$ /THF solution under moderate stirring. It should be noted that the reaction between the two solutions is extremely exothermic, and mixing the solutions should be carried out slowly, otherwise excessive solution foaming and THF evaporation may take place. The mixture was allowed to stir for 30 minutes. While Al Electrodeposition can be carried out at this point, the excessive hydride activity due to the elevated temperature in the solutions can be problematic. For this reason, the mixture was allowed to rest (without stirring) for several hours before measuring the oxidative stability of the electrolyte. (See Supporting Information Figure 4.8) The chloride-based electrolytes were prepared according to the same procedures using appropriate amounts of AlCl_3 (0.23 g), to ensure the total concentration of [Al] is the same in both electrolytes. Both electrolytes used for the 4 hour chronoamperometry experiments contained the same total concentration of Al. As for the electrolyte used for the 18 hours chronoamperometry experiment, the concentration was higher, and the electrolyte consisted of 0.4 g of LiAlH_4 and 1.23 g of $\text{Al}(\text{OTf})_3$ in 5 ml of THF.

4.2.3 Materials characterization

All electrochemical measurements were conducted in an argon-filled glovebox using a potentiostat (Gamry). Cyclic voltammetry experiments were carried out using a standard three-electrode set up using a gold working electrode, an Al wire pseudo-reference, and an Al wire as the counter electrode. A 50 mV/s scan rate was used. Chronoamperometry experiments were carried out using a Cu substrate as the working electrode, an Al wire as a pseudo-reference, and an Al wire as the counter electrode.

Immediately after the chronoamperometry experiments were done, the Cu substrates were rinsed with THF in the glovebox. Chronoamperometry for the 4 hours samples from both triflate-based and the chloride-based electrolytes were done by setting the potential to -0.25 V (vs Al/Al³⁺). For the 18 hour sample from the OTF⁻-based electrolyte, electrodeposition was conducted at -0.2 V (vs Al/Al³⁺) from a highly concentrated solution consisting of 0.4 g of LiAlH₄ and 1.23 g of Al(OTF)₃ in 5 ml of THF.

Fourier transform infrared spectroscopy (FTIR) experiments were done in attenuated total reflectance (ATR) mode using a Vertex 70 spectrometer. A 4 cm⁻¹ resolution and 64 scans were used.

X-ray photoelectron spectroscopy (XPS) measurements were carried out using a Nexsa spectrometer. Etching experiments were conducted using argon. In all cases, 10 scans were collected.

X-ray diffraction spectroscopy (XRD) measurements were carried out using a PANalytical X'Pert PRO X-ray diffractometer, using a Co-K α source. The spectra were then converted to Cu-K α source using the HighScore software. The sample holders for the XRD were filled with polyethylene glycol (PEG) and the Cu substrates were laid on top of the PEG. Electron microscopy experiments were conducted using a field emission scanning electron microscope (Zeiss Gemini SEM 500) and optical microscopy images were obtained using an ECLIPSE LV150A microscope.

4.3 Results and Discussion

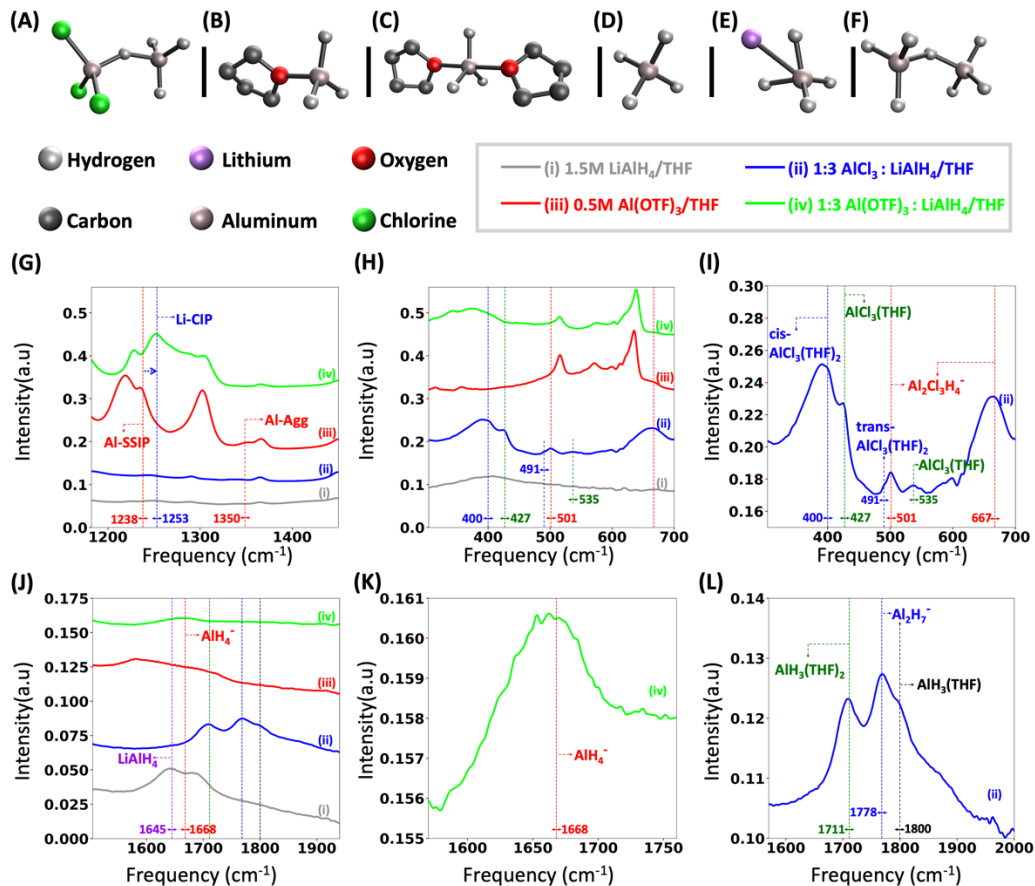


Figure 4.1 Optimized structures (hydrogens only shown for Al—H bonds) of various Al-complexes and FTIR spectra of various THF-based Al electrolytes. (A) $\text{Al}_2\text{Cl}_3\text{H}_4^-$, (B) $\text{AlH}_3(\text{THF})$, (C) $\text{AlH}_3(\text{THF})_2$, (D) AlH_4^- , (E) LiAlH_4 , (F) Al_2H_7^- , (G) $\nu_{\text{as}}\text{SO}_3$ shifting corresponding to OTF^- transfer from Al to Li ions, (H) Al-chloride speciation region for all electrolyte solutions, (I) Al-chloride speciation region for the Cl^- -based electrolyte, (J) Al-hydride speciation region, (K) zoomed in Al—H stretching region for the OTF^- -based electrolyte, (L) zoomed in Al—H speciation region for the Cl^- -based electrolyte. SSIP : solvent-separated ion pairs, CIP : contact ion pairs, Agg : aggregates.

The electrolytes were prepared by slowly adding a solution of $\text{LiAlH}_4/\text{THF}$ to a solution of either AlCl_3/THF or $\text{Al}(\text{OTF})_3/\text{THF}$. The experimental details can be found in the Supporting Information.

Identifying the Al species that are likely to be found in the studied electrolytes is crucial to elucidate the electrochemical mechanism for reversibly plating and stripping Al from the OTF^- -based electrolyte. DFT calculations for several Al complexes were performed and the optimized structures are shown in Figure 4.1A-F. A summary of the calculated vibrational frequencies can be found in Table 4.1 in the Supporting Information. To experimentally substantiate the existence of such species, FTIR spectra for four electrolyte solutions were collected, and different regions of the spectra are shown in Figure 4.1G-L.

Motivated by the exceptional work conducted by Frech et al.^{45–48} on the spectroscopic attributes of the OTF⁻ anions, in our previous work on Al(OTF)₃/THF we described a new method that allows for the determination of the reaction progress between Al(OTF)₃ and Li-based salts by exploiting the computed and measured spectroscopic features of the OTF⁻.³⁴ Indeed, these results are well represented by the FTIR measurements shown in Figure 4.1G. Upon the addition of LiAlH₄ to the Al(OTF)₃/THF electrolyte at 1:3 mole ratio's, a shift in frequency from 1238 to 1253 cm⁻¹, corresponding to the transfer of the triflate anion from Al to Li ions, is observed. Additionally, the peak at 1350 cm⁻¹ associated with the presence of Al-OTF aggregates (Al-Agg) disappears, further indicating that the OTF⁻ are no longer associated with Al ions.

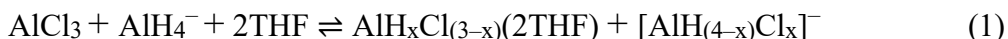
FTIR spectra for the Cl⁻-based electrolytes shown in Figure 4.1H,I reveals that the bands associated with AlCl₃(THF), cis- and trans-AlCl₃(THF)₂, those previously identified in an AlCl₃/THF solution,^{34,49} remain intact.

However, peaks attributable to a new species are observed at 501 and 667 cm⁻¹. Our DFT calculations suggest that these peaks are associated with the asymmetric stretch ($\nu_{\text{as}}(\text{Al}-\text{Cl})$) and AlH₃ group bending (δAlH_3) of Al₂Cl₃H₄⁻, respectively. Moreover, the $\nu_{\text{as}}(\text{Al}-\text{Cl})$ band for AlCl₃(THF)₂ was measured at 490 cm⁻¹ in the AlCl₃/THF electrolyte.^{34,49} The shift in frequency for the $\nu_{\text{as}}(\text{Al}-\text{Cl})$ mode from 490 to 501 cm⁻¹ suggest that strong ionic association is taking place. It is important to note that the presence of AlCl₃H⁻ in a H⁻ rich environment was confirmed by the detailed NMR studies conducted by Lefebvre and Conway,⁴² however, computational and experimental evidence for the ionic association of AlCl₃H⁻ with AlH₃ is presented here for the first time. Next, we examine the region associated with the hydride species. Inspecting the LiAlH₄ spectra (i) in Figure 4.1J, one can clearly see two adjoint peaks at 1645 and 1668 cm⁻¹. Our DFT calculations suggest that these bands are attributed to the Al—H asymmetric stretch ($\nu_{\text{as}}(\text{Al}-\text{H})$) of the AlH₄⁻, and LiAlH₄ species, respectively. (Table 4.1 in Supporting Information)

In the triflate based electrolyte, however, the peak associated with LiAlH₄ disappears. These results are also consistent with the fact that the Li ions in the OTF⁻-based electrolyte are associated with the OTF⁻, weakening the interaction between Li and AlH₄⁻, thus, resulting in free AlH₄⁻ species, which dominates the ionic profile of the OTF⁻-based electrolyte. Comparatively, the spectrum for the Cl⁻-based electrolyte shown in Figure 4.1L reveals several bands associated with three distinct Al-hydride complexes.

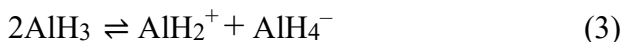
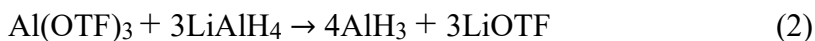
According to our DFT calculations, the bands at 1711 and 1800 cm⁻¹ are attributable to the AlH₃(THF)₂ and AlH₃(THF), respectively. Furthermore, DFT results for the Al₂H₇⁻ suggests that this species exhibits two strong vibrational modes associated with $\nu_{\text{as}}(\text{Al}-\text{H})$ at 1778 and 1800 cm⁻¹. These results suggest that the existence of a hydride bridge between two AlH₃ is likely to occur in the Cl⁻-based electrolytes, particularly because the calculated bond length between the bridging hydride and the AlH₃ is ca. 1.71 Å as shown in (Supporting Information Figure 4.6), this bond length is equal to Al—H bond length reported for solid AlH₃.⁵⁰ Interestingly, these bands are absent from the OTF⁻-based electrolyte. Clearly, the ionic profiles of both systems are radically distinct.

The discrepancy between the Al-hydride species in OTF⁻-based and Cl⁻-based electrolytes arises from the unique bonding profiles of Al(OTF)₃ in THF and AlCl₃ in THF. In the former, the coordination of Al with the OTF⁻ is relatively weak, which results in the presence of free OTF⁻, contact ion pairs (CIP) and aggregates (Agg) upon dissolving Al(OTF)₃ in THF.^{32,34} When a Li-based salt is added at 1:3 mole ratio's, complete transfer of the OTF⁻ from Al to Li ions occurs, as demonstrated in this work and our previous work.³⁴ As for the later, Cl⁻ are never completely detached from Al due to the strong and covalent nature of the Al—Cl bond,³⁰ which results in mixed speciation when LiAlH₄ is added to AlCl₃/THF solutions. It has been proposed that Al speciation in the Cl⁻-based electrolyte occurs according to the Schlesinger reaction^{42,43,51}:



It is worth emphasizing that in the previous studies by Lefebvre and Conway, it was proposed that the high Lewis acidity of the AlCl₃ facilitates solution decompositions in the Cl⁻-based electrolytes.⁴²

Based on these results, we propose the following dissociation reaction mechanism in the OTF⁻-based electrolytes at 1:3 mole ratio of Al(OTF)₃ to LiAlH₄ in THF:



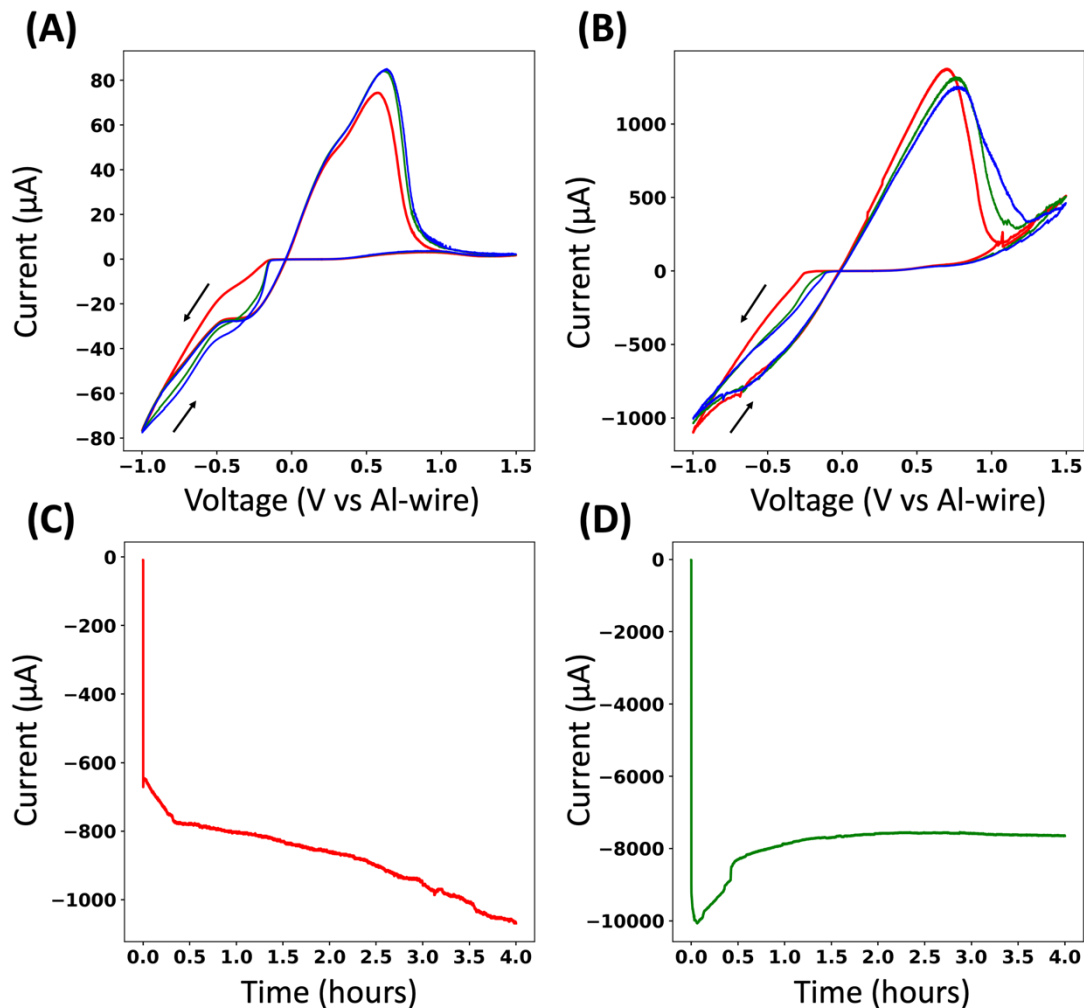


Figure 4.2 Cyclic voltammograms (first scan is red, second is green, and third is blue) on gold working electrode at 50 mV/s of (A) 1:3 Al(OTF)₃:LiAlH₄/THF, (B) 1:3 AlCl₃:LiAlH₄/THF, and corresponding chronoamperograms on Cu substrate of (D)1:3 Al(OTF)₃:LiAlH₄/THF, and (E) 1:3 AlCl₃:LiAlH₄/THF.

The plating/stripping behavior of Al from the chloride- and the OTF⁻-based electrolytes were evaluated by cyclic voltammetry using a gold working electrode in a three-electrode electrochemical cell. Prior to mixing the LiAlH₄/THF with the AlOTF₃/THF solutions, it is essential to first record a cyclic voltammogram (CV) for the LiAlH₄/THF. The CV is shown in (Supporting information Figure 4.7). Our measurements are consistent with those of Lefebvre and Conway,⁴³ revealing a reversible electrochemical process between -1 and 0 V (vs Al/Al³⁺), likely associated with deposition of Li and possibly the co-deposition of Al. This is perhaps due to the strong interaction between Li ions and AlH₄⁻ as revealed by the above-mentioned DFT and FTIR results.

Figure 4.2A shows a typical CV for the 1:3 Al(OTF)₃:LiAlH₄/THF electrolytes. Upon sweeping to a more negative potential, a cathodic current is immediately measured ca. -0.2 V (vs Al/Al³⁺), and a CV typical to reversible electrochemical deposition is recorded.

On the reverse sweep, stripping of the deposited Al takes place ca. 0V (vs Al/Al³⁺), with minimal plating/stripping potential hysteresis. The oxidative stability of the electrolyte is ca. 1.8 V (vs Al/Al³⁺), which to the best of our knowledge, is the highest measured oxidative stability for an active-halide-free Al organic electrolyte. (see Supporting Information Figure 4.8A) Comparatively, the CV for the Cl⁻-based electrolyte shown in Figure 4.2B exhibits a similar profile, with the appearance of an Al nucleation loop during the negative potential sweep. In this electrolyte, however, oxidative decomposition occurs ca. +1.1V (vs Al/Al³⁺), consistent with the measurements of Lefebvre and Conway.⁴³

Furthermore, while recoding the CVs for the OTF⁻-based electrolyte, an unusual feature in the CVs is observed ca. +1V (vs Al/Al³⁺) (Supporting Information Figure 4.8A). This feature was investigated by sweeping the potential from 0 to +1.5 V (vs Al/Al³⁺), which is shown in Supporting information Figure 4.8B. This oxidation reaction can be attributed to side reaction involving H₂ generation as shown in reaction (5). It is worth noting that this feature is usually amplified within the first 30 minutes after the electrolyte has been prepared as shown in (Supporting Information Figure 4.8C,D), likely due to the elevated temperature of the solution which arises from the highly exothermic reaction between Al(OTF)₃ and LiAlH₄. According to these results, we propose the following electrochemical reaction mechanisms at 1:3 mole ratio of Al(OTF)₃ to LiAlH₄ in THF:



Our hypothesis is that the H⁻ adsorb to the electrode surface enabling reversible Al plating in a process similar to that of the Cl⁻ in the magnesium aluminum chloride complex electrolytes.⁵²

In the OTF⁻-based electrolyte, this process is dictated by the equilibrium proposed in reaction (4) and the AlH₃ species are electrochemically reduced to Al metal during the electrochemical reduction reaction, increasing the concentration of free H⁻ at the interface, which, unfortunately, not only allows for stripping of the deposited Al, but also makes the electrolyte susceptible to parasitic reactions involving the oxidative generation of H₂.

To confirm Al electrodeposition from both electrolytes, chronoamperometry, optical microscopy and scanning electron microscopy experiments were conducted. Electrodeposition of Al on a Cu substrate from both electrolytes was achieved by holding the potential at either -0.25V (vs Al/Al³⁺) for 4 hours or -0.2V (vs Al/Al³⁺) for 18 hours. As was the case for the cyclic voltammetry experiments shown in Figure 4.2A,B, the measured currents during the chronoamperometry experiments in the Cl⁻-based electrolyte (Figure 4.2D) are one order of magnitude higher than that of the OTF⁻-based electrolytes (Figure 4.2C), re-enforcing the fact that the Cl⁻ significantly facilitate the plating process, as we have demonstrated in our previous report.³⁴ These results strongly suggest that a more facile nucleation process from the Cl⁻-based electrolyte is to be expected.

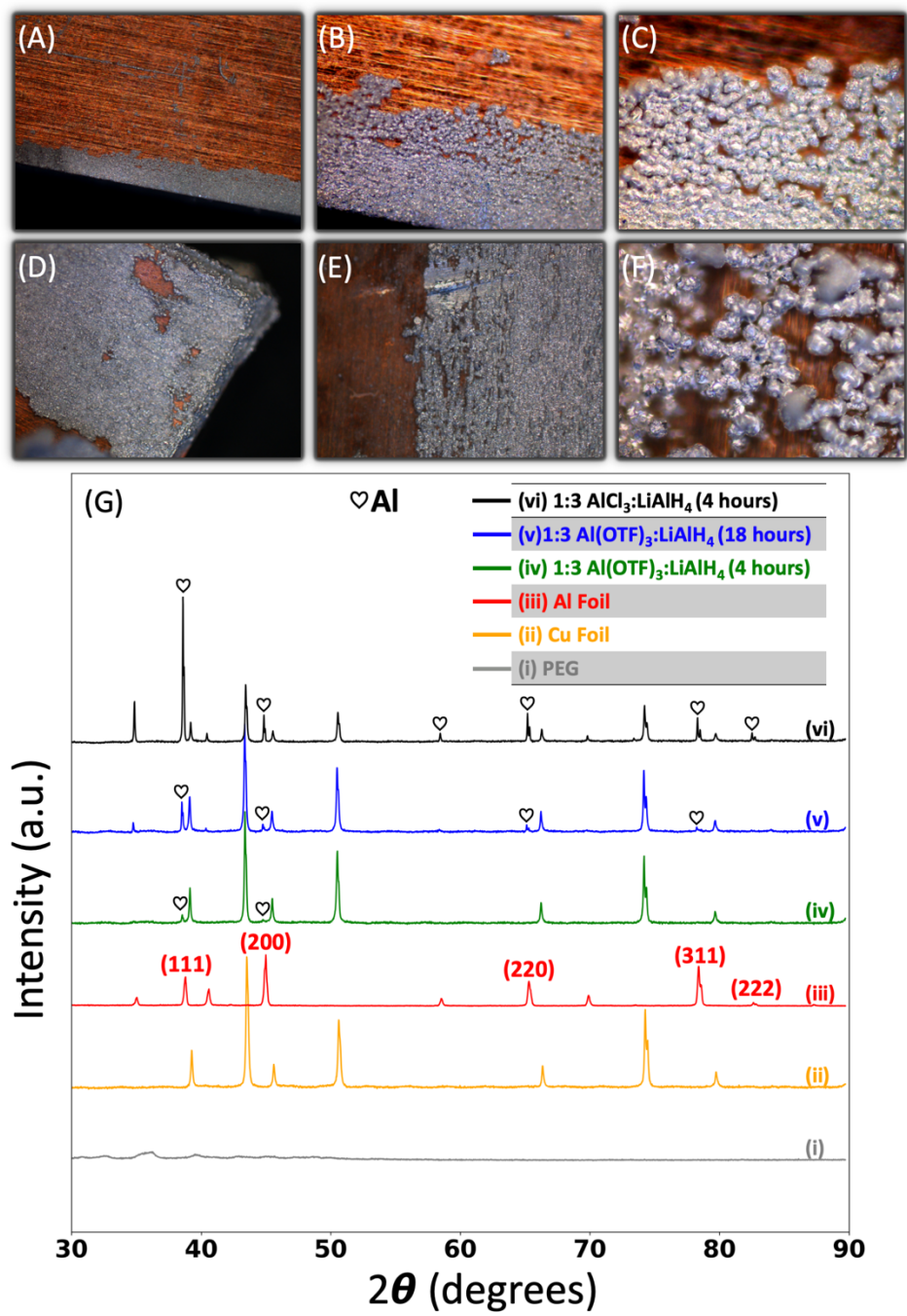


Figure 4.3 Optical microscopy images of Al electrodeposits on Cu substrate from 1:3 Al(OTF)₃:LiAlH₄/THF at -0.25V (vs Al/Al³⁺) for 4 hours at magnification of (A) 5x , (B) 20x, (C) 50x, and Al electrodeposits on Cu substrate after 18 hours at -0.2 V (vs Al/Al³⁺) from highly concentrated 1:3 Al(OTF)₃:LiAlH₄/THF electrolyte at magnification of (D) 5x and from AlCl₃:LiAlH₄/THF at magnification of (E) 5x and (F) 20x. (G) X-ray diffraction pattern of aluminum electrodeposits on Cu substrates.

The optical microscopy images and XRD patterns of the Al deposits from the OTF^- -based and the Cl^- -based electrolytes are shown in Figure 4.3. The overall effectiveness of the OTF^- -based electrolyte for electrodeposition of Al is evident from the optical microscopy images Figure 4.3A-D and the photographic images in Supporting Information Figure 4.9A,B in. To verify that the grain-like deposits observed on the Cu substrate corresponds to crystalline Al, XRD spectra were compared to that of an untreated Cu substrate and an Al foil. Clearly, the Al deposits from both the OTF^- -based and Cl^- -based electrolytes exhibit a diffraction pattern which is identical to that of the Al foil.

The surface morphology of the Al deposits were further examined by a scanning electron microscope (SEM) and the results are displayed in Figure 4.4. Clear dissimilarities in the grain sizes are indicative of the beneficial role chlorides play in facilitating the plating process. As mentioned earlier, the higher currents achieved suggest that nucleation rate is expected to be higher in the Cl^- -based electrolyte. Indeed, this is manifested by significantly larger Al deposits as shown in the Figure 4.4D,H.

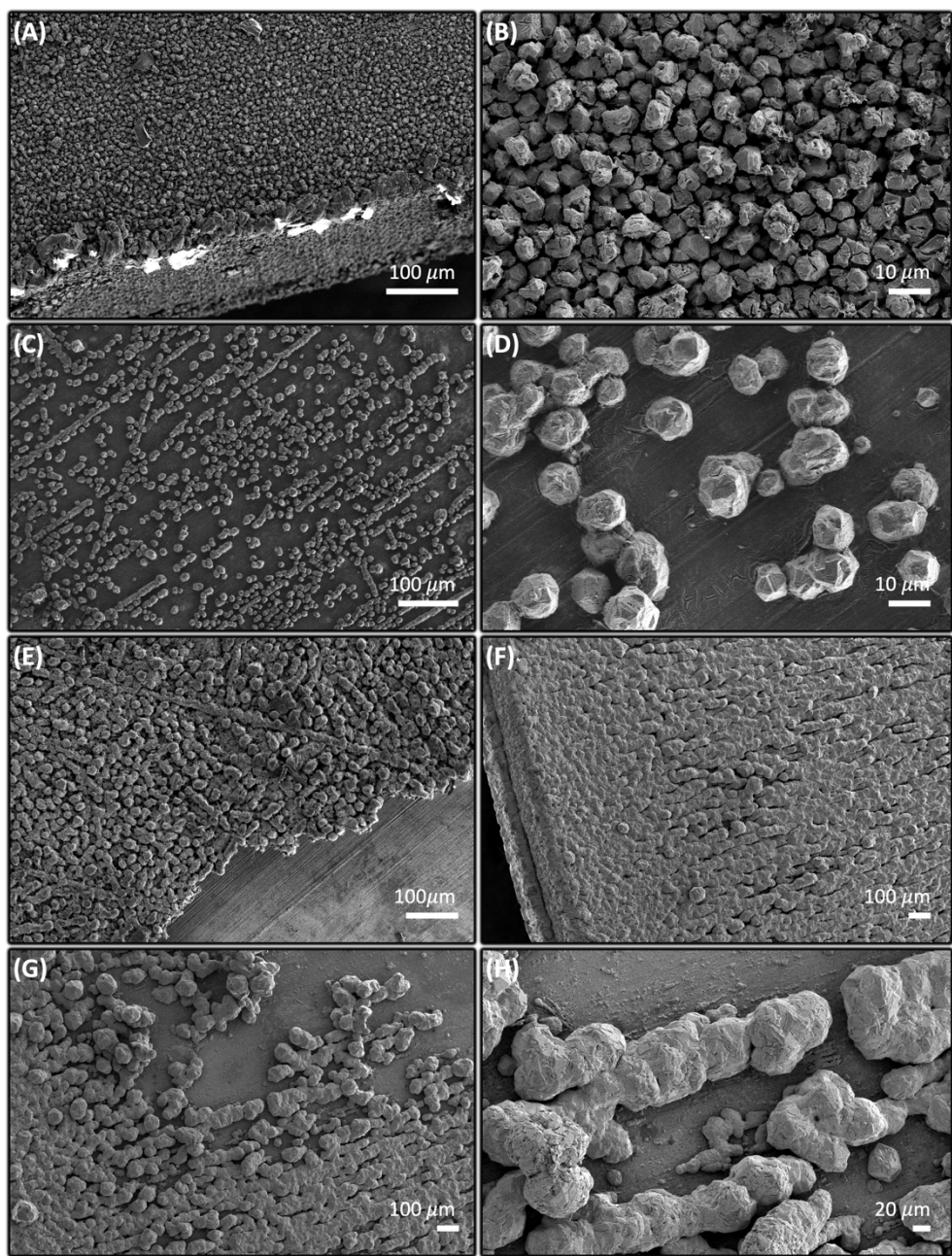


Figure 4.4 SEM micrographs of Al electrodeposits on Cu substrate from 1:3 $\text{Al}(\text{OTf})_3:\text{LiAlH}_4/\text{THF}$ after 4 hours at -0.25V (vs Al/Al^{3+}) at region 1 (A,B), and region 2 (C,D), and (E) after 18 hours at -0.2V (vs Al/Al^{3+}) from highly concentrated 1:3 $\text{Al}(\text{OTf})_3:\text{LiAlH}_4/\text{THF}$ electrolyte, and from (F-H) 1:3 $\text{AlCl}_3:\text{LiAlH}_4/\text{THF}$ after 4 hours at -0.25V (vs Al/Al^{3+}).

To uncover the chemical composition of the electrodeposited Al films, the Cu substrates were characterized by depth-profile XPS analyses and the results are shown in Figure 4.5. The Al 2p spectra for the Al deposits obtained from the OTF⁻-based electrolytes shown in Figure 4.5A, strongly indicates that Al metal, Al₂O₃, and AlF₃ are present. Upon etching the thin Al film with argon for 5 minutes, the peak attributed to the Al-metal at 72.8 eV remains unchanged, while the peaks attributed to Al₂O₃ and AlF₃ became more prominent. Also, the AlF₃ peak becomes broader due to the contribution from the Cu 3p at ca. 80 eV. A clear distinction between the peaks of the Al 2p of AlF₃ and the Cu 3p of the Cu substrate, in addition to the peaks associated with organic- and metallic-fluorine was made by examining another region of the electrode surface (region 2), where the surface coverage of Al on Cu is significantly lower than that of region 1. A comparison of the XPS spectra of the two regions is shown in the Supporting Information Figure 4.10. Additionally, before etching, a weak-intensity peak is observed at 933 eV in the Cu 2p spectrum. After etching, the relative intensity of this peak increases along with the appearance of a peak at 952.8 eV, indicating that a significant portion of the Al film has been completely removed exposing the Cu substrate. To experimentally confirm this result, after completing the XPS experiment, the Cu substrate was re-examined by a SEM and the result revealing the residual Al on Cu is shown in Supporting Information Figure 4.11.

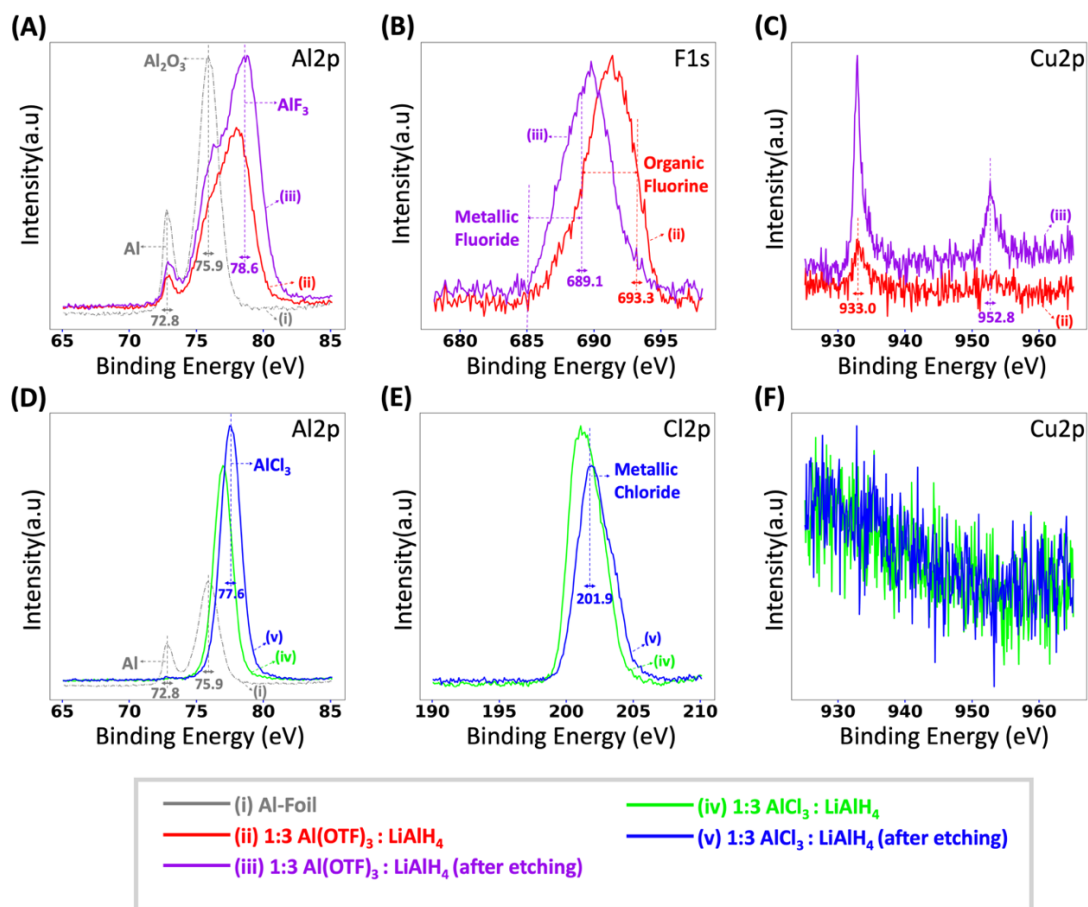


Figure 4.5 XPS spectra for aluminum electrodeposits (region 1) from (A-C) 1:3 Al(OTF)₃:LiAlH₄/THF, and Al electrodeposits (region 1) from (D-F) 1:3 AlCl₃:LiAlH₄/THF.

In contrast, the Al 2p spectra of the unetched Al film obtained from the Cl⁻-based electrolyte shown in Figure 4.5D suggests that the film is primarily comprised of AlCl₃ and Al₂O₃. Examining another region of the electrode, a small, yet significant peak at 72.8 eV associated with metallic Al is observed as shown in spectrum (v) in Supporting Information Figure 4.10.

In addition to the reactivity of the Al film with the electrolyte components during the plating process, the high degree of oxide- and chloride-components of the Al film can be attributed to the participation of AlX₃(THF)_n (where X is Cl or H, and n= 0, 1 or 2) species in the plating process.

Moreover, despite etching the Al film for 5 mins, no peaks associated with the Cu substrate were detected in the Cu 2p region as shown in Figure 4.5F, substantiating our visual examination (see photographic images in Supporting Information Figure 4.9) and confirming that the Al film obtained from the Cl⁻-based electrolyte is thicker than the Al film obtained from the OTF⁻-based electrolyte despite identical plating conditions, that is, total concentration of Al, plating potential and duration.

Also, the Cl 2p peak persists even after etching as shown in Figure 4.5E, confirming that Cl is not only found as a surface contaminant, but also within the Al film.

The results in this report indicate potential application of an active-halide-free organic electrolyte in rechargeable Al batteries. By introducing a LiAlH_4 additive to an $\text{Al}(\text{OTf})_3/\text{THF}$ electrolyte, we have demonstrated that the H^- play an integral role in plating/stripping Al in organic electrolytes, allowing the process to occur in the absence of any active-halides. Al deposits, although visually evident on the Cu substrates, were also confirmed by several characterization techniques including optical microscopy, SEM, XRD and XPS. XPS etching experiments confirm that significant reactivity occurs between the freshly-plated Al and the electrolyte components as evident by the F- and Cl-XPS spectra from the OTf^- and Cl^- -based electrolytes, respectively. Results from DFT and FTIR have shown that the strategy employed to evaluate the hydride additive by relying on the spectroscopic attributes of the OTf^- , can allow for the evaluation of other Li-based additives not just LiCl as we have previously demonstrated.³⁴ Lastly, preferential Al plating/stripping occurs in the Cl^- -based electrolyte, highlighting the role of both Al-chloride and Al-hydride species in the Al plating/stripping process.

4.4 Outlook and Future Work

While the work demonstrated in this report overcomes a milestone in organic electrolyte development for rechargeable Al batteries, much work is still needed. In addition to evaluating this electrolyte with several cathode materials, perhaps those less prone to hydride reactivity, studying the reaction in other organic solvents will be necessary. Ideally, the choice of the organic solvent should be limited to those compatible with LiAlH_4 . For instance, our preliminary cyclic voltammetry evaluation of an electrolyte consisting of $\text{Al}(\text{OTf})_3$ and LiAlH_4 in diglyme reveals a reversible electrochemical process ca. 0V (vs Al/Al^{3+}), likely associated with reversible Al plating and stripping, as shown in the Supporting Information Figure 4.14. We speculate that borohydrides (BH_4^-) can have similar effect on the plating and stripping behavior of Al-ions, especially because of the critical role BH_4^- play in magnesium⁵³ and calcium⁵⁴⁻⁵⁶ electrolyte chemistries. Preliminary cyclic voltammetry evaluation of the LiBH_4 additive on electrolytes consisting of either $\text{Al}(\text{OTf})_3/\text{THF}$ or AlCl_3/THF reveal promising reversible Al electrochemistry as shown in Supporting Information Figure 4.15. Future work will focus on confirming Al electrodeposition from these solutions and exploring ionic speciation in both systems. We also speculate that a similar plating/stripping behavior can occur in the absence of the F-component, this hypothesis will be explored by replacing the $\text{Al}(\text{OTf})_3$ salt with a halide-free and THF-soluble Al salts.

4.5 Supporting Information

Table 4.1 Measured and computed vibrational frequencies of aluminum complexes ν = bond stretch, τ = twisting, δ = group angle deformation, subscript s = symmetric, subscript as = asymmetric, $\text{OTF}^- = \text{CF}_3\text{SO}_3^-$

Species	Mode	Computed (cm ⁻¹)	Measured (cm ⁻¹)	Literature
[Al(THF) ₄ (OTF)][OTF] ¹⁺	Outer sphere $\nu_{\text{as}}\text{SO}_3$	1238.28	1238	This work and our previous work ³⁴
[Al(THF) ₂ (OTF) ₂] ¹⁺	Inner sphere $\nu_{\text{as}}\text{SO}_3$	1351.58	1350	This work and our previous work ³⁴
		1357.27		
Li(THF) ₃ (OTF)	Inner sphere $\nu_{\text{as}}\text{SO}_3$	1252.60	1253	Previous work and ref ⁴⁶
trans-AlCl ₃ (THF) ₂	$\nu_{\text{as}}(\text{Al}-\text{Cl})$	487.86	491	Previous work ³⁴
		476.34		
	$\nu(\text{Al}-\text{Cl})$	-	490	Ref ⁴⁹
cis-AlCl ₃ (THF) ₂	-	-	329	Ref ⁴⁹
			407 (Broad peak)	Previous work ³⁴
AlH ₃ (THF)	Al-H twisting	503.04 & 513.07	500 (broad)	This work
	$\nu_{\text{as}}(\text{Al}-\text{H})$	1806.10	1800 (broad)	
	$\nu_{\text{as}}(\text{Al}-\text{H})$	1825.67		
AlH ₃ (THF) ₂	$\nu_{\text{s}}(\text{Al}-\text{H})$	1799.65		This work
	$\nu_{\text{as}}(\text{Al}-\text{H})$	1742.15 (strong)	1711 (broad)	This work

	$\nu_{as}(Al-H)$	1762.46 (strong)	1768 (broad)	
AlH_4^-	$\nu_{as}(Al-H)$ Triply degenerate	1670.85	1668	This work
$LiAlH_4$	$\nu_{as}(Al-H)$	1651.49	1645	This work
$Al_2H_7^-$	$\nu_{as}(Al-H)$ bridging hydride (very strong)	1778.21	1778 (broad)	
	$\nu_{as}(Al-H)$ Quadruply degenerate	1802.10, 1808.92 and 1811.28 (very strong)	1800 (shoulder)	
$Al_2Cl_3H_4^-$	$\nu_{as}(Al-Cl)$	501.28	501	This work
		507.48		
	δAlH_3	672.70 (very strong)	667	This work

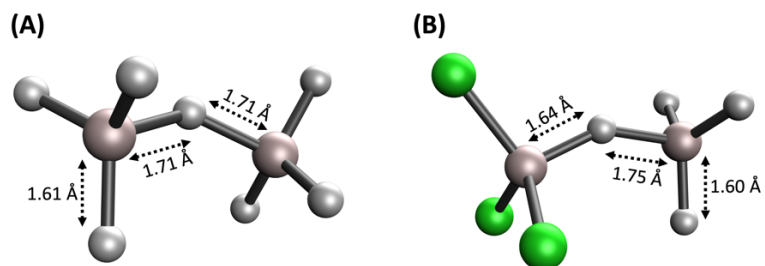


Figure 4.6 Showing the DFT calculated Al—H bond lengths in (A) $Al_2H_7^-$ and (B) $Al_2Cl_3H_4^-$

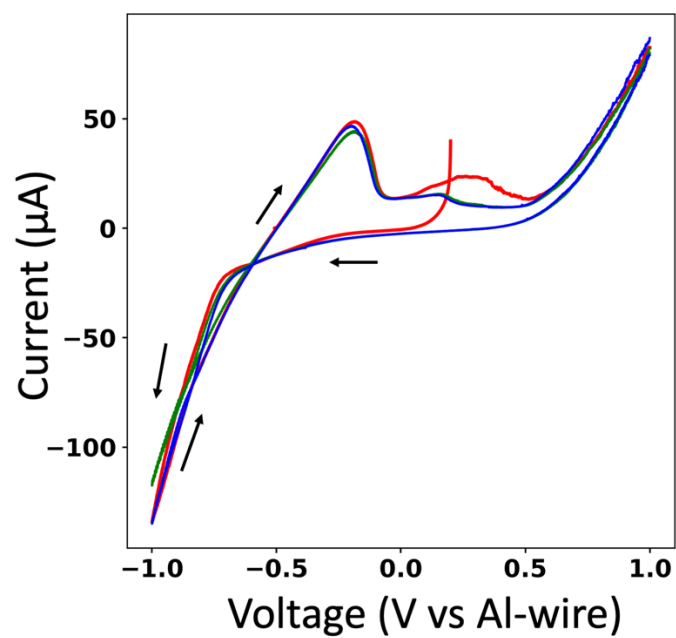


Figure 4.7 Cyclic voltammogram for 1.5 M $\text{LiAlH}_4/\text{THF}$ on gold working electrode (first scan is red, second is green, and third is blue)

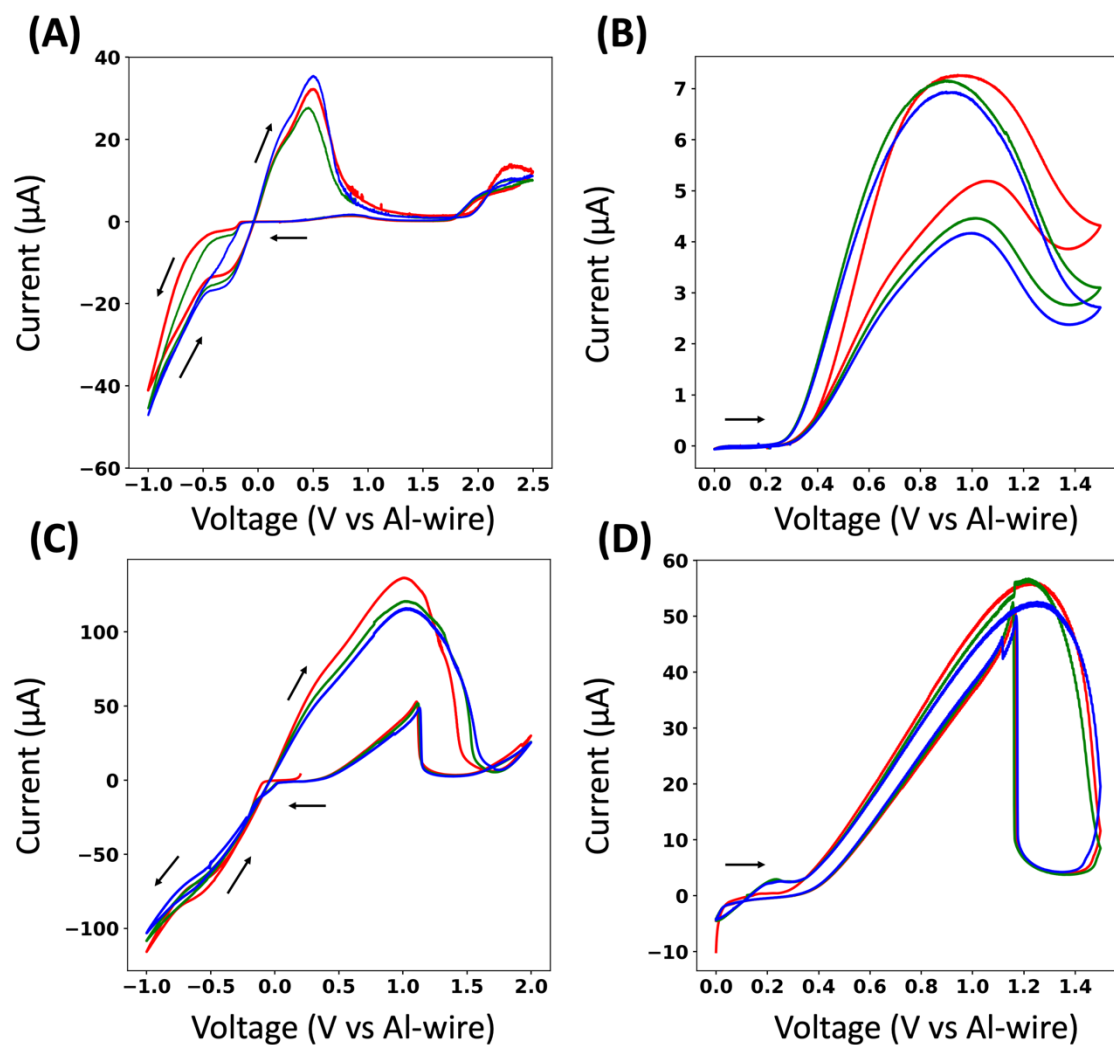


Figure 4.8 Cyclic voltammograms showing hydride activity on gold working electrode for 1:3 $\text{Al}(\text{OTf})_3:\text{LiAlH}_4/\text{THF}$. After resting the electrolyte for several hours (A) -1 to +2.5 V voltage window and (B) 0 to +1.5 V voltage window. Showing contributing from hydride 30 minutes after the electrolyte has been prepared (C) -1 to +2.5 V voltage window and (D) 0 to +1.5 V voltage window. (first scan is red, second is green, and third is blue)

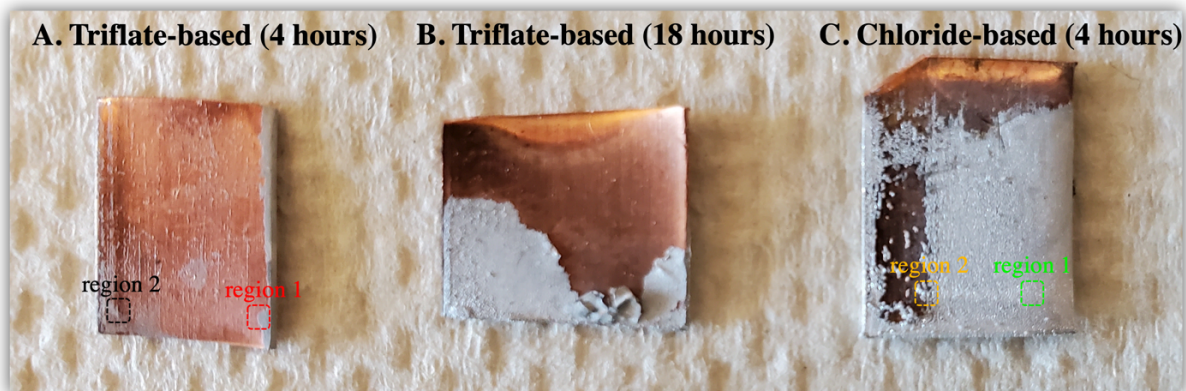


Figure 4.9 Showing photographic images of Al electrodeposit on Cu substrate from (A) & (B) OTF⁻-based and (C) Cl⁻-based electrolytes and the regions (1) & (2) for XPS experiments

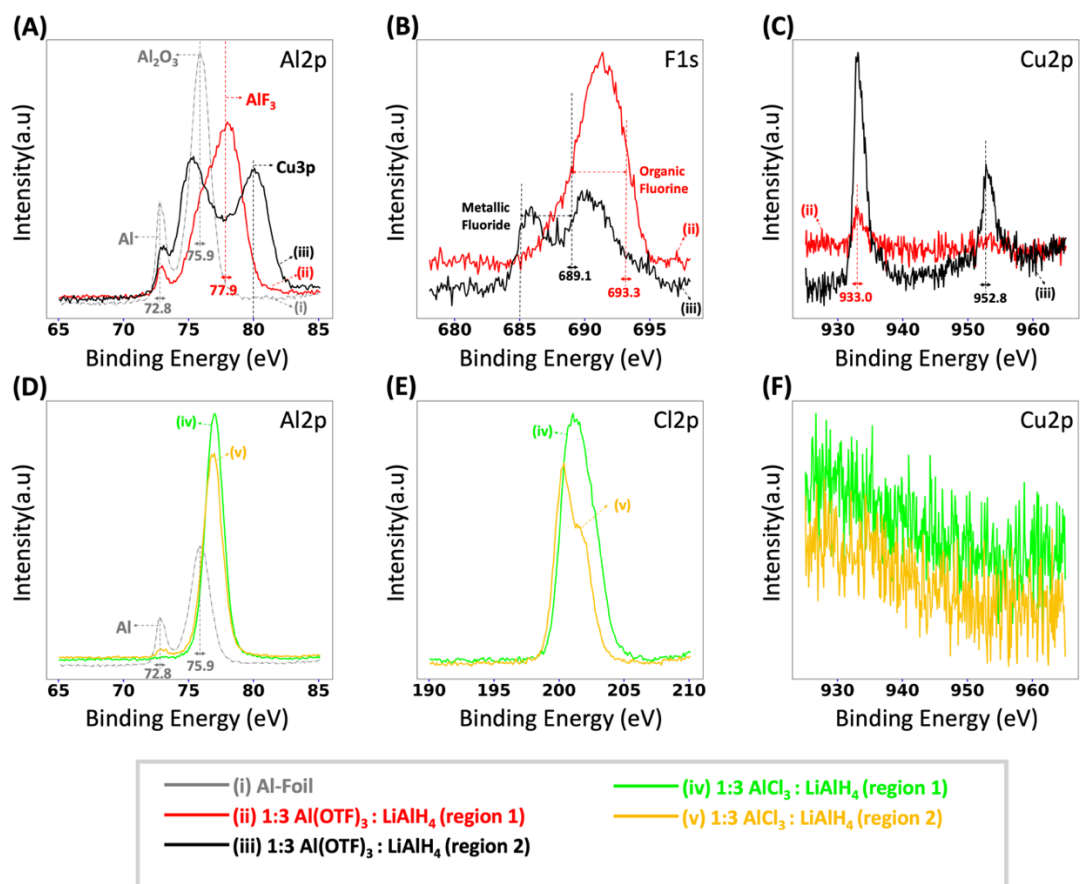


Figure 4.10 XPS spectra comparison of region 1 (before etching) and region 2 for Al electrodeposits from (A-C) 1:3 Al(OTF)₃:LiAlH₄/THF, and from (D-F) 1:3 AlCl₃:LiAlH₄/THF

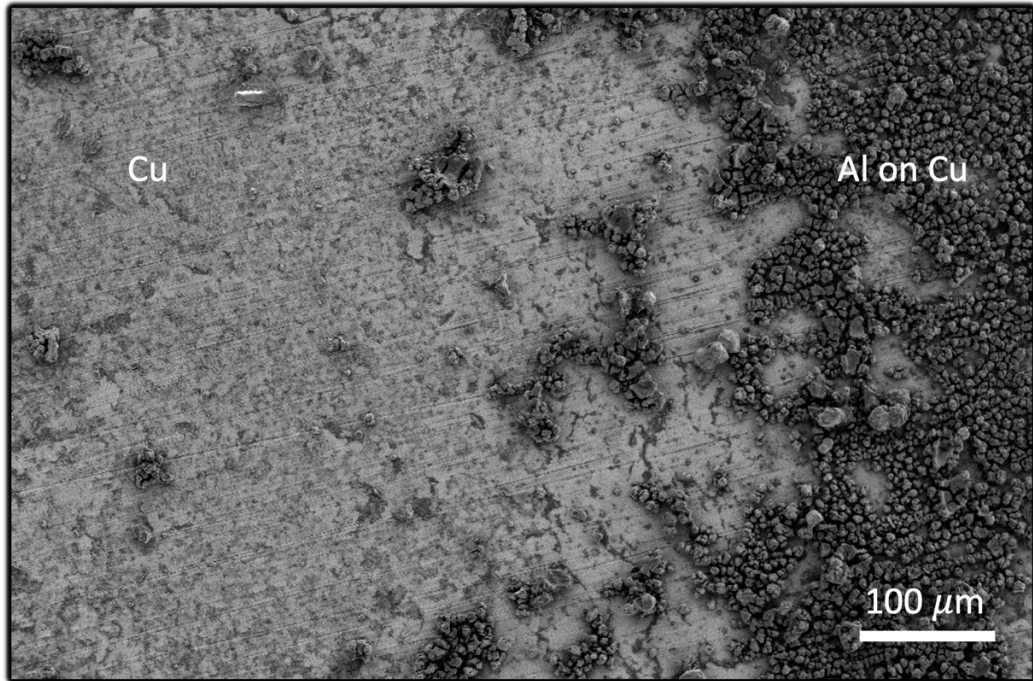


Figure 4.11 SEM image of remaining Al electrodeposits on Cu substrate after etching experiments at region 1

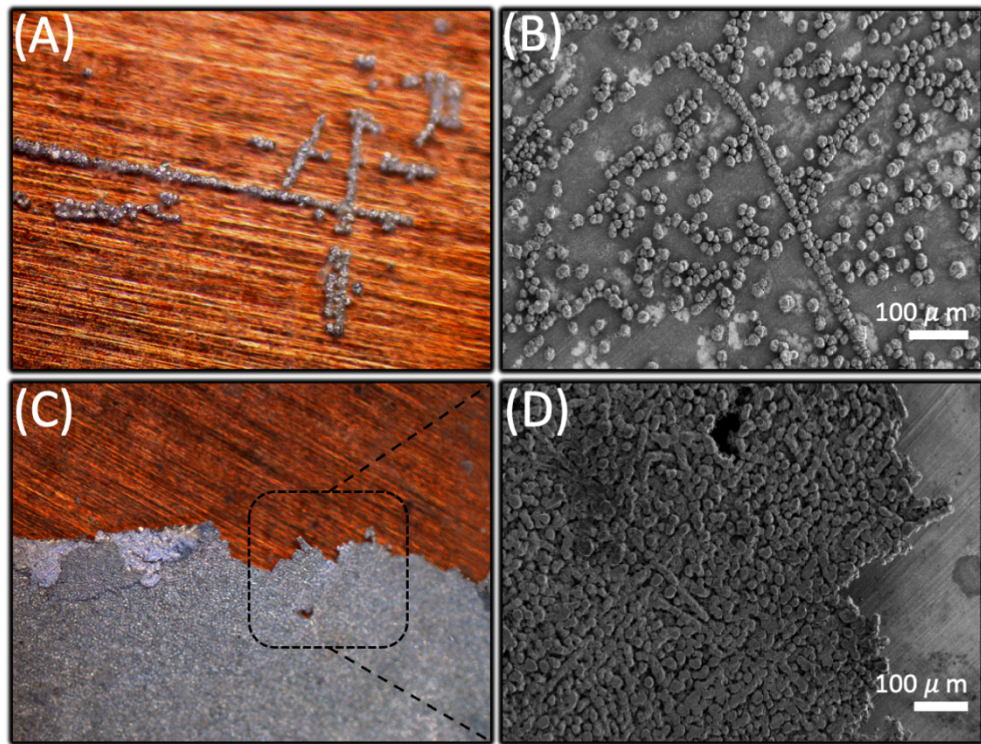


Figure 4.12 Showing (A) optical image and (B) SEM image of Al electrodeposits streaking patterns on Cu from 1:3 $\text{Al}(\text{OTF})_3:\text{LiAlH}_4/\text{THF}$ after 4 hours of plating. Showing (C) Al film obtained after 18 hours of plating from highly concentrated 1:3 $\text{Al}(\text{OTF})_3:\text{LiAlH}_4/\text{THF}$ and (D) corresponding SEM image

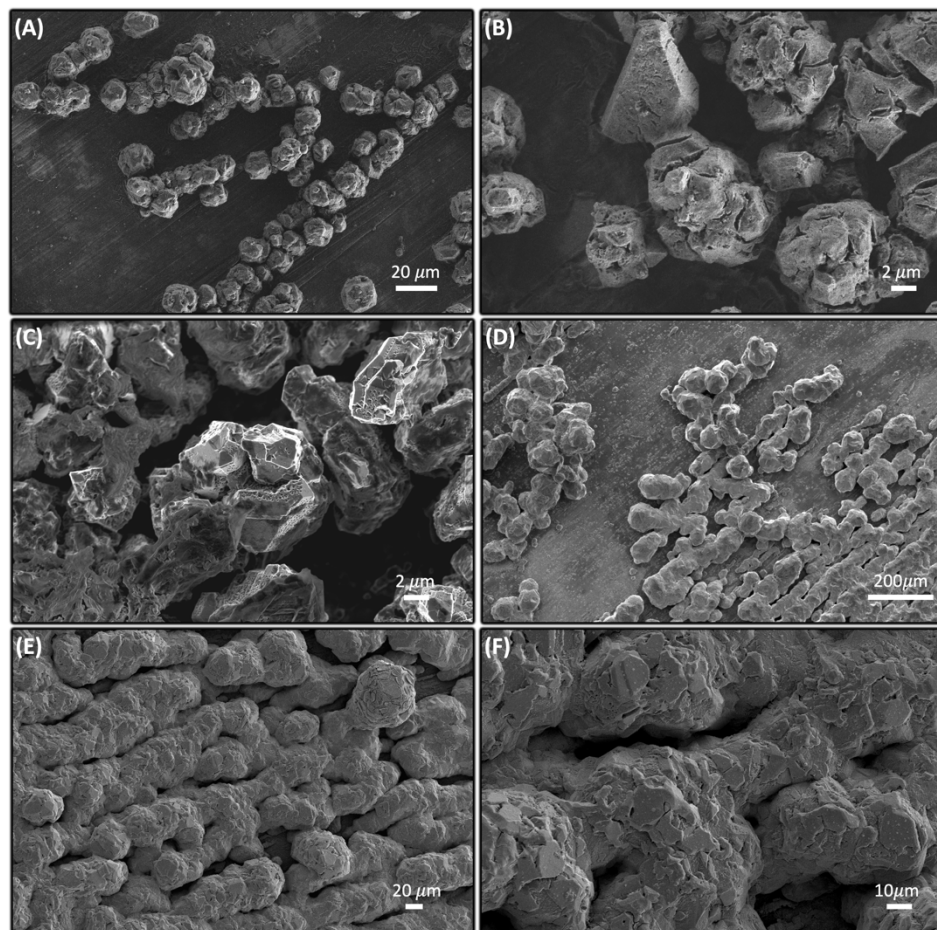


Figure 4.13 High magnification SEM images of Al electrodeposits (4 hours) from (A-C) 1:3 $\text{Al}(\text{OTf})_3:\text{LiAlH}_4/\text{THF}$ and from (D-F) 1:3 $\text{AlCl}_3:\text{LiAlH}_4/\text{THF}$.

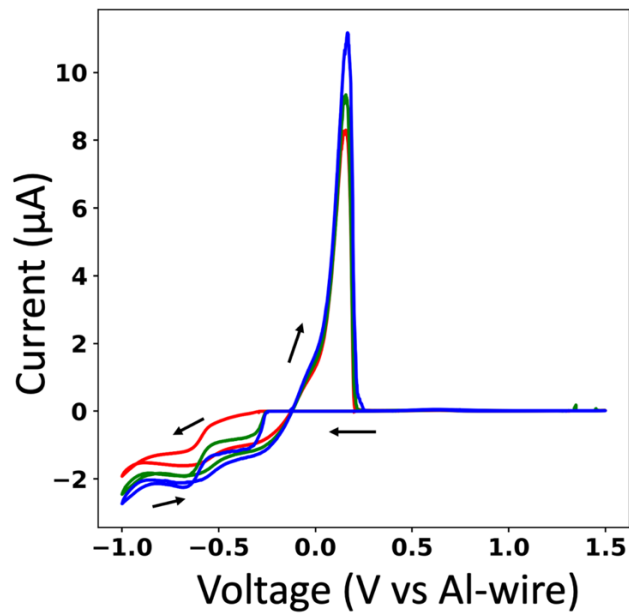


Figure 4.14 Cyclic voltammogram on gold working electrode for 1:3 Al(OTF)₃:LiAlH₄/diglyme (first scan is red, second is green, and third is blue).

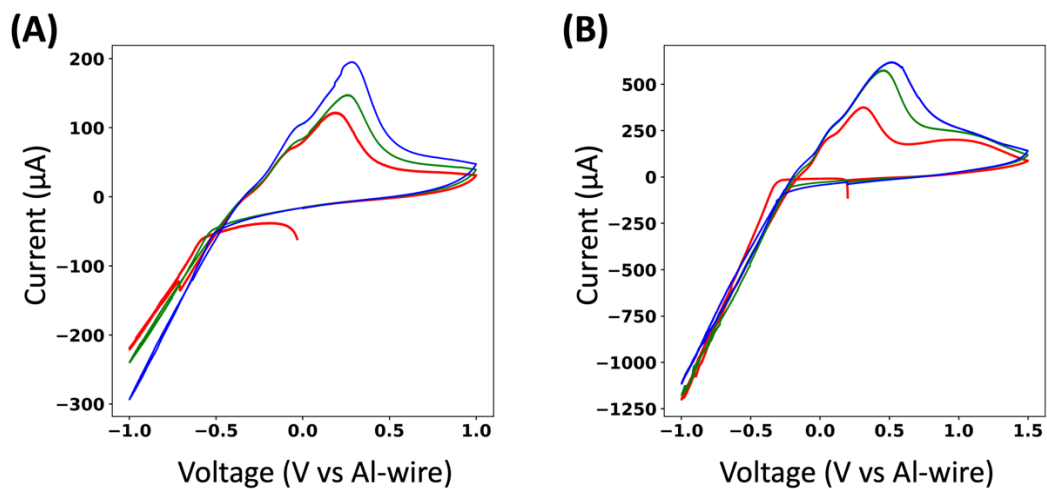


Figure 4.15 Cyclic voltammograms on gold working electrode for (A) 1:3 Al(OTF)₃:LiBH₄/THF and (B) 1:3 AlCl₃:LiBH₄/THF (first scan is red, second is green, and third is blue).

4.6 References

- (1) Elia, G. A.; Marquardt, K.; Hoeppe, K.; Fantini, S.; Lin, R.; Knipping, E.; Peters, W.; Drillet, J.-F.; Passerini, S.; Hahn, R. An Overview and Future Perspectives of Aluminum Batteries. *Adv. Mater.* **2016**, *28* (35), 7564–7579.
- (2) Tu, J.; Song, W.-L.; Lei, H.; Yu, Z.; Chen, L.-L.; Wang, M.; Jiao, S. Nonaqueous Rechargeable Aluminum Batteries: Progresses, Challenges, and Perspectives. *Chem. Rev.* **2021**, *121* (8), 4903–4961.
- (3) Gifford, P. R.; Palmisano, J. B. An Aluminum/Chlorine Rechargeable Cell Employing a Room Temperature Molten Salt Electrolyte. *J. Electrochem. Soc.* **1988**, *135* (3), 650.
- (4) Jayaprakash, N.; Das, S. K.; Archer, L. A. The Rechargeable Aluminum-Ion Battery. *Chem. Commun.* **2011**, *47* (47), 12610–12612.
- (5) Reed, L. D.; Menke, E. The Roles of V₂O₅ and Stainless Steel in Rechargeable Al-Ion Batteries. *J. Electrochem. Soc.* **2013**, *160* (6), A915–A917.
- (6) Geng, L.; Lv, G.; Xing, X.; Guo, J. Reversible Electrochemical Intercalation of Aluminum in Mo₆S₈. *Chem. Mater.* **2015**, *27* (14), 4926–4929.
- (7) Wang, H.; Bai, Y.; Chen, S.; Luo, X.; Wu, C.; Wu, F.; Lu, J.; Amine, K. Binder-Free V₂O₅ Cathode for Greener Rechargeable Aluminum Battery. *ACS Appl. Mater. Interfaces* **2015**, *7* (1), 80–84.
- (8) Lin, M.-C.; Gong, M.; Lu, B.; Wu, Y.; Wang, D.-Y.; Guan, M.; Angell, M.; Chen, C.; Yang, J.; Hwang, B.-J. An Ultrafast Rechargeable Aluminium-Ion Battery. *Nature* **2015**, *520* (7547), 324–328.
- (9) Gao, T.; Li, X.; Wang, X.; Hu, J.; Han, F.; Fan, X.; Suo, L.; Pearse, A. J.; Lee, S. B.; Rubloff, G. W. A Rechargeable Al/S Battery with an Ionic-Liquid Electrolyte. *Angew. Chem.* **2016**, *128* (34), 10052–10055.
- (10) Stadie, N. P.; Wang, S.; Kravchyk, K. V.; Kovalenko, M. V. Zeolite-Templated Carbon as an Ordered Microporous Electrode for Aluminum Batteries. *ACS Nano* **2017**, *11* (2), 1911–1919.
- (11) Elia, G. A.; Hasa, I.; Greco, G.; Diemant, T.; Marquardt, K.; Hoeppe, K.; Behm, R. J.; Hoell, A.; Passerini, S.; Hahn, R. Insights into the Reversibility of Aluminum Graphite Batteries. *J. Mater. Chem. A* **2017**, *5* (20), 9682–9690.
- (12) Kravchyk, K. V.; Wang, S.; Piveteau, L.; Kovalenko, M. V. Efficient Aluminum Chloride–Natural Graphite Battery. *Chem. Mater.* **2017**, *29* (10), 4484–4492.
- (13) Tian, H.; Zhang, S.; Meng, Z.; He, W.; Han, W.-Q. Rechargeable Aluminum/Iodine Battery Redox Chemistry in Ionic Liquid Electrolyte. *ACS Energy Lett.* **2017**, *2* (5), 1170–1176.
- (14) Walter, M.; Kravchyk, K. V.; Böfer, C.; Widmer, R.; Kovalenko, M. V. Polypyrenes as High-Performance Cathode Materials for Aluminum Batteries. *Adv. Mater.* **2018**, *30* (15), 1705644.
- (15) Wang, S.; Kravchyk, K. V.; Filippin, A. N.; Müller, U.; Tiwari, A. N.; Buecheler, S.; Bodnarchuk, M. I.; Kovalenko, M. V. Aluminum Chloride-Graphite Batteries with Flexible Current Collectors Prepared from Earth-Abundant Elements. *Adv. Sci.* **2018**, *5* (4), 1700712.

- (16) Muñoz-Torrero, D.; Leung, P.; García-Quismondo, E.; Ventosa, E.; Anderson, M.; Palma, J.; Marcilla, R. Investigation of Different Anode Materials for Aluminium Rechargeable Batteries. *J. Power Sources* **2018**, *374*, 77–83.
- (17) Chen, H.; Xu, H.; Wang, S.; Huang, T.; Xi, J.; Cai, S.; Guo, F.; Xu, Z.; Gao, W.; Gao, C. Ultrafast All-Climate Aluminum-Graphene Battery with Quarter-Million Cycle Life. *Sci. Adv.* **2017**, *3* (12), eaao7233.
- (18) Yang, C.; Wang, S.; Zhang, X.; Zhang, Q.; Ma, W.; Yu, S.; Sun, G. Substituent Effect of Imidazolium Ionic Liquid: A Potential Strategy for High Coulombic Efficiency Al Battery. *J. Phys. Chem. C* **2019**, *123* (18), 11522–11528.
- (19) Kim, D. J.; Yoo, D.-J.; Otley, M. T.; Prokofjevs, A.; Pezzato, C.; Owczarek, M.; Lee, S. J.; Choi, J. W.; Stoddart, J. F. Rechargeable Aluminium Organic Batteries. *Nat. Energy* **2019**, *4* (1), 51–59.
- (20) Wen, X.; Liu, Y.; Jadhav, A.; Zhang, J.; Borchardt, D.; Shi, J.; Wong, B. M.; Sanyal, B.; Messinger, R. J.; Guo, J. Materials Compatibility in Rechargeable Aluminum Batteries: Chemical and Electrochemical Properties between Vanadium Pentoxide and Chloroaluminate Ionic Liquids. *Chem. Mater.* **2019**, *31* (18), 7238–7247.
- (21) Zhou, Q.; Wang, D.; Lian, Y.; Hou, S.; Ban, C.; Wang, Z.; Zhao, J.; Zhang, H. Rechargeable Aluminum-Ion Battery with Sheet-like MoSe₂@ C Nanocomposites Cathode. *Electrochimica Acta* **2020**, *354*, 136677.
- (22) Tseng, C.-H.; Chang, J.-K.; Chen, J.-R.; Tsai, W. T.; Deng, M.-J.; Sun, I.-W. Corrosion Behaviors of Materials in Aluminum Chloride–1-Ethyl-3-Methylimidazolium Chloride Ionic Liquid. *Electrochem. Commun.* **2010**, *12* (8), 1091–1094.
- (23) Wang, H.; Gu, S.; Bai, Y.; Chen, S.; Zhu, N.; Wu, C.; Wu, F. Anion-Effects on Electrochemical Properties of Ionic Liquid Electrolytes for Rechargeable Aluminum Batteries. *J. Mater. Chem. A* **2015**, *3* (45), 22677–22686.
- (24) Lai, P. K.; Skyllas-Kazacos, M. Electrodeposition of Aluminium in Aluminium Chloride/1-Methyl-3-Ethylimidazolium Chloride. *J. Electroanal. Chem. Interfacial Electrochem.* **1988**, *248* (2), 431–440.
- (25) Carlin, R. T.; Crawford, W.; Bersch, M. Nucleation and Morphology Studies of Aluminum Deposited from an Ambient-Temperature Chloroaluminate Molten Salt. *J. Electrochem. Soc.* **1992**, *139* (10), 2720.
- (26) Shi, J.; Zhang, J.; Guo, J. Avoiding Pitfalls in Rechargeable Aluminum Batteries Research. *ACS Energy Lett.* **2019**, *4* (9), 2124–2129.
- (27) Reed, L. D.; Ortiz, S. N.; Xiong, M.; Menke, E. J. A Rechargeable Aluminum-Ion Battery Utilizing a Copper Hexacyanoferrate Cathode in an Organic Electrolyte. *Chem. Commun.* **2015**, *51* (76), 14397–14400.
- (28) Reed, L. D.; Arteaga, A.; Menke, E. J. A Combined Experimental and Computational Study of an Aluminum Triflate/Diglyme Electrolyte. *J. Phys. Chem. B* **2015**, *119* (39), 12677–12681.
- (29) Mandai, T.; Johansson, P. Al Conductive Haloaluminate-Free Non-Aqueous Room-Temperature Electrolytes. *J. Mater. Chem. A* **2015**, *3* (23), 12230–12239.
- (30) Mandai, T.; Johansson, P. Haloaluminate-Free Cationic Aluminum Complexes: Structural Characterization and Physicochemical Properties. *J. Phys. Chem. C* **2016**, *120* (38), 21285–21292.

- (31) Chiku, M.; Matsumura, S.; Takeda, H.; Higuchi, E.; Inoue, H. Aluminum Bis (Trifluoromethanesulfonyl) Imide as a Chloride-Free Electrolyte for Rechargeable Aluminum Batteries. *J. Electrochem. Soc.* **2017**, *164* (9), A1841.
- (32) Slim, Z.; Menke, E. J. Comparing Computational Predictions and Experimental Results for Aluminum Triflate in Tetrahydrofuran. *J. Phys. Chem. B* **2020**, *124* (24), 5002–5008.
- (33) Wen, X.; Zhang, J.; Luo, H.; Shi, J.; Tsay, C.; Jiang, H.; Lin, Y.-H.; Schroeder, M. A.; Xu, K.; Guo, J. Synthesis and Electrochemical Properties of Aluminum Hexafluorophosphate. *J. Phys. Chem. Lett.* **2021**, *12*, 5903–5908.
- (34) Slim, Z.; Menke, E. J. Aluminum Electrodeposition from Chloride-Rich and Chloride-Free Organic Electrolytes. *J. Phys. Chem. C* **2022**, *126* (5), 2365–2373.
- (35) Couch, D. E.; Brenner, A. A Hydride Bath for the Electrodeposition of Aluminum. *J. Electrochem. Soc.* **1952**, *99* (6), 234.
- (36) Ishibashi, N.; Yoshio, M. Electrodeposition of Aluminium from the NBS Type Bath Using Tetrahydrofuran—Benzene Mixed Solvent. *Electrochimica Acta* **1972**, *17* (8), 1343–1352.
- (37) Yoshio, M.; Ishibashi, N. High-Rate Plating of Aluminium from the Bath Containing Aluminium Chloride and Lithium Aluminium Hydride in Tetrahydrofuran. *J. Appl. Electrochem.* **1973**, *3* (4), 321–325.
- (38) Daenen, T. E. G. Cyclic Reaction Mechanism in the Electrodeposition of Aluminium. *Nature* **1979**, *280* (5721), 378–380.
- (39) Galová, M. Conductometric Study of the Composition of Aluminum Chloride-Lithium Aluminium Hydride $\text{AlCl}_3\text{—LiAlH}_4$ Electrolyte in Tetrahydrofuran. *Chem. Pap.* **1982**, *36* (6), 791–797.
- (40) Graef, M. W. M. The Mechanism of Aluminum Electrodeposition from Solutions of AlCl_3 and LiAlH_4 in THF. *J. Electrochem. Soc.* **1985**, *132* (5), 1038.
- (41) Badawy, W. A.; Sabrah, B. A.; Hilal, N. H. Y. A New Bath for the Electrodeposition of Aluminium. II. Kinetics and Mechanism of the Deposition and Dissolution Processes. *J. Appl. Electrochem.* **1987**, *17* (2), 357–369.
- (42) Lefebvre, M. C.; Conway, B. E. ^{27}Al NMR Spectroscopy Studies on Speciation of Al Complex Ions in $\text{AlCl}_3 + \text{LiAlH}_4$ Solutions in Tetrahydrofuran for Electroplating of Al. *J. Electroanal. Chem.* **1998**, *448* (2), 217–227.
- (43) Lefebvre, M. C.; Conway, B. E. Elementary Steps and Mechanism of Electrodeposition of Al from Complex Hydride Ions in Tetrahydrofuran Baths. *J. Electroanal. Chem.* **2000**, *480* (1–2), 34–45.
- (44) Lefebvre, M. C.; Conway, B. E. Nucleation and Morphologies in the Process of Electrocrystallization of Aluminium on Smooth Gold and Glassy-Carbon Substrates. *J. Electroanal. Chem.* **2000**, *480* (1–2), 46–58.
- (45) Frech, R.; Huang, W. Ionic Association in Poly (Propylene Oxide) Complexed with Divalent Metal Trifluoromethanesulfonate Salts. *Solid State Ion.* **1993**, *66* (1–2), 183–188.
- (46) Frech, R.; Huang, W. Anion-Solvent and Anion-Cation Interactions in Lithium and Tetrabutylammonium Trifluoromethanesulfonate Solutions. *J. Solut. Chem.* **1994**, *23* (4), 469–481.
- (47) Huang, W.; Frech, R. Dependence of Ionic Association on Polymer Chain Length in Poly (Ethylene Oxide)-Lithium Triflate Complexes. *Polymer* **1994**, *35* (2), 235–242.


- (48) Huang, W.; Frech, R.; Wheeler, R. A. Molecular Structures and Normal Vibrations of Trifluoromethane Sulfonate (CF₃SO₃⁻) and Its Lithium Ion Pairs and Aggregates. *J. Phys. Chem.* **1994**, *98* (1), 100–110.
- (49) Derouault, J.; Granger, P.; Forel, M. T. Spectroscopic Investigation of Aluminum Trihalides-Tetrahydrofuran Complexes. 2. Solutions of Aluminum Chloride or Bromide in Tetrahydrofuran and in (Tetrahydrofuran-Dichloromethane). *Inorg. Chem.* **1977**, *16* (12), 3214–3218.
- (50) Yartys, V. A.; Denys, R. V.; Maehlen, J. P.; Frommen, C.; Fichtner, M.; Bulychev, B. M.; Emerich, H. Double-Bridge Bonding of Aluminium and Hydrogen in the Crystal Structure of γ -AlH₃. *Inorg. Chem.* **2007**, *46* (4), 1051–1055.
- (51) Finholt, A. E.; Bond Jr, A. C.; Schlesinger, H. I. Lithium Aluminum Hydride, Aluminum Hydride and Lithium Gallium Hydride, and Some of Their Applications in Organic and Inorganic Chemistry. *J. Am. Chem. Soc.* **1947**, *69* (5), 1199–1203.
- (52) See, K. A.; Chapman, K. W.; Zhu, L.; Wiaderek, K. M.; Borkiewicz, O. J.; Barile, C. J.; Chupas, P. J.; Gewirth, A. A. The Interplay of Al and Mg Speciation in Advanced Mg Battery Electrolyte Solutions. *J. Am. Chem. Soc.* **2016**, *138* (1), 328–337.
- (53) Mohtadi, R.; Matsui, M.; Arthur, T. S.; Hwang, S.-J. Magnesium Borohydride: From Hydrogen Storage to Magnesium Battery. *Angew. Chem.* **2012**, *124* (39), 9918–9921.
- (54) Wang, D.; Gao, X.; Chen, Y.; Jin, L.; Kuss, C.; Bruce, P. G. Plating and Stripping Calcium in an Organic Electrolyte. *Nat. Mater.* **2018**, *17* (1), 16–20.
- (55) Ta, K.; Zhang, R.; Shin, M.; Rooney, R. T.; Neumann, E. K.; Gewirth, A. A. Understanding Ca Electrodeposition and Speciation Processes in Nonaqueous Electrolytes for Next-Generation Ca-Ion Batteries. *ACS Appl. Mater. Interfaces* **2019**, *11* (24), 21536–21542.
- (56) Melemed, A. M.; Skiba, D. A.; Gallant, B. M. Toggling Calcium Plating Activity and Reversibility through Modulation of Ca²⁺ Speciation in Borohydride-Based Electrolytes. *J. Phys. Chem. C* **2022**.


Appendix A

Copyright permission for chapter 2

Rightslink® by Copyright Clearance Center

4/8/22, 7:47 PM

Home Help Live Chat Sign in Create Account



Comparing Computational Predictions and Experimental Results for Aluminum Triflate in Tetrahydrofuran
Author: Zaher Slim, Erik J. Menke
Publication: The Journal of Physical Chemistry B
Publisher: American Chemical Society
Date: Jun 1, 2020
Copyright © 2020, American Chemical Society

PERMISSION/LICENSE IS GRANTED FOR YOUR ORDER AT NO CHARGE

This type of permission/license, instead of the standard Terms and Conditions, is sent to you because no fee is being charged for your order. Please note the following:

- Permission is granted for your request in both print and electronic formats, and translations.
- If figures and/or tables were requested, they may be adapted or used in part.
- Please print this page for your records and send a copy of it to your publisher/graduate school.
- Appropriate credit for the requested material should be given as follows: "Reprinted (adapted) with permission from {COMPLETE REFERENCE CITATION}. Copyright (YEAR) American Chemical Society." Insert appropriate information in place of the capitalized words.
- One-time permission is granted only for the use specified in your RightsLink request. No additional uses are granted (such as derivative works or other editions). For any uses, please submit a new request.

If credit is given to another source for the material you requested from RightsLink, permission must be obtained from that source.

[BACK](#) [CLOSE WINDOW](#)


© 2022 Copyright - All Rights Reserved | [Copyright Clearance Center, Inc.](#) | [Privacy statement](#) | [Terms and Conditions](#)
Comments? We would like to hear from you. E-mail us at customer@copyright.com

Copyright permission for chapter 3

Rightslink® by Copyright Clearance Center

4/8/22, 7:35 PM

Home Help ▾ Live Chat Sign in Create Account



Aluminum Electrodeposition from Chloride-Rich and Chloride-Free Organic Electrolytes
Author: Zaher Slim, Erik J. Menke
Publication: The Journal of Physical Chemistry C
Publisher: American Chemical Society
Date: Feb 1, 2022
Copyright © 2022, American Chemical Society

PERMISSION/LICENSE IS GRANTED FOR YOUR ORDER AT NO CHARGE

This type of permission/license, instead of the standard Terms and Conditions, is sent to you because no fee is being charged for your order. Please note the following:

- Permission is granted for your request in both print and electronic formats, and translations.
- If figures and/or tables were requested, they may be adapted or used in part.
- Please print this page for your records and send a copy of it to your publisher/graduate school.
- Appropriate credit for the requested material should be given as follows: "Reprinted (adapted) with permission from {COMPLETE REFERENCE CITATION}. Copyright {YEAR} American Chemical Society." Insert appropriate information in place of the capitalized words.
- One-time permission is granted only for the use specified in your RightsLink request. No additional uses are granted (such as derivative works or other editions). For any uses, please submit a new request.

If credit is given to another source for the material you requested from RightsLink, permission must be obtained from that source.

[BACK](#) CLOSE WINDOW

© 2022 Copyright - All Rights Reserved | [Copyright Clearance Center, Inc.](#) | [Privacy statement](#) | [Terms and Conditions](#)
Comments? We would like to hear from you. E-mail us at customercare@copyright.com